Development and applications of a distributed hydrological model for water resources assessment at the Chao Phraya River Basin under a changing climate

Supattana Wichakul

2014

Development and applications of a distributed hydrological model for water resources assessment at the Chao Phraya River Basin under a changing climate

by

Supattana Wichakul

A dissertation

submitted in partial fulfillment of the requirement

for the degree of Doctor of Philosophy

Dept. of Civil and Earth Resources Engineering

Kyoto University, Japan

2014

Declaration of authorship

I, Miss Supattana Wichakul, hereby declare that this thesis titled ‘Development and applications of a distributed hydrological model for water resources assessment at the Chao Phraya River Basin under a changing climate’ and the work presented in its entirely are my own investigation, except where I have consulted the work of others, this is always clearly stated. I confirm that this work has not been submitted for a degree or any other qualification at this University or any other institution.

Supattana Wichakul

Acknowledgement

I would like to express my gratitude and appreciation to all those who gave me the possibility to complete this thesis.

Greatly thanks to my best academic advisor Prof. Yasuto Tachikawa, who helped, stimulating suggestions and encouragement, taught me to coding the computer programming with a numerical simulation and assisted me to conduct my research.

I would also like to acknowledge with much appreciation other professors of Hydrology and Water Resources Research Laboratory – Prof.Michiharu Shiiba, Prof. Kazuaki Yorozu, and Prof. Sunmin Kim – who gave me helpful suggestion and discussion.

I would like to thank the Royal Irrigation Department of Thailand, for supporting recorded rainfall data and observed discharge. I greatly appreciate Team Consulting Engineering and Management Co., Ltd., in their kind support during our site visit to the Chao Phraya River Basin.

Special thanks go to my Lab mates and my friends, who in one way or another have given all their support and encouragement.

I also expressed my deep gratitude to the Japanese Government (Monbukagakusho: MEXT) Scholarship for providing the scholarship during staying in Japan, giving me a chance to study here, Kyoto University.

Finally, I would like to say a million thanks to my family and my boyfriend. They always make me smile and warm me up when I feel down during the time I am far from home. They always believe in me and are looking forward to seeing my success.

Abstract

In the second half year of 2011, Thailand has encountered with a devastating flood caused by continuous intense precipitation, occurred in the Chao Phraya River Basin (CPRB). From the losses of life and properties caused from this huge flood, I realized that it is critical to assess the vulnerability of river systems and water-related disasters to predict the future situation and avoid those losses.

Therefore, Chapter 2 aims to develop a regional distributed hydrological model for water resources assessment. The regional hydrologic model is composed of a runoff generation model based on an infiltration capacity, and the flow routing model including the effects of dam control. The model is applied to the Chao Phraya River basin to reproduce floods in 1995, 2008, 2010, and 2011. By using the model application, the effects of the existing dams operations and the new dam construction on flood control were numerical evaluated.

Chapter 3 is to include the inundation effect into the distributed flow routing model. The flow routing model is modified based on the concept of a diffusive tank model to present overbank flow. The overbank flow is estimated by using a broad crested weir equation. The inundation model had provided a good fit for observed and simulated discharge in 2011 at the C.2 Station at Nakhon Sawan.

To take the impacts of climate change on water resources into account, chapter 4 presents an application of the developed regional distributed hydrologic forcing with outputs of the super-high-resolution general circulation model version MRI-AGCM3.2S

without any bias correction for three different climate experiments: the present climate (1979-2008), near future climate (2015-2044), and future climate (2075-2104). The C.2 gauging station is selected to monitor changes in river discharge. The results showed water availability considerably to increase in the future climate experiment and drought risk to increase in the near future climate experiment.

Furthermore, for precious result of the discharge projection, it is necessary to remove the existing biases before conducting hydrological simulation. The bias correction processes are presented in Chapter 5. Two bias correction methods, (1) Empirical distribution method and (2) Quantile-quantile method, were applied to the GCM precipitation. APHRODITE data was used as reference observation data for training period of 29 years (1979-2007). Both two methods were basically based on a comparison of cumulative distribution functions (CDFs) of the GCM precipitation and CDFs of observation data. Additionally, to remove bias in GCM evapotranspiration, two simple methods adjusting mean monthly evapotranspiration were introduced. I obtained a reference crop evapotranspiration (ET_o) calculated by the FAO Penman-Monteith method using recorded climatology data for the 30 years to be the truth reference data. Both two correction methods, the multiplicative factor and the different factor, completely improved the mean monthly GCM evapotranspiration.

Finally, Chapter 6 shows the hydrograph simulated by using the bias-corrected precipitation by the quantile-quantile method with the bias-corrected evapotranspiration by the different factor achieved a well fit with the reference observed discharge at the C.2 station. Finally, projection discharge of the Chao Phraya River for the near climate future and the future climate experiments by using the bias-corrected GCM data set

presents that 1) the mean annual discharge tends to increase in both near future and future projection periods, 2) During a dry season the tendency of low flow in the near future period leads to decrease. However, the flood frequency analysis using Generalized Extreme Value distribution (GEV) indicates that flood risk in the future will have more severities and damages to the country; especially in the near future (2015-2043) the magnitude of 80-year return period flood is greater than the devastating 2011 Thai flood.

Contents

List of figures

List of tables

Chapter 1

Introduction

1.1 Background

Water resources are the main component of the environment and fundamental element for all life on earth. For the past half-century, human consumption is rapidly growth and all human activities influence a climate change. It results in a limited usage of the water resources during the last two decades. So water resources should be reasonably used for human society to achieve the demands of the present and future and to maintain a desirable environment (Shiklomanov, 2000). According to the report of Intergovernmental Panel on Climate Change (IPCC) in 2007, the definition of climate change has been stated as a change in the state of the climate that can be identified by changes in the mean and/or the variability of its properties and that persists for an extended period, typically decades or longer. It refers to any change in climate over time, due to not only natural variability but also as a result of human activity (IPCC, 2007a).

The IPCC (2007b) also concludes that the proportion of total rainfall from heavy precipitation events is very likely to increase over most areas of the global and tropical and high latitude areas are particularly likely to experience increases in both the frequency and intensity of heavy precipitation events and also future tropical cyclones will likely become more intense, with larger peak wind speeds and heavier precipitation.

General circulation model (GCM) is the effective tool to study the interaction of the atmosphere, ocean, land surface, and ice for understanding of a changing climate behavior in long term. Currently, the GCMs that have been being developed for different climatologies are now available for 24 models, as of April, 22 2014 (IPCC, 2007c). Generally, the GCM contains of 9 variables that are specific humidity, precipitation flux, air pressure at sea level, surface downwelling shortwave flux in air, air temperature, air temperature daily maximum, air temperature daily minimum, eastward wind, and northward wind. The utilities of GCM are to analyze and project a change in those variables for various purposes.

Apart from the general circulation model, a vital tool for a further detailed study of the effects of the climate on the water resources for continental and regional scale basins is a hydrological model (rainfall-runoff model), that is one of the most important tools for water supply and long-term average monthly river discharge estimates (Wood et al., 1997). In the past two decades, numerous distributed hydrological models have been developed while traditional models are lumped. The lumped one cannot be used in many case to predict the effects of changes in land use, especially cannot be coupled with output from the GCM to predict the impacts of changes in climate on water resources. On the other hand, a distributed hydrological model can predict water resources effects by land use change and climate change (Jha et al., 1997). For the global scale scientific studies of climate change impacts on hydrological aspect lots of researches have already conducted. Hirabayashi et al. (2008) simulated daily discharge using the output from a climate change simulation model, MIROC, to investigate future projections of extremes in river discharge by considering the frequencies of future floods and droughts as estimated. Mizuta et al. (2011) used the MRI-AGCM3.2 to

simulate heavy monthly-mean precipitation and the global distribution of tropical cyclones. Nakaegawa et al. (2013) projected how discharge of major global rivers in late 21st century effected by a changing climate.

Not only the global scale researches were evaluated for the impacts of climate change, but the regional level researches were conducted also. For example, Aldous et al. (2011) evaluated climates change impacts and developing adaptation strategies in the western USA and south-eastern Australia. In China, Piao et al. (2010) reviewed the climate change impacts on water resources and agriculture and Yang et al. (2012) studied the impacts especially on flood and drought events in Huaihe River Basin. Potential impacts of climate change on heavy rainfall events, floods and droughts in the Australia were explored by Whetton et al. (1993). Also evaluation a change on discharge on major Asian rivers, including the Chao Phraya River, Thailand, was carried out by using the observation and model-based projections of discharge, and the result shown that changes in river discharge extremes are particularly important (Kundzewicz et al., 2009).

The several grid-based hydrological models have been developed for the purpose of continental and regional hydrological studies, i.e. predict floods, droughts and future water resources (Bemporad et al., 1997; Jha et al., 1997; Kite et al., 1994; Shiiba et al., 1999; Tachikawa et al., 2000; Wood et al., 1997). In Thailand, recent studies to utilize the application of the distributed hydrological model with the GCM output without any bias correction were conducted by Hunukumbura and Tachikawa (2012) to project future river discharge to detect hotspots in river discharges in the Chao Phraya River Basin (CPRB) using MRI-AGCM3.1s. Duong et al. (2013) used runoff data generated by MRI-AGCM3.2s to project a change in river discharge in the Indochina Peninsula region that also includes the CPRB.

However, for a reliable prediction result and reducing of systematic errors, the bias correction should be applied to the GCM output. Previous studies on bias correction in the Chao Phraya River Basin (CPRB) have been carried out by Koontanakulvong and Chaowiwat (2010) using Standard Deviation ratio downscaled rainfall and Modified Rescale downscaled rainfall to remove the bias from the MRI-AGCM3.1 precipitation and temperature datasets. In the Ping River basin, sub-basin of the CPRB, Sharma et al. (2007) improved the quality of EHCHAM4/OPYC SERS A2 and B2 precipitation by applying a gamma-gamma transformation bias-correction to evaluate the stream flow pattern.

In the second half year of 2011, Thailand has encountered with a devastating flood caused by continuous intense precipitation, occurred in the Chao Phraya River Basin in Thailand. The nation's economic system was severely disrupted, people lost their homes and lives. From these situations, I realized that it is critical to assess the vulnerability of river systems and water-related disasters. This disaster indicated that evaluation of the impacts of climate change is critical by using a suitable hydrological model for a basin scale. At this moment, I could not clearly indicate whether the Thailand's Great Flood in 2011, which resulted in the countless calamity causing tremendous losses on livelihood, social and economic of the nation, was the impact of climate change in the Southeast-Asia. Nevertheless, only a better understanding of the regional scale hydrological processes and effectively utilizing of the output from the available GCMs are necessary to envisage future water resources situation and to initiate an adaptive measures for sustainable protection system and development for the sever future situations whether it is flood or drought.

1.2 Objective

The main goals of this thesis are to develop and evaluate a distributed hydrological model that is applicable to the regional scale for future discharge prediction under a changing climate. The specific objectives of each interested are as follows.

- To develop a regional distributed hydrological model that composed of a runoff generation model (hydrological model) and a flow routing model for the Chao Phraya River Basin, Thailand.
- To improve the accuracy of flood movement simulation for the extreme flood event by including a dam operation and inundation effect.
- To identify the optimum model parameters that are suitable to topographical and hydrogeological conditions by using the data of historical floods in the Chao Phraya River Basin.
- To predict future discharge of the Chao Phraya River for the future water resources assessment by using the MRI-AGCM3.2S variables, such as precipitation and evapotranspiration.
- To propose statistical bias correction methods for the daily GCM precipitation and daily GCM evapotranspiration.
- To evaluate performance of the proposed bias correction methods for discharge simulations of the Chao Phraya River.
- To project future discharge of the Chao Phraya River and assess flood and drought risks of the Chao Phraya River Basin by using the bias corrected GCM data.

1.3 Outline of the thesis

This thesis is mainly focused on the development and evaluation of rainfall-runoff model for future discharge prediction. Therefore, all contents in total seven (7) chapters are related to the step-by-step developments of a distributed hydrological model, and the future discharge simulations by coupling with the GCM output data. The objectives of this thesis are described in the previous section.

Chapter 2 illustrates a regional distributed hydrological model developed for water resources assessment. The regional hydrologic model was developed with a concept of the variable infiltration capacity and the kinematic wave equation. The effects of dam control were also included in the flow routing model. The model was applied to reproduce the historical floods in the Chao Phraya River basin for the model parameters identification. Using an application of this developed model, I examined the effect of existing dams operations and the new dam construction on flood control.

Chapter 3 is to mainly modify the regional distributed hydrological model based on the concept of a diffusive tank model to take the inundation effect into account. Overbank flow was estimated by using a broad crested weir equation. The massive flood occurring in the Chao Phraya River Basin in 2011 has been reproduced by the modified model.

Chapter 4 is to test our developed model for discharge prediction and future water resources assessment in the Chao Phraya River Basin directly using the outputs of super-high-resolution general circulation model, version MRI-AGCM3.2S, without conducting bias-correction for three different climate experiments: the present climate (1979–2008), near future climate (2015–2044), and future climate (2075–2104).

However, the results of discharge prediction in the Chao Phraya River were still afflicted with biases to a degree that precludes its direct use of the GCM variables, precipitation and evapotranspiration. Consequently, to overcome this bias problem I proposed two bias correction methods, empirical distribution method and quantile-quantile method, for removing biases for the GCM precipitation, and also introduced the bias correction to the evapotranspiration. Thus, I provided the detail of the bias correction in Chapter 5.

Chapter 6 is to conduct river discharge simulation by using the corrected GCM precipitation and evapotranspiration. The best combination of the corrected precipitation and evapotranspiration based on discharge time series simulation was selected to further conduct future river discharge simulation under a changing climate condition. Future river discharge assessment for the Chao Phraya River was implemented.

Finally, the last chapter 7 presents concluding remark of thesis.

Chapter 2

Developing a regional distributed hydrological model for water resources assessment and its application to the Chao Phraya River Basin

2.1 Introduction

Due to the continuous and intense precipitation occurring in the upper part of Chao Phraya River Basin (CPRB), the unforeseen devastating flood occurred in the basin especially in the lower part of the basin from July 2011 until the end of the year. There are many losses in term of human, social and economic losses. Thai Ministry of Interior revealed that 815 people were killed and 3 were missing during the inundated period, as of January 20, 2012. The World Bank has estimated 1,425 billion baht (US$ 45.7 Bn) in economic damages and losses due to flooding, as of December 1, 2011. That is the worst recorded damage in Thailand. Therefore many hydrologists are interested to study about this flood and looking for the future situation of the basin.

In the recent past, using the atmospheric general circulation model (GCM) output data has been studied to predict the future hydrological situation in various basins around the world. There are also some studies about the future of hydrological situation under climate change impacts in the CPRB. For example; Ogata et at., 2012 applied the geomorphology-based hydrological model (GBHM) with using different three GCM outputs to forecast discharge from 2010 to 2040 in the CPRB, and Kure and Tebakari (2012) used Japan Meteorological Research Institute (MRI) atmospheric general circulation model 3.1 and 3.12 output data as input data to a watershed hydrologic model, DHI MIKE 11, to perform river discharge projections in the CPRB. Hunukumbura and Tachikawa (2012) projected future river discharge using MRI-AGCM3.1S to detect the hotspots on rivers discharge in the CPRB.

In 2002, Jayawardena et al. (2002*)* developed a meso-scale hydrological model by coupling a land surface model and a river routing model to predict river flow in

Mekong and Chao Phraya basins using GCM output. They applied several versions of the variable infiltration capacity (VIC) models. In the beginning, VIC model was developed by Wood et al. (1992), they simplified and reduced the number of parameters in the Xinanjiang (XAJ) model that has been widely and successfully applied in humid and semi-humid areas in China. Originally, the XAJ model was developed in 1973 and published in 1980 by Zhao et al. under the main concept of runoff formation on repletion of storage with three layers of soil moisture model and also the XAJ model was extended to include an evapotranspiration term.

The main objective of this paper is to develop a regional distributed hydrological model which is up-to-date and can reproduce historical floods in the CPRB. The model is applicable to assess a river plan under a changing climate. Using this developed regional hydrological model, I examine the effect of existing dams on reducing flood and a new dam construction on flood control.

2.2 Study area

The Chao Phraya River originates in the north region of Thailand and flow direction is from north to south. There are two parts of the CPRB, upper and lower part with an area of 157,925 km^2. The upper part of the basin consists of four principal sub-basins, the Ping River (catchment area 33,898 km^2), the Wang River (catchment 10,791 km^2), the Yom River (catchment area 23,616 km^2) and the Nan River basin (catchment area 34,330 km^2. The Upper Chao Phraya basin covers the area of 102,635 square kilometers representing 65% of the total basin area. The confluence of the Ping and Nan River at Nakorn Sawan province is the beginning of the Chao Phraya River. The Chao Phraya River including its tributaries are gently slope rivers, particularly in the lower part of the

basin and the downstream parts of the Yom and Nan Rivers, where the river gradients is around 1/10,000 to 1/15,000 (Komori et al., 2012).

Flow of the Chao Phraya River is significantly influenced by the operation of two main dams in the Ping River basin (Bhumiphol Dam) and the Nan River basin (Sirikit Dam). **Figure 2.2-1** illustrates a diagram of the CPRB including the satellite image of inundated area during flood 2011.

2.3 Input data

Rainfall accumulating in 2011 in the upper CPRB was 1,152 mm for the Ping, 1,430 mm for the Wang, 1,618 mm for the Yom, and 1,744 for the Nan River basins. The average 2011 annual rainfall for these subbasins is 36% larger than the average annual rainfall over a 30-year period from 1980 to 2009, whereas the average 2011 annual rainfall in the lower CPRB was 2% higher than the 30-year average. Therefore, in this study, I focused on runoff generated in upper sub-basins of the CPRB as observed at the C.2 station (15°40'N and 100°06'E).

Evapotranspiration data were obtained from reference crop evapotranspiration calculated by the Royal Irrigation Department of Thailand (RID) using the Penman-Monteith method and recorded climatology data for the 30 years from 1981 to 2010. Rainfall data were collected from 26 stations throughout the CPRB. List of station names and locations are shown in Appendix A. Both rainfall and evapotranspiration are the point data, I have transferred data format to a grid based with the same resolution of the rainfall-runoff model.

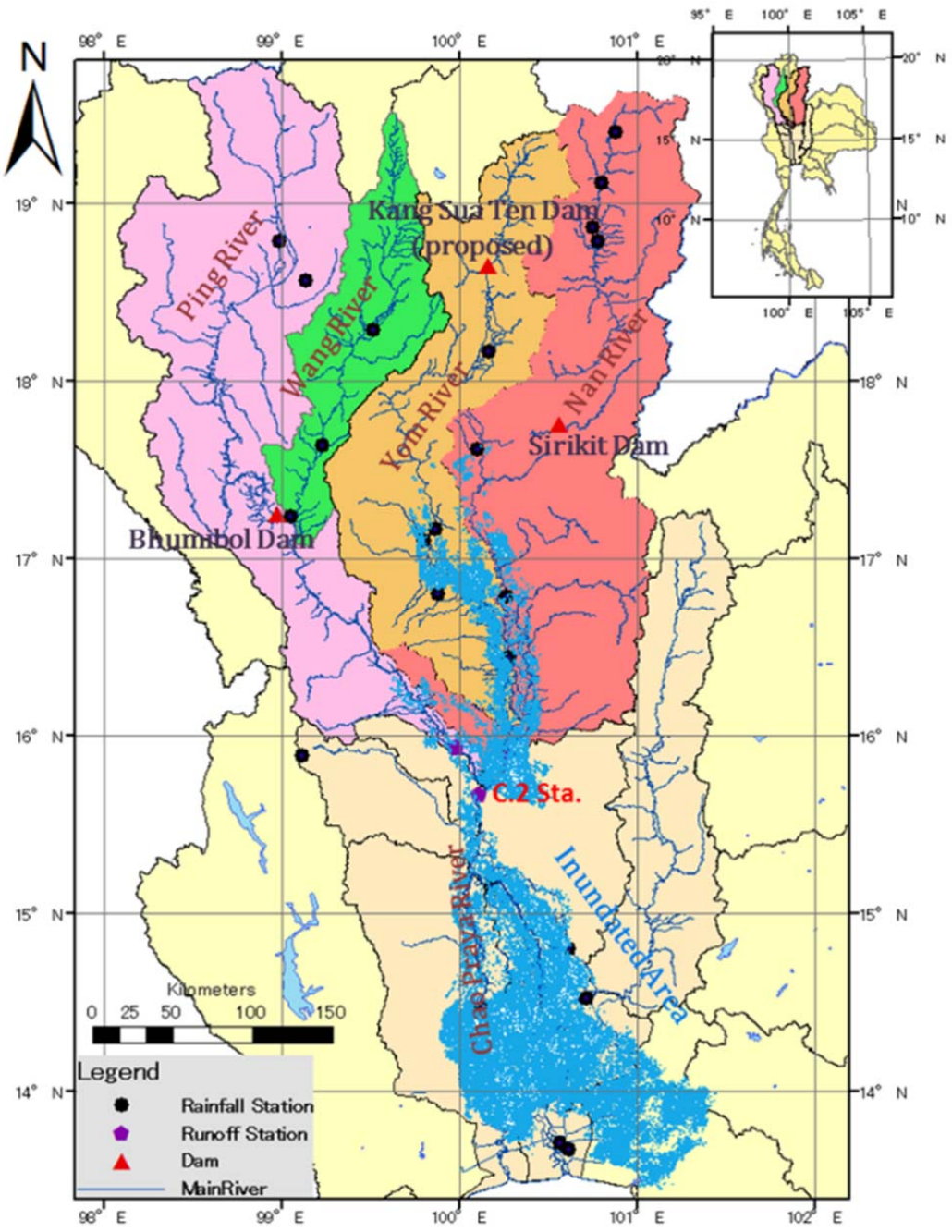

Figure 2.3-1 Diagram of the Chao Phraya River basin of Thailand

2.4 Modeling approach

Principally, a distributed hydrological model consists of a hydrologic model and a flow routing model. In this study both hydrologic and flow routing models were founded as a grid-based model. In order to reproduce the realistic runoff situation in the CPRB, a dam operation model has been combined in the flow routing model. The overall framework of the distributed hydrological model to achieve the simulated discharge in the river at each focused point can be schematized as in **Figure 2.4-1**.

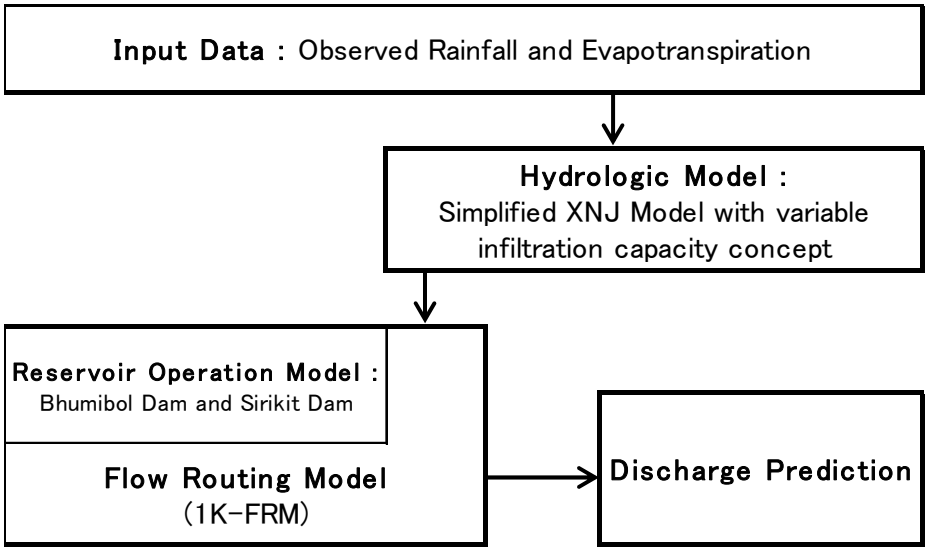

Figure 2.4-1 Framework of the distributed hydrological model

2.4.1 Hydrological model

To develop the hydrologic model, I simplified the Xinanjiang (XAJ) model by reducing the number of parameters and modifying sub-layers in the model for surface and subsurface runoff generations. Additionally, the concept of the modified XAJ model, the tension water storage variation and aquifer condition proposed by Nirupama et al. (1996), were adapted in this study as well.

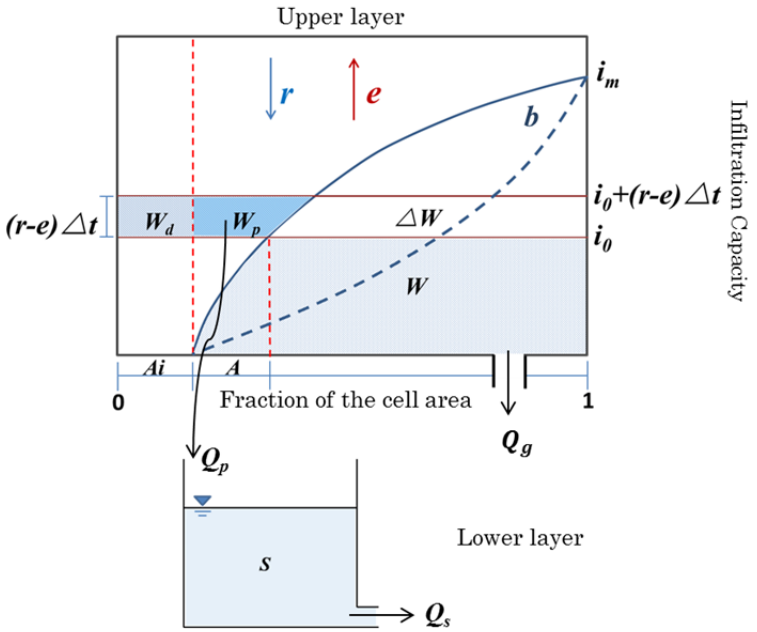

Figure 2.4-2 The distribution of runoff and infiltration as a function of grid wetness and infiltration capacity.

Based on assumption that infiltration capacities over the study area vary due to variations in topography, soil, and land cover (refer to **Figure 2.4-2**), the infiltration capacity i over an area can be represented as the following equation,

$$i = \begin{cases} 0 & if\ 0 \le A \le A_i \\ i_m \left[1 - \left(1 - \frac{A - A_i}{1 - A_i}\right)^{1/b}\right] & if\ A_i \le A \le 1 \end{cases} \quad (2\text{-}1)$$

where i_m represents the maximum infiltration capacity, A is the fraction of the cell area takes values between 0 and 1, A_i is the portion of direct runoff generation areas in the cell, and b is an empirical parameter showing a shape of the storage water capacity curve.

By integrating the function of the infiltration capacity i (**Eq.2-1**) from A_i to 1, the maximum tension water storage of the cell W_m can be expressed as

$$W_m = \frac{i_m}{1+b}(1 - A_i) \tag{2-2}$$

From **Eq.2-1**, the area fraction *A* can be written as

$$A = 1 - (1 - A_i)\left(1 - \frac{i}{i_m}\right)^b \tag{2-3}$$

Therefore, the current soil moisture *W* corresponding to initial infiltration capacity i_0 is obtained by the following derivation.

$$W = i_o \times 1.0 - \int_0^{i_0} A di \tag{2-4a}$$

$$W = W_m\left\{1 - \left(1 - \frac{i_0}{i_m}\right)^{b+1}\right\} \tag{2-4b}$$

According to **Figure 2.4-2**, during the precipitation event, rainfall *r* and potential evapotranspiration *e* are taken as input to the model. From the runoff generation area, the direct runoff depth W_d is generated which is shown as

$$W_d = Q_d \Delta t = A_i(r - e)\Delta t \tag{2-5}$$

where Δt is time interval. From the previous area, surface runoff depth W_p is calculated by using the following relationships;

Case 1: If $i_m \leq i_0 + (r - e)\Delta t$ (i.e., severe rainfall occurs and/or soil is saturated)

$$W_p = (r - e)(1 - A_i)\Delta t - W_m + W \tag{2-6a}$$

Case 2: If $i_m > i_0 + (r - e)\Delta$t(i.e., normal rainfall occurs and/or soil is unsaturated)

$$W_p = (r - e)(1 - A_i)\Delta t - W_m + W + W_m\left(1 - \frac{i_0 + (\mathrm{r-e})\Delta \mathrm{t}}{i_m}\right)^{1+b} \tag{2-6b}$$

To avoid confusion of the parameters unit, the runoff depth which is generated by the upper layer (refer to **Figure 2.4-2)**, are conversed to millimeter per hour by

$$Qd = \frac{W_d}{\Delta t} \tag{2-7a}$$

$$Qp = \frac{W_p}{\Delta t} \tag{2-7b}$$

where Q_d is the direct runoff generated in the runoff generation area (impervious area), and Q_p is the surface runoff provided by the infiltration capacity concept in previous area.

As show in **Figure 2.4-2**, due to the shallow aquifer underneath in some part of the CPRB (Dept. of Groundwater Resources, 2012), I included the effect of the groundwater component into the upper layer of the model to separate some amount of infiltrated water for recharging to the shallow aquifer. The soil water storage contributes to the groundwater Q_g expressed as the function of a non-linear reservoir relationship. The equation presents as

$$\mathrm{s} = k_g {Q_g}^{p_g} \tag{2-8a}$$

$$Q_g = \left(\frac{W}{k_g}\right)^{1/p_g} \tag{2-8b}$$

where k_g is the groundwater coefficient (hr) and p_g is the empirical parameter of aquifer storage. Thus, the updated soil moisture W is determined according to the water balance in the upper layer of the model by the following equation,

$$W_{(t+\Delta t)} = W_t + (r - e)\Delta t - W_p - Q_g \Delta t \tag{2-9}$$

Remark that the values W vary between 0 to W_m. By referring to **Eq. 2-4b**, the W is a

function of i_0. Hence, the values i_0 can solved as well.

The surface runoff Q_p infiltrates to be inputs of the subsurface runoff (base flow) component of the model as shown in the **Figure 2.4-2** (lower layer). The subsurface runoff component of the model is approximated by a relationship of a non-linear reservoir and continuity equation conveyed by

$$\frac{ds}{dt} = Q_p - Q_s \tag{2-10}$$

and $$s = k_s Q_s^{p_s} \tag{2-11a}$$

$$Qs = \left(\frac{S}{k_s}\right)^{1/p_s} \tag{2-11b}$$

where Q_s represents the subsurface runoff, s is the subsurface storage, k_s is the subsurface coefficient (hr), p_s is the empirical parameter of subsurface storage. Then the storage of each time step is calculated by the combination of **Eq.2-10**, **Eq.2-11a** and **Eg.2-11b** shown as

$$s_{(t+\Delta t)} = \left[\bar{Q}_p + \frac{s_{(t)}}{\Delta t} - \left(\frac{s_{(t)}}{k_s}\right)^{1/p_s}\right]\Delta t \tag{2-12}$$

where $\bar{Q}_p$ is the mean value of Q_p. This equation can be solved by using the Runge-Kutta method and fourth-order method was selected to avoid the numerical errors. Finally, Total runoff Q produced for a cell is obtained as

$$Q = Q_d + Q_p \tag{2-13}$$

The simplified Xinanjiang model has seven parameters in total, A_i, W_m, b, k_s, k_g, p_s, and p_g. They were identified in the process of model calibration. The model was applied for the CPRB at the 1/4 degree resolution and the model represents about 560 (20 columns

and 28 rows) computational grid cells covering the basin, and 1-hr time step of the calculation. Hereafter, I would refer to the simplified Xinanjiang Model as the SXAJ model. The outputs from the SXAJ model obtained as total discharge depth (millimeter per hour) at each computational grid cell were used as inputs to a flow routing model. The outputs from the SXAJ model, total discharge obtained as depth (millimeter per hour) at each particular computational grid cell, and they are used as inputs to a flow routing model.

2.4.2 Flow routing model

Generally, excess rainfall is easily routed by lumped approaches, such as the unit hydrograph, flow isochrones or linear reservoir modeling in computational of overland flow and channel flow, but it is difficult to represent land cover and topography as spatially distributed on a basin scale (Liu et al., 2009). Hence, the 1-km distributed flow routing model, 1K-FRM, was chosen for routing in this study (Tachikawa et al. 2011).

There are two parts inside the model, catchment model and flow model. A digital elevation model, DEM, was applied for the catchment model. The 8-direction method, used to define the flow direction of the catchment, assumes the flow direction 1-dimensionally to steepest downward slope to an immediately neighboring cell as illustrated in **Figure 2.4-3**. The topographic data used in the 1K-FRM were the 30 arc-second DEM and flow direction stored in HydroSHED (USGS, 2011).

The flow model is based on the one-dimensional kinematic wave model. According to the flow direction shown in **Figure 2.4-3**, each cell has a routing order from upstream to downstream. Then runoff generated by the SXAJ model becomes river discharge. The one-dimension kinematic wave equation for each cell is given by

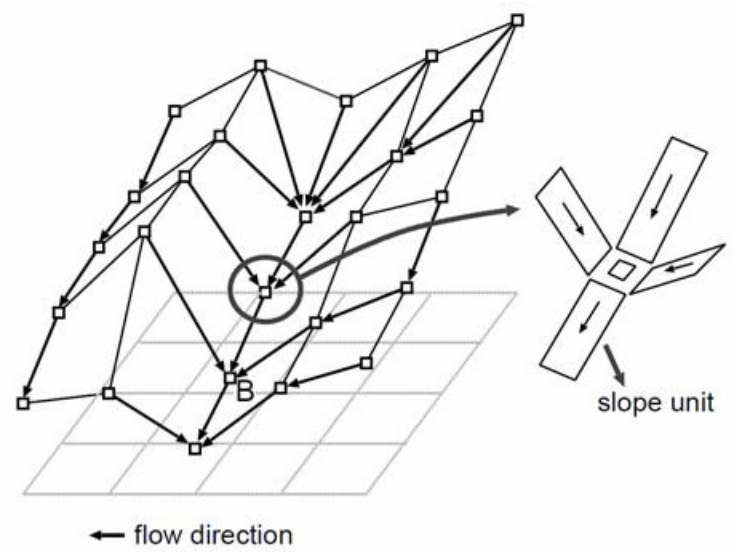

Figure 2.4-3 Schematic diagram of a catchment model using DEMs.

$$\frac{\partial A}{\partial t} + \frac{\partial Q}{\partial x} = q(t) \tag{2-14}$$

where *t* is time, *x* is the distance from the top of the rectangular grid, *A* is cross section area on the regular grid, *Q* is discharge, and *q(t)* is the lateral inflow per unit length of channel unit given as runoff generated by the SXAJ model. The Manning relation type of the discharge and cross-sectional area was joined with the continuity equation to route the water for each cell. There are two types of the cross sections used in this study, rectangular and quadratic shapes. The relationship of the discharge to the cross section area is given as follows;

$$Q = \alpha A^m \tag{2-15}$$

For a rectangular cross-section shape (m = 1.67), and a quadratic function shape ($y = \alpha x^2$) (m = 1.44), respectively;

$$\alpha = \frac{\sqrt{g_0}}{n}\left(\frac{1}{B}\right)^{m-1} \tag{2-16a), and}$$

$$\alpha = \frac{\sqrt{g_0}}{n}\left(\frac{a}{6}\right)^{2/9} \quad \text{(2-16b)}$$

where g_0 is slope; s slope; n is the manning roughness coefficient; B is the width of flow; and a is cross-section parameter. The quadratic function was applied to flooded area where cross-section of the river was accordingly changed with the over bank flow. The criterion to distinguish the type of the cross section is set by the number of upstream grids. When the number is larger than 35,000 (about 35,000 km^2) the quadratic cross section is adopted for representing the inundated areas. The 1K-FRM parameters are *n, B* and *a*. In this study, I used the values of *n* and *B* same as the original model, n = 0.03 m$^{-1/3}$s and 11.0 m$^{-1/3}$s for channel and slope flow, respectively. The value of B is equal to $1.06C^{0.69}$; where C is catchment area at the points. These two values were determined and used in the Japanese catchment (Tachikawa et al., 2011). To reproduce the inundation phenomena of the flood 2011 in Thailand, I assumed the quadratic cross section shape. The cross section parameter a was set to 0.00012 to reproduce a flood discharge properly.

2.4.3 Dam operation model

As mention in the study area, flow in the Chao Phraya River was significantly influenced by the dams operation. Therefore, dam operation model was embedded into some particular grids of 1K-FRM where the dams locate. An algorithm to develop a general reservoir operating rules was a flexible function that can be adjusted for different dam features.

The kinds of information, which were required for input to the dam operation model,

are spillway capacity, downstream requirement, active storage, min/max storage, and upper/lower rule curves. The monthly operation basis of the dam model was to store water in wet season (May-December) and to release water in dry season (January-April).

Figure 2.4-4 is a flowchart depicting algorithms of the dam operation model. I obtained actual BB and SK dam operation data to develop an algorithm of operating rules based on actual 2011 data. There are two steps in the monthly operating rule basis. First, water released in the dry season (January-April) was determined by a minimum reservoir storage and downstream requirement. The downstream requirements were derived from actual data equal to 200 m^3/s for BB Dam and 250 m^3/s for SK Dam. Second, water released in the wet season (May-December) was determined by a min/max reservoir storage and spillway capacity. I found from the actual data that when reservoir storage was lower than maximum storage, both dams still released water approximately 15% and 30% of natural inflow to maintain downstream flow. Because storage capacity was limited, dams have to fully release water when storage reaches the maximum limit.

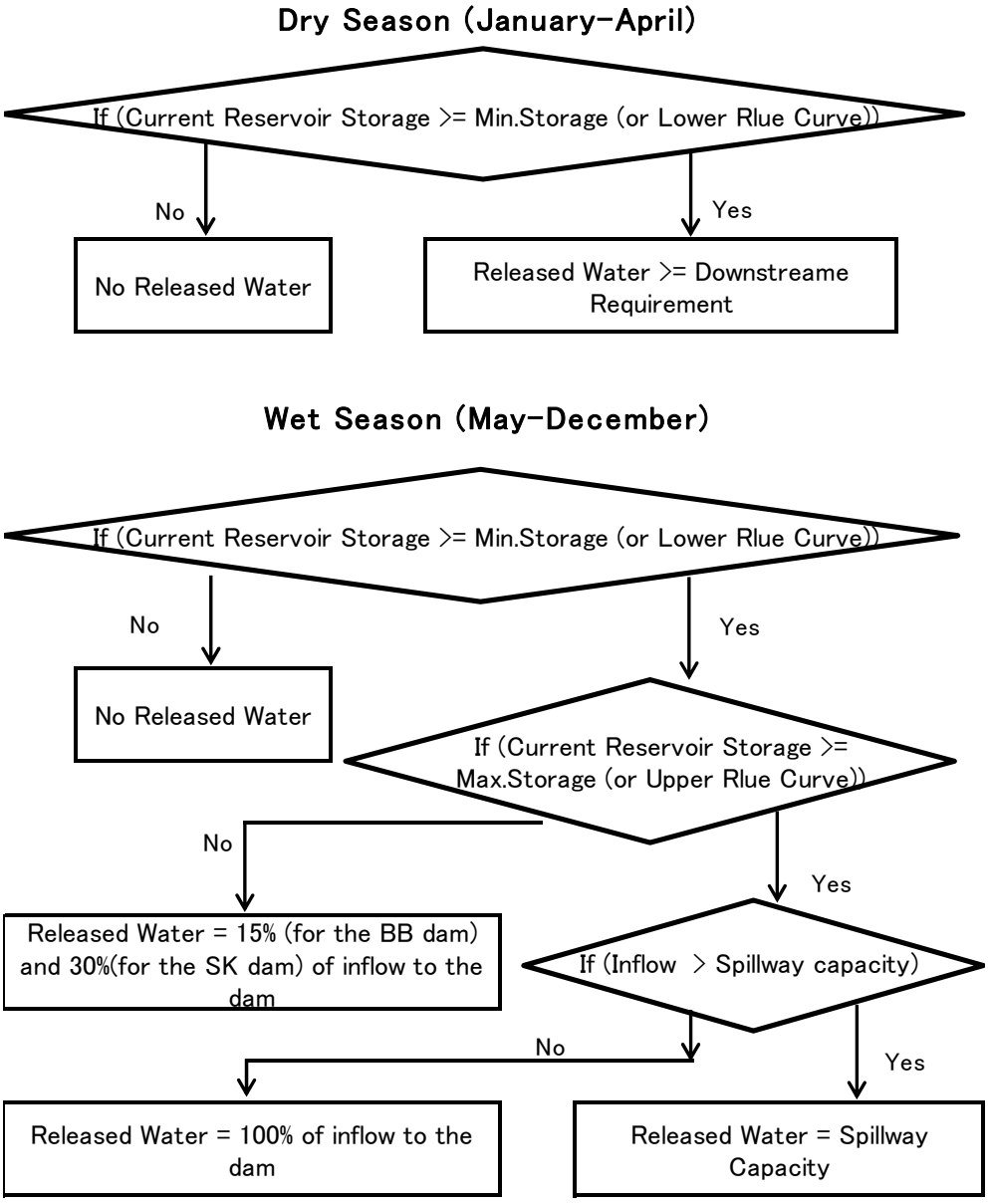

Figure 2.4-4 Flow chart of dam operating model algorithms.

2.5 Parameters identification

The SXAJ model have seven parameters, i.e., the shape parameter of the soil water storage curve b, the groundwater parameter k_g, the base flow parameter k_s, the parameter of groundwater storage p_g, the parameter of sub-surface storage p_s, the maximum soil

moisture storage W_m, and the fraction of the impervious area A_i; to be calibrated for each computational grid in the basin. According to the CPRB size (large), its non-homogenous geological, and its topographic characteristics, the best combination of the model parameter was estimated using the observed discharge data of the year 2011 at the C.2 station, Bhumibol dam and Sirikit dam. Also the observed data of year 1995 2008 and 2010 at those points was compared with the simulated discharge to verify the model parameters.

I, therefore, separated the set of parameters to three sets depended on the topographic and geologic conditions. The first set of parameters was applied to the lower part of the Yom and Nan River, the second set was proposed to the Ping River basin, and the last set was used for remaining areas over the CPRB.

To identify the parameters, the trial-and-error method and the following procedures were conducted for the model calibration in this paper: (a) setting initial values of the parameters by referring to the study of Nirupama et al. (1996) on the Ping River bas $0 < b \leq 1.5,\ 50 \leq W_m \leq 400, 100 \leq k_s \leq 300, 100 \leq k_g \leq 1000,\ 0.3 < p_s and\ p_g \leq 0.6, and\ 0 \leq Ai \leq 0$, (b) comparing simulated and observed discharge, (c) adopting a coarse step-size and then a finer step-size to identify the range of probable parameters and refine values, respectively.

The optimized SXAJ model parameters are given in **Table 2.5-1**. In the SXAJ model, a relationship between the k_g value and the effect of groundwater was not in direct proportion (**Eq. 2-8**). Consequently, the high values of k_g were obtained in the general grids and Ping River basin resulted from a lesser effect of shallow groundwater in those areas. With these sets of parameters, the SXAJ model generated runoff as an input for

the routing model, and initial condition of the routing model was set accordingly to the observed discharge.

The comparisons of simulated and observed discharge at the Bhumibol dam, Sirikit dam, and C.2 Station are respectively illustrated in **Figures 2.5-1 and 2.5-2** for the model calibration and **Figure 2.5-3** for the model verification. The model was calibrated by maximizing the Nash-Sutcliffe efficiency (NSE) of the daily discharge, and some error indicators, coefficient of determination R^2, and root mean square error RMSE, were used to justify the model performance. The summary of the model performance indicators of the calibration and verification stages are given in the **Table 2.5-2**.

Table 2.5-1 The SXAJ model parameters

Parameters	**General grids**	**Lower Yom & Nan River Basin**	**Ping River Basin**
Ai (-)	0.35	0	0.30
W_m (mm)	350	1500	400
b (-)	1.5	0.2	1.5
k_s ($hr^{0.6}mm^{0.4}$)	150	400	200
k_g ($hr^{0.6}mm^{0.4}$)	1500	40	1500
p_s (-)	0.6	0.6	0.5
p_g (-)	0.6	0.6	0.6

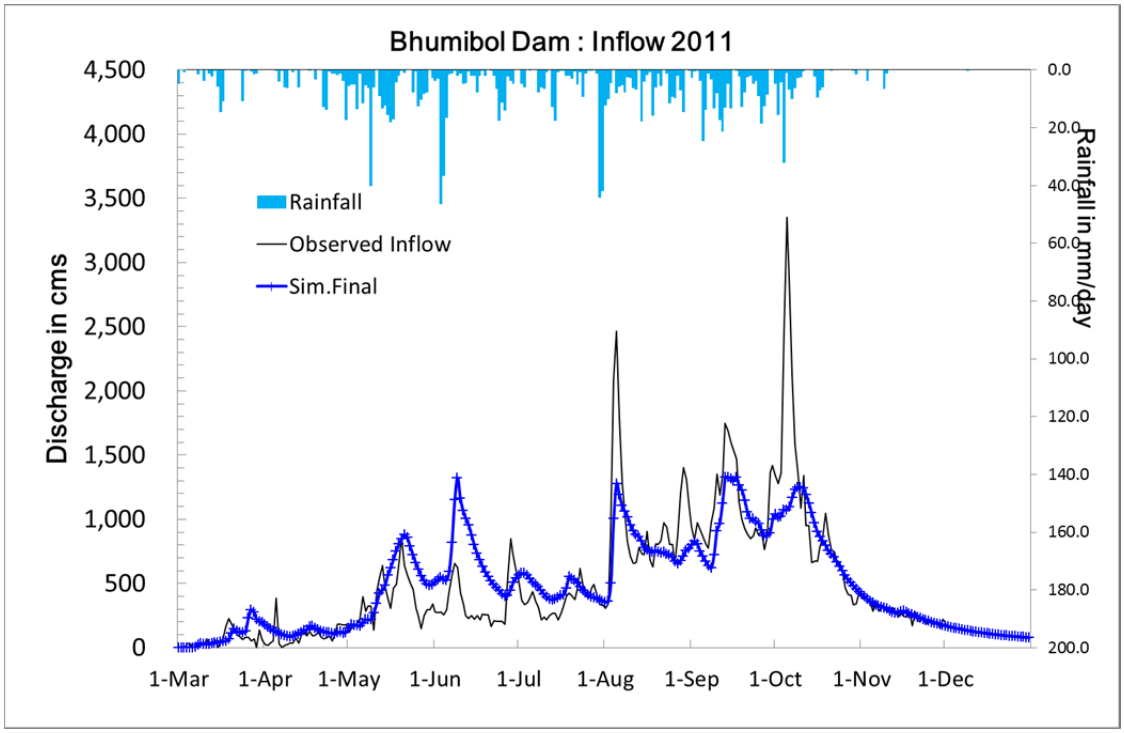

Figure 2.5-1 Comparison of discharge at the Bhumibol dam for the model calibration, 2011.

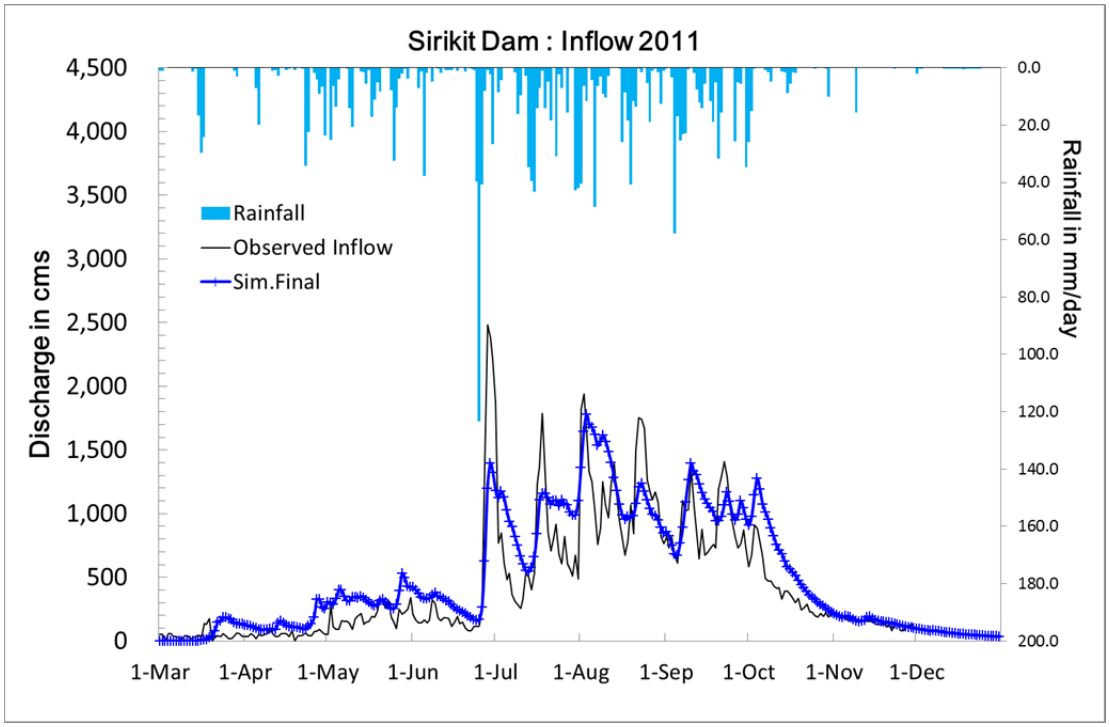

Figure 2.5-2 Comparison of discharge at the Sirikit dam for the model calibration, 2011.

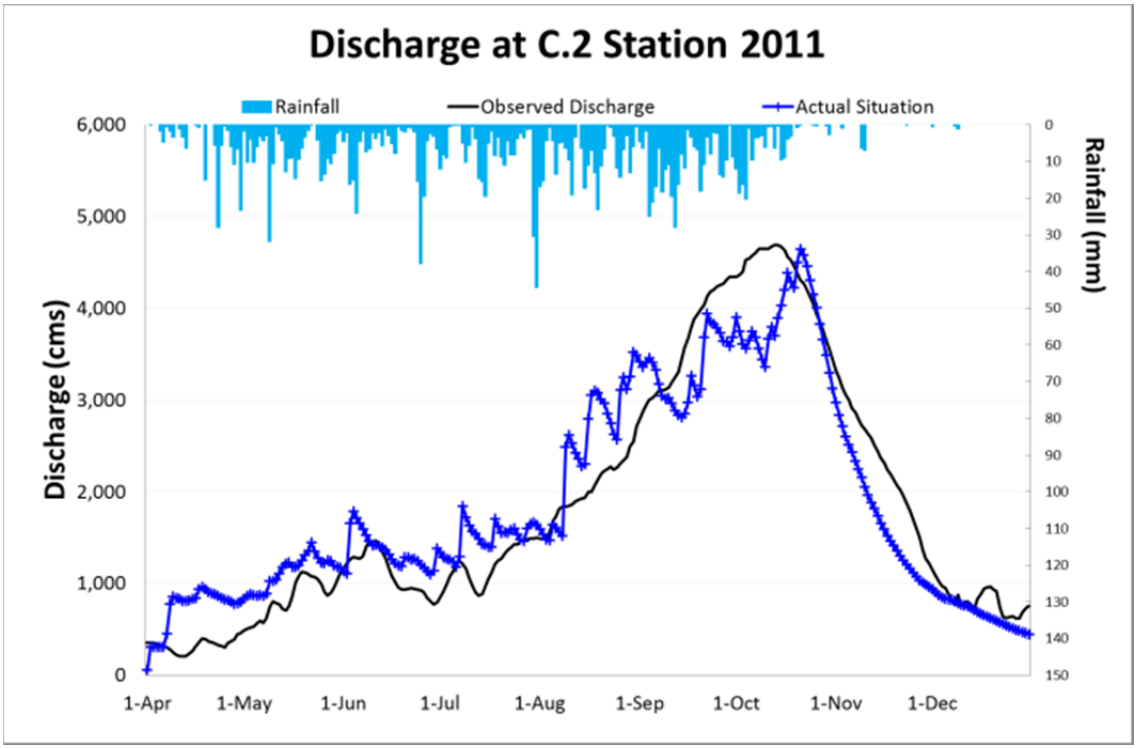

Figure 2.5-3 Comparison of discharge at the C.2 station for the model calibration, 2011.

Table 2.5-2 Summary of model performance indicators

Period		Statistical criterion	Location		
			BB Dam	SK Dam	C.2
Calibration	2011	NSE	0.62	0.71	0.87
		RMSE (m^3/s)	310.61	265.16	498.53
		R^2	0.63	0.75	0.87
Verification	2010	NSE	-0.28	0.47	0.49
		RMSE (m^3/s)	397.42	247.75	562.9
		R^2	0.56	0.77	0.85
	2008	NSE	0.2	0.75	0.55
		RMSE (m^3/s)	217.34	138.07	396.64
		R^2	0.75	0.77	0.6
	1995	NSE	0.53	0.68	0.7
		RMSE (m^3/s)	192.46	295.41	663.97
		R^2	0.67	0.71	0.77

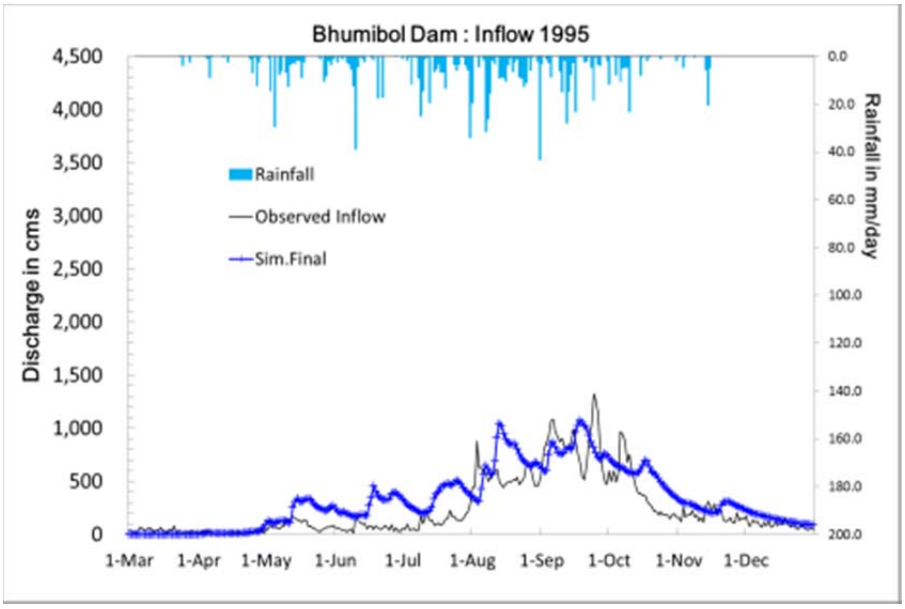

Figure 2.5-4 Comparisons of discharge at the Bhumibol dam for model verification, 1995.

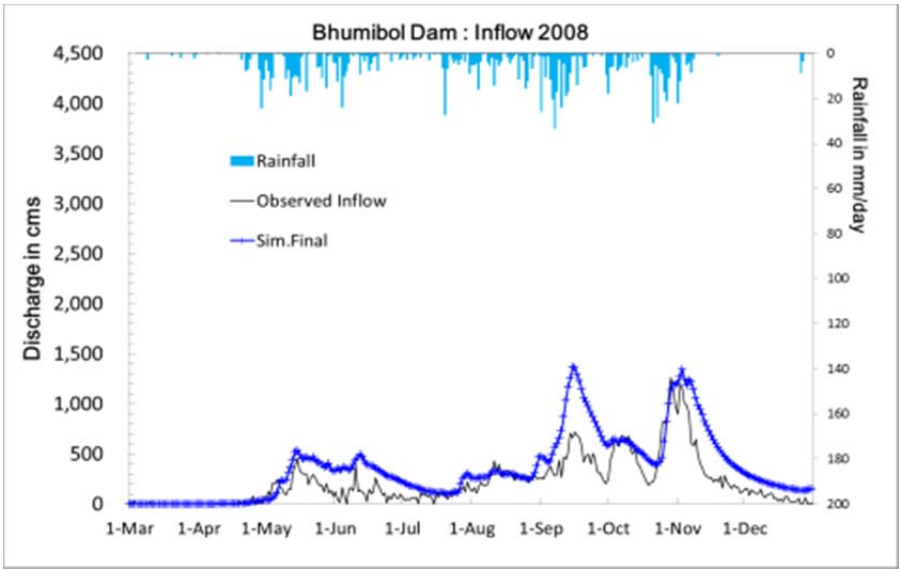

Figure 2.5-5 Comparisons of discharge at the Bhumibol dam for model verification, 2008.

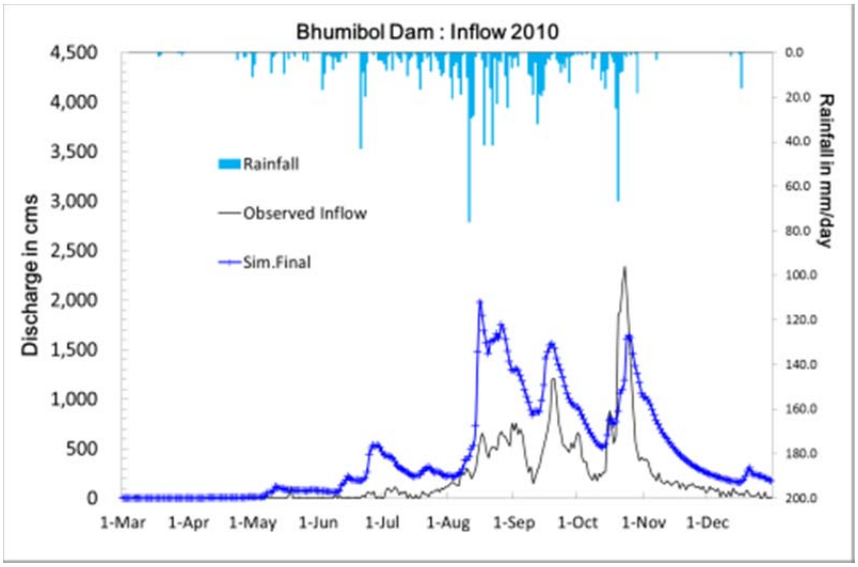

Figure 2.5-6 Comparisons of discharge at the Bhumibol dam for model verification, 2010.

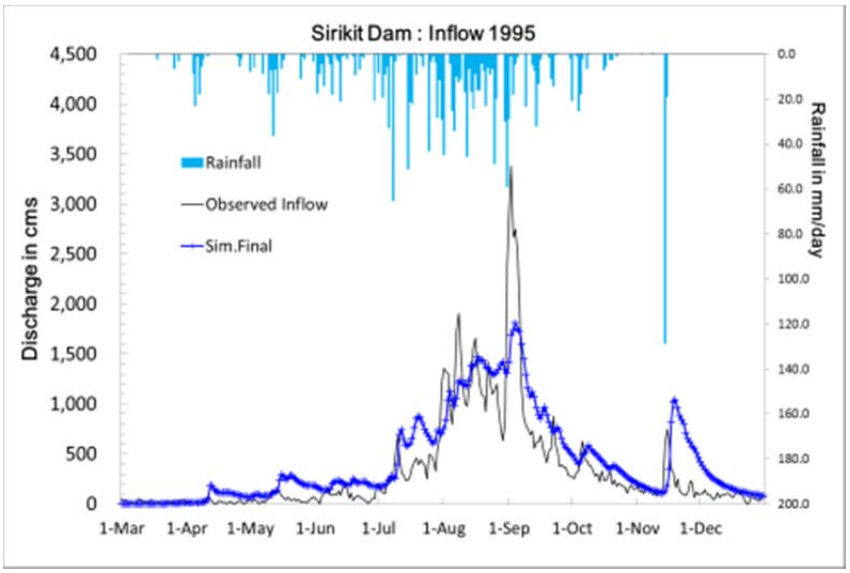

Figure 2.5-7 Comparisons of discharge at the Sirikit dam for model verification, 1995**.**

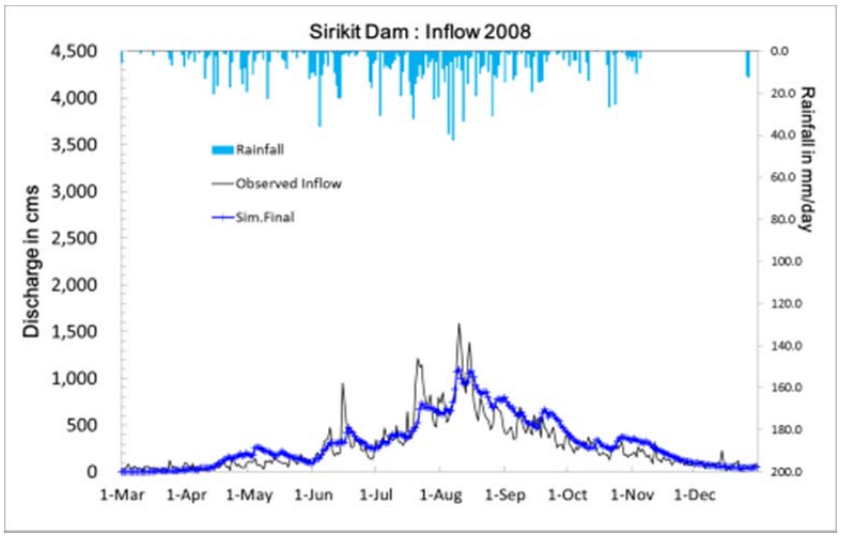

Figure 2.5-8 Comparisons of discharge at the Sirikit dam for model verification, 2008.

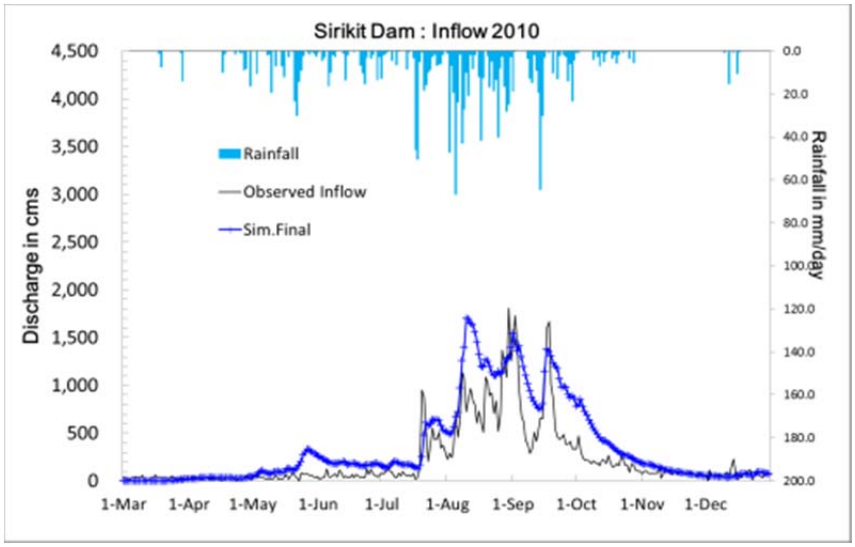

Figure 2.5-9 Comparisons of discharge at the Sirikit dam for model verification, 2010.

2.6 Model application

2.6.1 The effect of the Bhumibol and Sirikit dam

The Bhumibol (BB) dam was built in 1964 with the capacity 13,420 billion m^3 and the spillway capacity 6,000 m^3/s for the multi-purposes of water resources management in the Ping River basin. Afterwards, in 1974 the Sirikit (SK) dam was built with the capacity 9,510 billion m^3 and the spillway capacity 3,250 m^3/s for the multi-purposes in the Nan River basin. The catchment areas of the BB and SK dams are 26,400 $km^3$and 13,130 km^3 respectively. In the simulation shown in **Figure 2.6-1**, the dam operation of two dams was embedded into the 1K-FRM according to the actual operation data to the 1K-FRM with the condition of releasing water 200 m^3/s and 250 m^3/s during January-April and 15% and 30% of natural inflow during May-December for BB Dam and SK Dam, respectively. This condition was aimed to approach the best match of the real situation of the dams operation in year 2011. The comparisons between simulated and observed reservoir storage of those two dams are shown in **Figures 2.6-1** and **2.6-2**.

To assess the effect of dams on the flood 2011, I have done the simulation of the year 2011 by using the runoff input generated by the SXAJ model to the 1K-FRM without considering the dam operation model, as illustrated in **Figure 2.6-3**. The result shows the volume of simulated hydrograph without two dams was 54,812 million m^3, which was as much as a 23% increase when compared to the actual situation, focusing at the C.2 station during April-December 2011. Moreover, the dams facilitate water storage during the early stage of the flooding period by decreasing 15% of the peak discharge compared to the value obtained with no dams.

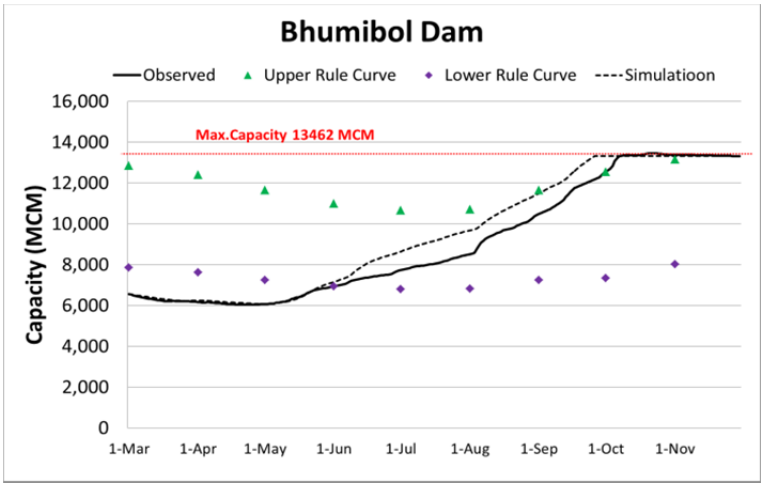

Figure 2.6-1 Reservoir capacity of the Bhumibol dam, March-November.

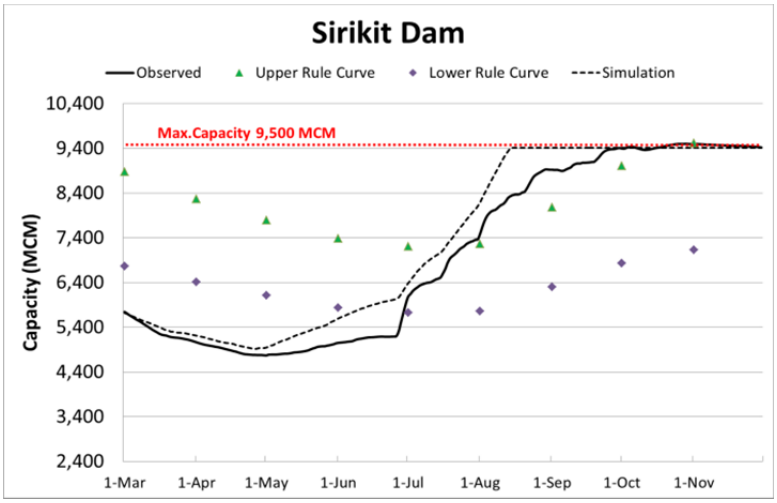

Figure 2.6-2 Reservoir capacity of the Sirikit dam, March-Novovember.

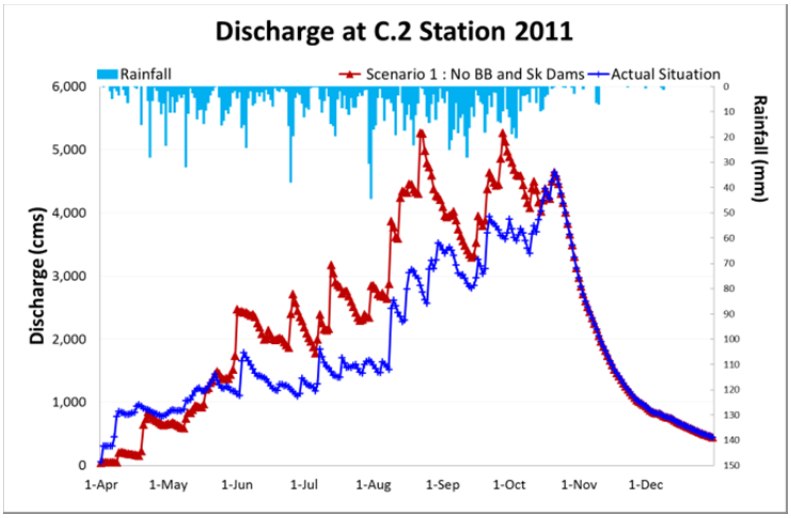

Figure 2.6-3 Comparison of simulated discharge between actual situation, and without the BB and SK dams at C.2 station.

2.6.2 The effect of proposed dam construction on the Yom River

Tentatively, the government of Thailand has proposed to develop one more dam named Kang Sue Ten (KST) dam in the Yom River basin to relieve water resources problems. The catchment area of the KST dam is 3,538 km^2. The active storage is 1,125 million m^3, and the spillway capacity is 5,355 m^3/s. In this study, I consider the dam for flood protection purpose only. The operation condition of this dam was made by optimizing the historical discharge data of 19 years (1992-2010) at Y.20 station to figure out the suitable downstream release flow. Dam operation conditions of the KST dam are releasing water 40 m^3/s during January-April and 40% of natural inflow during May-December. I assumed that what would happen to the flood 2011 if the KST dam had already been built.

The results show that there was insignificant effect on the overall water resources situation in the CPRB. The volume of the hydrograph at the C.2 station only a 1.5 % decreases as shown in **Figure 2.6-4**. However, the KST has significant effect on the water resources situation of the Yom River basin by increasing in dry season flow and also reducing about 50% of peak discharge during the wet season as presented **Figure 2.6-5**.

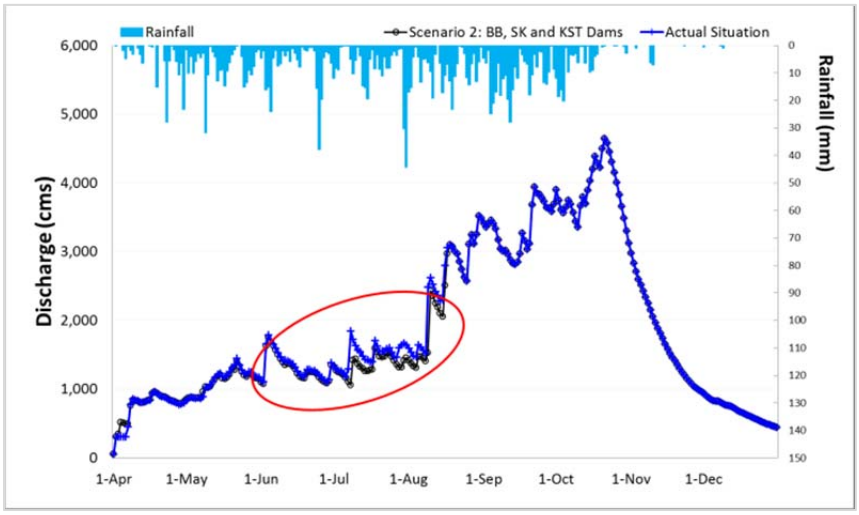

Figure 2.6-4 Comparison of simulated discharge between with and without the KST dam at C.2 Station.

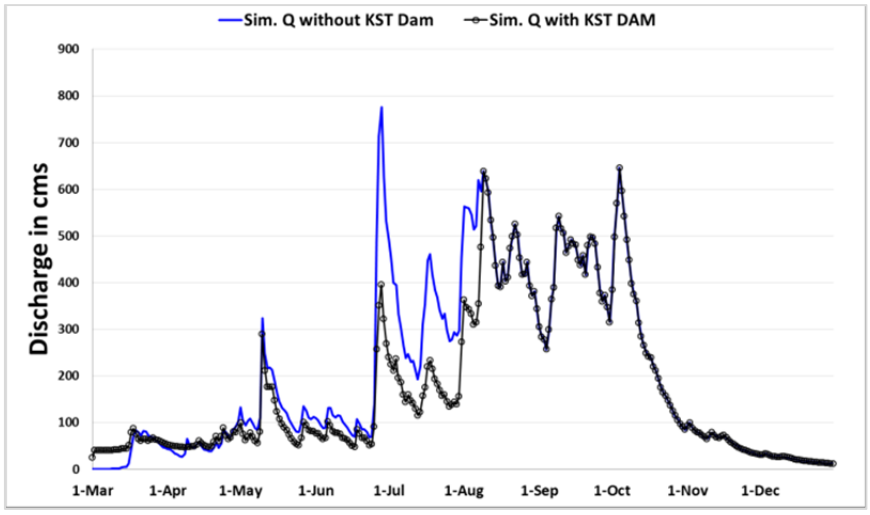

Figure 2.6-5 Comparison of the simulated discharge between with and without the KST dam at downstream of the dam.

2.7 Conclusion

In this study, I have successfully developed the regional distributed hydrological model associated with the dam operation model to reproduce the flood 2011 in the CPRB and to investigate the effect of dams to a water resources situation of the Chao Phraya River at C.2 station by using the model application.

The hydrological model was developed based on a concept of variable infiltration capacity including the effect of shallow groundwater. The model parameters were finalized into three sets of parameters depended on the topographic and geologic conditions of their location. Overall, the agreement between observed discharge and simulated discharge, and the water balance of simulated and observed hydrographs were satisfied by the NSE ranges from 0.62 to 0.87 and the R^2 ranges from 0.63 to 0.87 for the calibration period. This indicated that the SXAJ model and these sets of parameters were precise. As expected the NSE for the model validation is smaller than the model calibration. But the R^2 for the model validation, which ranges from 0.56 to 0.85, is almost the same range with the model calibration The dams in the upper part of the CPRB were proved that they are useful for the flood protection in the basin. However, it also depends on size of their reservoirs.

To modify the routing model, 1K-FRM, to reduce a fluctuation of the routed hydrograph by including inundation effect during high flow period, I will examine in the following chapter.

Chapter 3

Development of a flow routing model including inundation effect for the extreme flood in the Chao Phraya River Basin, Thailand 2011

3.1 Introduction

The flow routing model is an important tool for achieving all studies on the projection of the future situation of water resources. Specifically, after the extreme flooding in 2011, I realized that the flow routing process in the channel alone is not enough to reproduce phenomena of realistic river flow. The flood mark in a photo of the C.2 gauging station on the Chao Phraya River after a year of flooding **(Figure 3.1-1)** is one piece of evidence shows the occurrence of overbank flow. In this study, the effect of inundation was taken into account for developing a flow routing model which is the most important tool for further study of future situation under the changing climate of the CPRB.

Figure 3.1-1 Flood mark at maximum water level +26.88 m above sea level at the C.2 gauging station (October 2, 2012).

This paper focused on the development of the flow routing model by using the concept of a diffusive tank model to include the inundation effect to improve flood movement simulation of the extreme flood event of 2011.

3.2 Methodology

This chapter mainly is to include in inundation effect from overbank flow to the flow routing model. The hydrologic model was not modified; only the follow routing model was modified, so the model parameter was increased by the addition calculation part. Structure of modelling work process are illustrated in **Figure 3.2-1.**

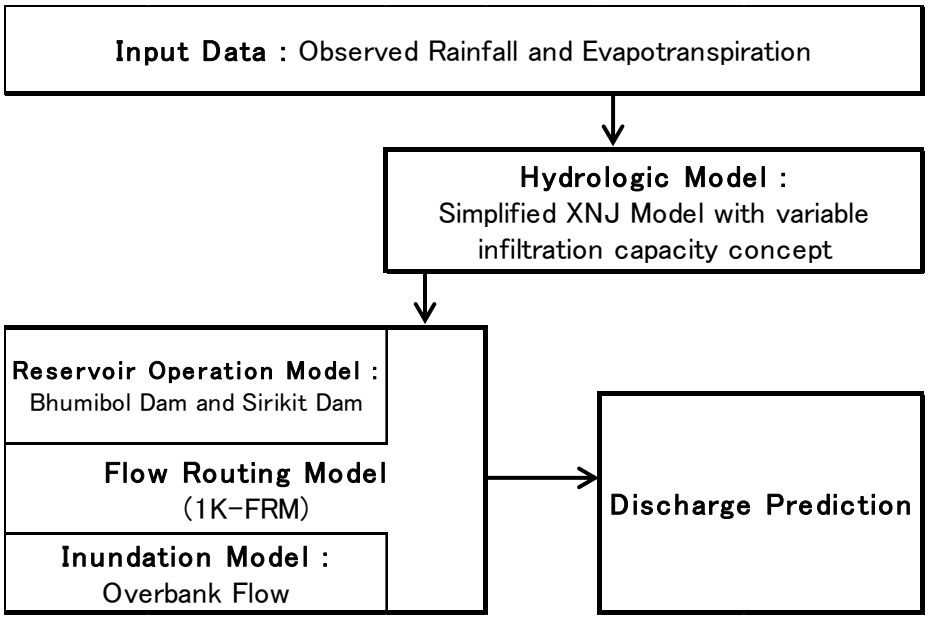

Figure 3.2-1 Framework of the distributed hydrological model including inundation model.

3.2.1 Flow routing model including inundation effect

For the purpose of including the effect of inundation in the 1K-FRM, I adopt the concept of the diffusive tank model (Moussa and Bocquillon, 2010) by considering the

drainage discrepancy between the main channel and floodplain ponds. Once the water height of the main channel exceeds bank height, water is drained into the adjacent floodplain, and then when the water height of floodplain ponds exceeds bank height and the water level in the main channel, water is drained back into the main channel. The cross-section of the main channel and floodplain is illustrated in **Figure 3.2-2**. To assemble the inundation model into the routing model, the kinematic wave equation (**Eq.3-1**) was modified as follows,

$$\frac{\partial A}{\partial t} + \frac{\partial Q}{\partial x} = q(t) - q_{li}(t) \tag{3-1}$$

where q_{li} is lateral overbank flow per unit width solved by this inundation model.

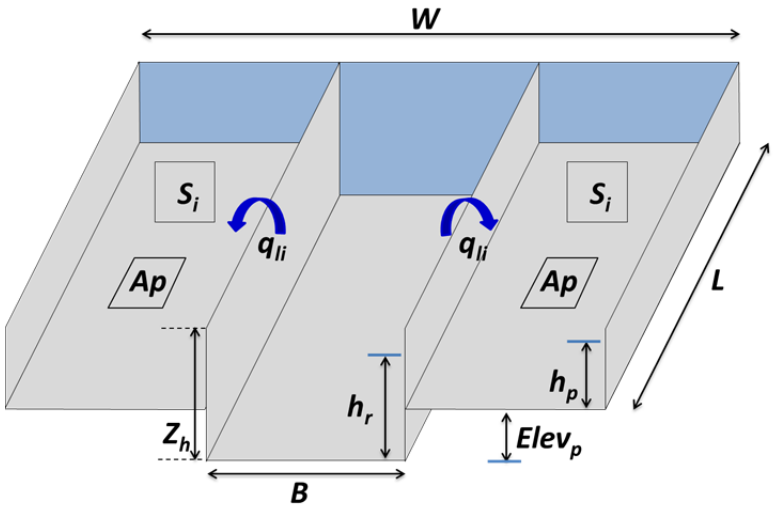

Figure 3.2-2 Sketch of a river channel and a floodplain pond defined for each computational grid. (Z_h is bank height, B is river width, h_r is water height in the river, S_i is storage volume of the floodplain pond, h_p is water height in the floodplain pond, W is floodplain width, $Elev_p$ is floodplain pond elevation, and A_p is surface area of the floodplain pond.)

The water balance of a floodplain pond is given as

$$\frac{dS_i}{dt} = Q_{li} - Loss \tag{3-2}$$

where S_i is the floodplain pond storage volume, Q_{li} is total lateral overbank flow, and *Loss* is pond-water loss due to evaporation and infiltration. Exchange lateral overbank flow between the channel and floodplain area is modeled using a broad crested weir equation for a clear overflow weir, expressed as

$$Q_{li} = C_{b-f} L(\Delta h)\sqrt{2g(\Delta h)} \tag{3-3a) or}$$

$$q_{li} = C_{b-f}(\Delta h)\sqrt{2g(\Delta h)} \tag{3-4b}$$

where C_{b-f} represents a constant value, Δh is the difference in head or water depth exceeding the bank, L is the channel length, and g is gravity (9.81 m/s^2). C_{b-f} and Δh depend on flow characteristics and shape. According to the value of Δh indicating the lateral flow direction, the lateral inflow can be either positive or negative. To calculate water height in the floodplain pond h_p, I set datum at the river bed and identify a suitable elevation for floodplain pond $Elev_p$. As mentioned above, **Eq.3-4b** is suitable for flows over the weir (river bank), so to determine the lateral flow of the recession process back to the channel (**Figure 3.2-3g**), I identified lateral flow q_{li} by modifying a concept of Darcy's law as

$$q_{li} = C_g(\Delta h) \tag{3-5}$$

where C_g is the constant value of underground flow in m/s. Δh is identified separately for each overbank flow process during stages of rise, equilibrium, and recession, as demonstrated in **Figure 3.2-3**.

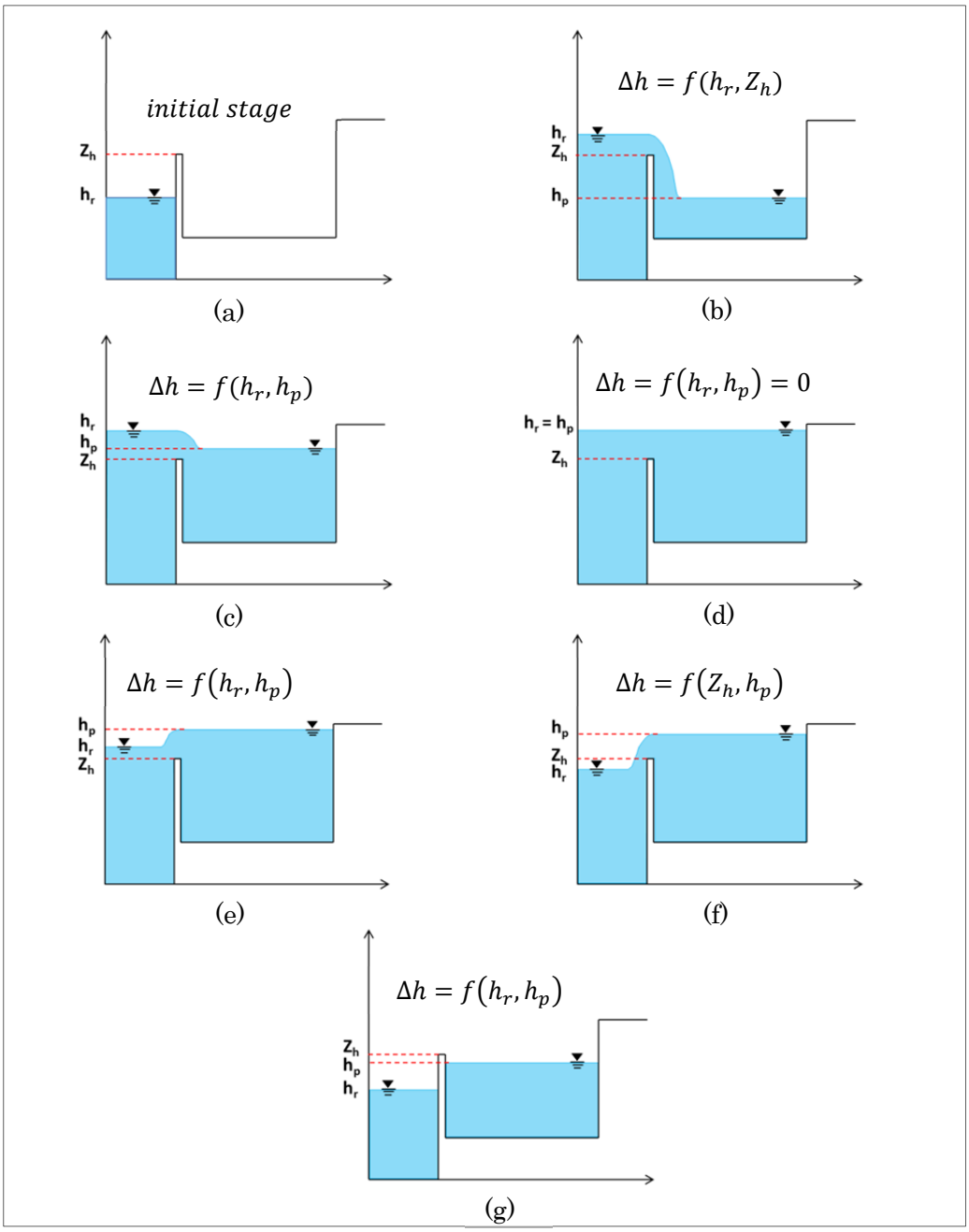

Figure 3.2-3 Overbank flow process during an initial stage (a), a rise stage (b and c), and equilibrium stage (d), and a recession stage (e f and g) in main river.

3.2.2 Model parameters

In this study, I identified model parameters of the 1K-FRM by comparing 2011 observed and simulated discharge at the C.2 station. The parameter for the 1K-FRM in the routing part was Manning's roughness coefficient n = 0.03 $m^{-1/3}s$ and 0.7 $m^{-1/3}s$ for channel and slope flows, respectively.

To improve the routing process, the inundation model was the main part that I developed based on the various parameters and variables listed in **Table 3.3-1**. There were ten model parameters, i.e., floodplain width *W,* floodplain elevation $Elev_p$, bank height Z_h, evaporation loss *Loss*, rise stage constants C_b and C_c, equilibrium stage constant C_d, recession stage constants C_e and C_f, and underground flow constant C_g. To set the initial value of *W*, I measured width from satellite imaging, i.e., about 50 km. I then used this value for simulation and gradually adjusted it until I obtained satisfactory results with respect to related parameters Z_h and $Elev_p$. Remarks: In the equilibrium stage($\Delta h = 0$) C_d does not reflect simulation results.

Table 3.2-1 Inundation model parameters and variables

Symbol	Name	Value
Parameters		
W	floodplain area width (unit: km)	100.0
$Elev_p$	flood plain pond elevation (unit: m)	2.5
Z_h	bank height (unit: m)	6.0
C_b	rise stage constant in **Figure 3.3-3b**	0.1
C_c	rise stage constant in **Figure 3.3-3c**	0.1
$C_{d,}$	equilibrium stage constant in **Figure 3.3-3d**	0.1
C_e	recession stage constant in **Figure 3.3-3e**	0.6
C_f	recession stage constant in **Figure 3.3-3f**	0.6
C_g	recession stage constant (underground flow) in **Figure 3.3-3g** (unit: m/s)	0.0022
Loss	loss due to evaporation and infiltration from water in pond (unit: mm/day)	8.0
Variables		
h_r	water height in river (unit: m)	
h_p	water height in floodplain pond (unit: m)	
S_i	storage volume of floodplain pond (unit: m^3)	
A_p	surface area of floodplain pond (unit: m^2)	

3.3 Result and discussion

To examine the applicability of the proposed method developed and embedded in the 1K-FRM, simulation was performed using input data obtained from the SXAJ model with model parameters listed in **Table 3.2-1**. Excess rainfall was then routed by the 1K-FRM, including the effects of dam release and inundation. Final results best fitting observed and simulated hydrographs are shown in **Figures 3.3-1, 3.3-2** and **3.3-3** for the BB and SK dams and the C.2 station, respectively. Because the BB and SK dams are located in the mountainous upper part of the CPRB (**Figure 2.3-1**), simulated flow was

not affected by the inundation effect. It is obvious that simulated inflow without considering the inundation effect was similar to the simulated inflow considering the inundation effect for both locations (**Figures 3.3-1** and **3.3-2)**. When data on simulated inflow including the inundation effect and observed inflow is analyzed, Nash-Sutcliffe efficiency (NSE) was 0.60 and 0.68, coefficient of determination (R^2) was 0.61 and 0.73, and root mean square error (RMSE) was 320 m^3/s and 275 m^3/s at the BB and SK dams, respectively. Peaks of both simulated inflows were significantly different from observed inflow, i.e., a 60% difference for the BB dam and a 20% difference for the SK dam. The water balance, however, agreed for both simulated and observed inflow.

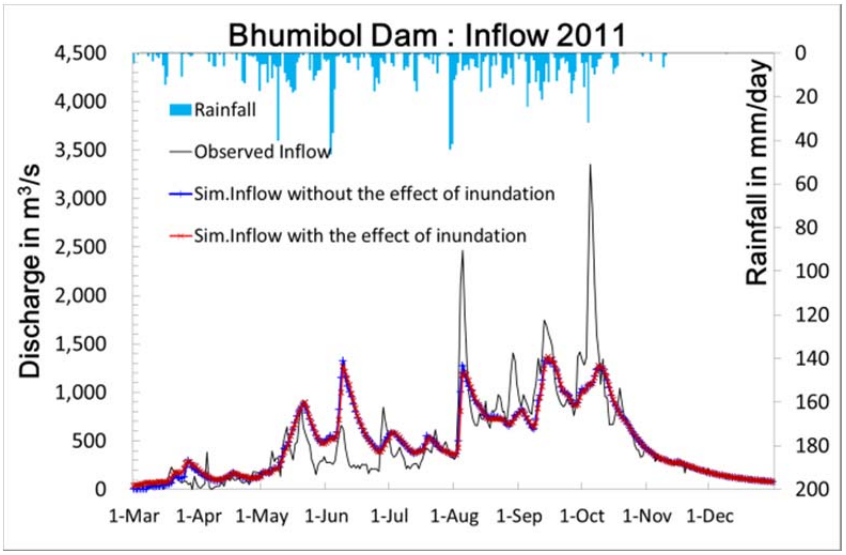

Figure 3.3-1 Comparison of inflow of Bhumibol dam for 2011 model parameter identification.

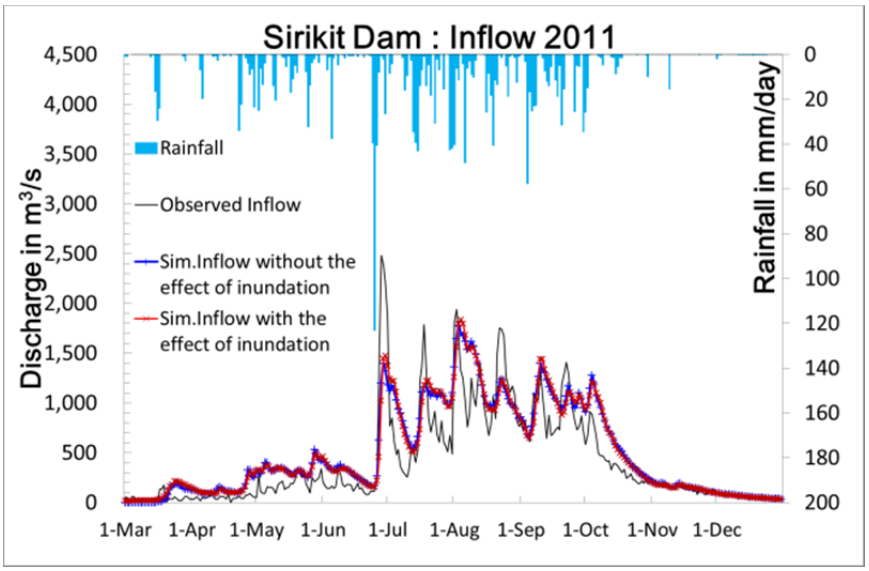

Figure 3.3-2 Comparison of inflow of Sirikit dam for 2011 model parameter identification.

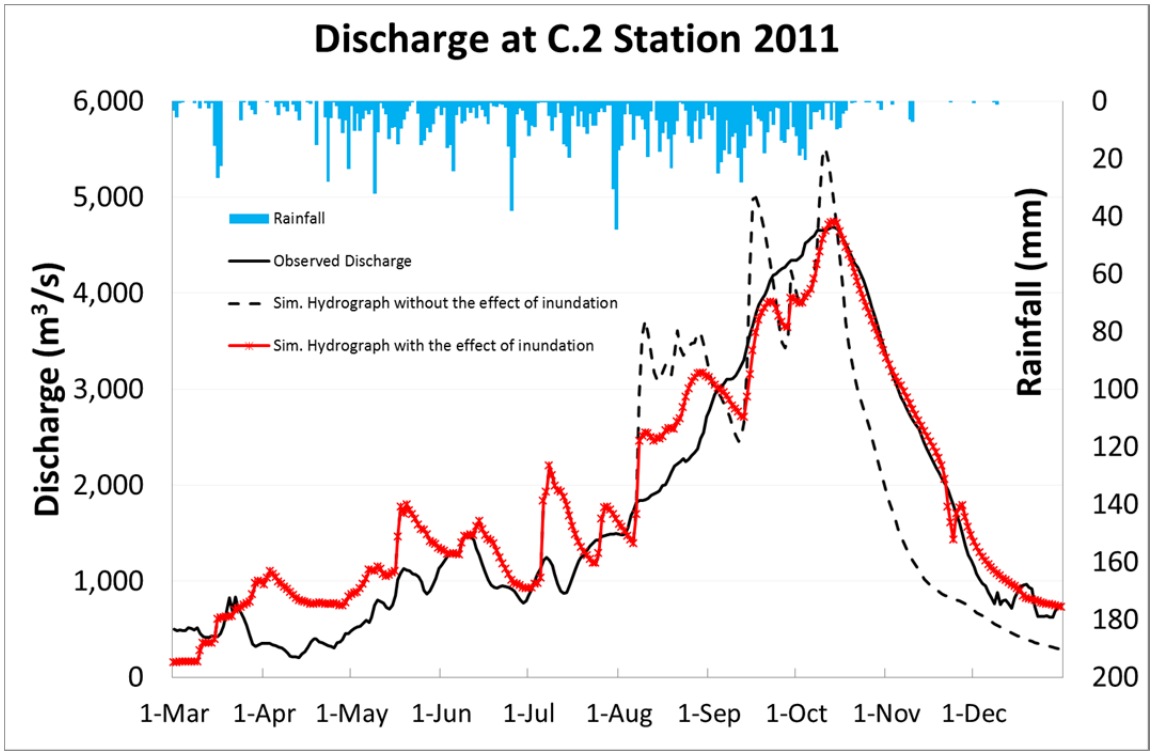

Figure 3.3-3 Comparisons of discharge at C.2 Station for the model parameter identification, 2011.

In the case of the C.2 station (**Figure 3.3-3**), values for the simulated hydrograph not considering the inundation effect were considerably different from values of observed

and simulated hydrographs that considered the inundation effect. Differences were in the hydrograph peak and shape during flooding period. The inundation effect influenced the flow regime significantly because the C.2 station is situated at downstream of the confluence of the Ping and Nan rivers, which were flooded at that time. A comparison of the observed hydrograph peak and shape to the simulated hydrograph peak and shape including the inundation effect showed altitudes of both hydrographs to have a good conformity. Agreement between observed and simulated discharge and simulated and observed hydrograph water balance were satisfied by NSE of 0.91, RMSE of 388 m^3/s, and R^2 of 0.94. Model simulation results at the C.2 station were more accurate than those at the BB and SK dams. Values of error indicators obtained in this study, however, were with in an acceptable range.

3.4 Conclusion

A flow routing model including the inundation effect has been developed to improve predicted discharge for the Chao Phraya River Basin. The Simplified Xinanjiang model based on the concept of the variable infiltration capacity was used for runoff generation. Flow routing was modeled using kinematic wave flow approximation including a reservoir operation model for the Bhumibol and Sirikit dams. I developed an inundation model and embedded it in the flow routing model. Overbank flow in the inundation model was estimated by a broad crested weir equation. The inundation model had ten parameters, which were manually identified by trial-and-error method based on experiences from the site investigation. Simulation has been done for 2011. Simulated discharge data was extracted and analyzed at three locations, i.e., the Bhumibol, Sirikit dams and the C.2 station.

Results have demonstrated that only river flow in downstream of the Ping and Nan River basins was influenced by the inundation effect. That is clearly shown by the similar shape of simulated hydrographs at the Bhumibol and Sirikit dams. The routing model including the inundation effect improved the simulated hydrograph at the C.2 station well. The volume of the simulated hydrograph was slightly larger (10%) than the volume of the observed hydrograph at the C.2 station.

Model performance was satisfactory with NSE of 0.60 for the Bhumibol dam, 0.69 for the Sirikit dam, and 0.91 for the C.2 station. The model still needs to be verified, however, for other extreme flood events in the Chao Phraya River Basin. By using this model, I plan to further study water resources projection and prediction under the changing climate conditions in the Chao Phraya River Basin.

Chapter 4

Prediction of water resources in the Chao Phraya River Basin, Thailand

4.1 Introduction

Climate change has an obvious impact on water resources. The magnitude and frequency of water related disasters, e.g. floods and droughts, are more likely to increase worldwide (Arora and Boer, 2001). Consequently, assessments and projections on the impacts of climate change are necessary. Several studied have been conducted around the world – for example, Aldous et al. (2011) evaluated climates change impacts and developing adaptation strategies in the western USA and south-eastern Australia. In China, Piao et al. (2010) reviewed the climate change impacts on water resources and agriculture and Yang et al. (2012) studied the impacts especially on flood and drought events in Huaihe River Basin. Potential impacts of climate change on heavy rainfall events, floods and droughts in the Australia were explored by Whetton et al. (1993). Olesen et al. (2007) considered uncertainties in projected impacts of climate change between 1961–1990 and 2071–2100 on European agriculture and terrestrial ecosystems based on scenarios from regional climate models. Also evaluation a change on discharge of large Asian rivers, including the Chao Phraya River, Thailand, was carried out by using the observation and model-based projections of discharge and the result shown that changes in river discharge extremes are particularly important (Kundzewicz et al., 2009).

In the second half year of 2011, Thailand has encountered with a devastating flood caused by continuous intense precipitation, occurred in the Chao Phraya River Basin (CPRB) in Thailand. The nation's economic system was severely disrupted, people lost their homes and lives were lost. From these situations it is realized that it is critical to assess the vulnerability of river systems and water-related disasters. This disaster

indicated that evaluation of the impacts of climate change by using a suitable hydrological model for a basin scale is critical. There are some studies related to the impact of climate change in the CPRB. Hunukumbura and Tachikawa (2012) projected future river discharge to detect hotspots in river discharges in the CPRB using MRI-AGCM3.1s. Duong et al., (2013) used runoff data generated by MRI-AGCM3.2S to project a change in river discharge in the Indochina Peninsula region. As a distributed hydrological model is an important tool for achieving the study of future situations of water resources, Wichakul et al. (2013b) developed a regional distributed hydrological model including a dam operation model and inundation effects for the CPRB and tested the model performance with the 2011flood and other historical extreme events.

This chapter is focused on projecting the impacts of climate change on the water resources situation of the CPRB, especially flow in the Chao Phraya River, by utilizing outputs of the latest 20 km spatial resolution general circulation model (MRI-AGCM3.2S) with the regional distributed hydrological model.

4.2 Global Circulation Model (GCM)

General Circulation Model (GCM) is the effective tool available today for well understanding of the interaction of the atmosphere, ocean, land surface, and ice for understanding of a changing climate behavior in long term. Nowadays, more than twenty GCMs have been developed in many research institutes around the world. The GCM, which exhibits excellent climate reproducibility is the one produced by the Meteorological Research Institute (MRI), Japan Meteorology Agency.

The first generation of MRI's atmospheric general circulation model (AGCM) is

MRI-GCM-I (Tokioka et al., 1984). This model was then coupled to a global ocean general circulation model (OGCM) to generate MRI's first-generation atmosphere-ocean coupled global climate model (MRI-GCM1). This MRI-GCM1 was used to study the global warming due to the gradual increase in the atmospheric concentration of greenhouse gases about 1%/year (Tokioka et al., 1995). In 2001, a new version of the MRI GCM, referred to as MRI-GCM2, was made to reduce the drawbacks of the former version (Yukimoto et al., 2001).The MRI-GCM3 was developed to improve the representation of regional-scale phenomena and local climate, by increasing horizontal resolution to be 20-km mesh by Mizuta et al. (2006). Mizuta et al. (2012) very slightly revised the previous model (MRI-AGCM3.1; Kitoh et al., 2009) by adding parameterization schemes for various physical processes and performed a present-day climate experiment using observed sea surface temperature. This lasted version of MRI GCM is MRI-AGCM3.2S. The model has a horizontal resolution of triangular truncation 959 (TL959), and the transform grid uses 1920 x 960 grid cells, corresponding to approximately a 20-km grid interval with 64 vertical layers (top at 0.01 hPa).

4.2.1 Precipitation data

Among the GCM output variables, PRECIPI, which is total precipitation above a canopy, mainly composes of rainfall reaching to soil layer (PRCSL) and snow melt water to soil layer (SN2SL). In case of a hydrological simulation in a tropical area such as Thailand, the SN2SL variable was neglected. Therefore, I used PRCSL without bias-correction as input rainfall to a distributed hydrological model for runoff generation. A primary unit of PRCSL was indicated as $kg/m^2/s$ in daily time step. It was

converted into hourly time step to correspond to calculation time step of the distributed hydrological model (SXAJ model).

4.2.2 Evapotranspiration data

To conduct a distributed hydrological model simulation, total evapotranspiration is ones of the input data. For the GCM output variables, the total evapotranspiration can be obtained from evaporation from bare soil (EVPSL) and transpiration from root zone soil (TRNSL). The summation of these two variables was input as total evapotranspiration into the model without bias correction. The unit of EVPSL and TRNSL is $kg/m^2/s$ in daily time step. I had to convert the unit into hourly time step to correspond to calculation time step of the distributed hydrological model (SXAJ model) as well. **Figure 4.2-1** shows a schematic of GCM variables that I obtained for the output of MRI-AGCM3.2S.

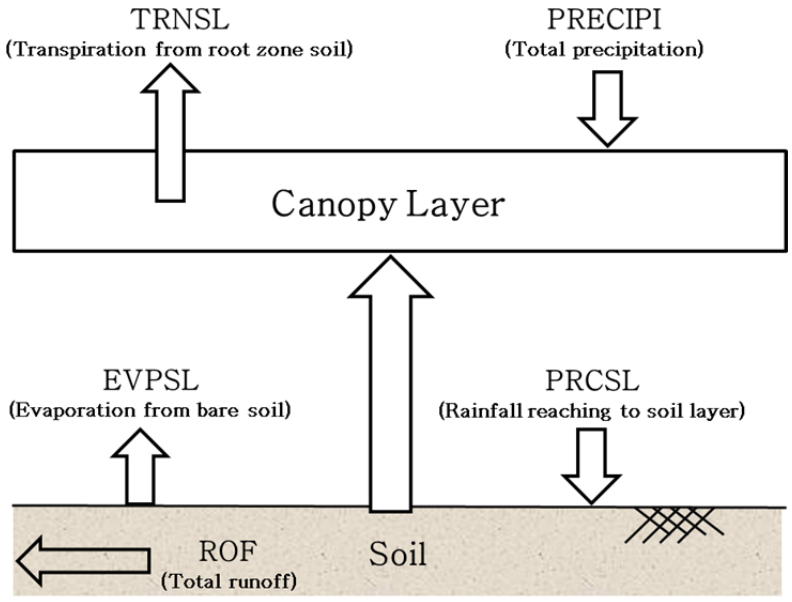

Figure 4.2-1 Schematic of obtained GCM output variables.

4.3 Methodology

I used gridded output data from the lasted version of a super-high-resolution general circulation model, MRI-AGCM3.2S (S means super-high resolution) for conducting a simulation. The products of MRI-AGCM3.2S represented the present climate experiment (1979–2008), the near future climate experiment (2015–2044), and the future climate experiment (2075–2104), which were simulated under a global warming A1B emission scenario of the SRES in the 2007 IPCC Fourth Assessment Report . I analyzed annual mean rainfall and evapotranspiration derived from GCM outputs, PRCSL (rainfall on the land surface), EVPSL (evaporation from bare soil) and TRSNL (transpiration) for three different climate experiments.

Figure 4.3-1 shows the framework of model simulation. PRCSL, EVPSL and TRNSL that were used to be the input data to the SXAJ model to generate runoff intensity represented 1120 (28 columns and 40 rows) grid cells covering the CPRB. The generated runoff in unit of millimeter per hour was input into the flow routing model, 1K-FRM, that already modified by including the reservoir operation model and inundation model. The overall model performance achieved a Nash-Sutcliffe model efficiency coefficient of 0.91 and a squared correlation coefficient of 0.94 for the calibrated period at C.2 station (Wichakul et al., 2013a,b). Details of these two models development were explained in Chapter 2 and Chapter 3.

The 1K-FRM represents 288,000 (480 columns and 600 rows) computational grid cells and undertook a 10-min time step of calculation. Topographic data used in the 1K-FRM were the 30-arc-second DEM and flow direction stored in HydroSHED. The final result of the models simulations was predicted discharge that can be obtained any points in the

river channel. To evaluate a river discharge in the Chao Phraya River basin, the C.2 gauging station at Nakhon Sawan, located about 5 km downstream of the beginning of the river (15°40′N and 100°06′E), was selected as a monitoring station that represents the overall situation of the CPRB.

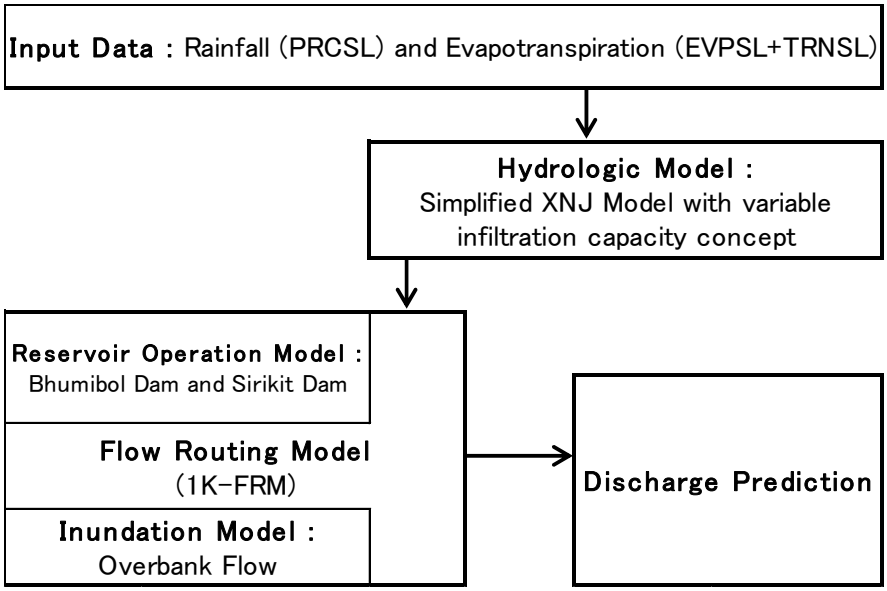

Figure 4.3-1 Framework of the distributed hydrological model including inundation model by using the GCM output.

4.4 Assessment on climate change

4.4.1 Variability and trends of GCM outputs

By analysing rainfall and evapotranspiration data derived from GCM outputs for three different climate experiments, **Table 4.4-1** presents mean annual rainfall and evapotranspiration presented at the C.2 gauging station grid located at the middle of the entire CPRB (**Figure 2.3-1**). Mean annual rainfall slightly decreased in the near future climate experiment and significantly increased in the future climate experiment. Annual

evapotranspiration also trends to be constant in the near future climate experiment. That change varied by less than 1% from the present climate annual evapotranspiration. In contrast, in the future climate experiment, both rainfall and evapotranspiration shows a rising trend of approximately 5% and 4% from the present climate, respectively. **Figure 4.4-1(a)** shows that fluctuation of mean annual rainfall during the future climate experiment and the difference of the lowest and highest values. Mean annual evapotranspiration shows similar fluctuations for all three climate experiments, as presented in **Figure 4.4-1(b)**.

Table 4.4-1 Mean annual rainfall and evapotranspiration

At C.2 gauging station grid	Present (SPA)	Near Future (SNA)	Future (SFA)
(1) Rainfall on the land surface in mm	1192	1169	1247
(2) Evapotranspiration in mm	957	951	996
(3) Approximated runoff in mm (1)–(2)	235	218	251

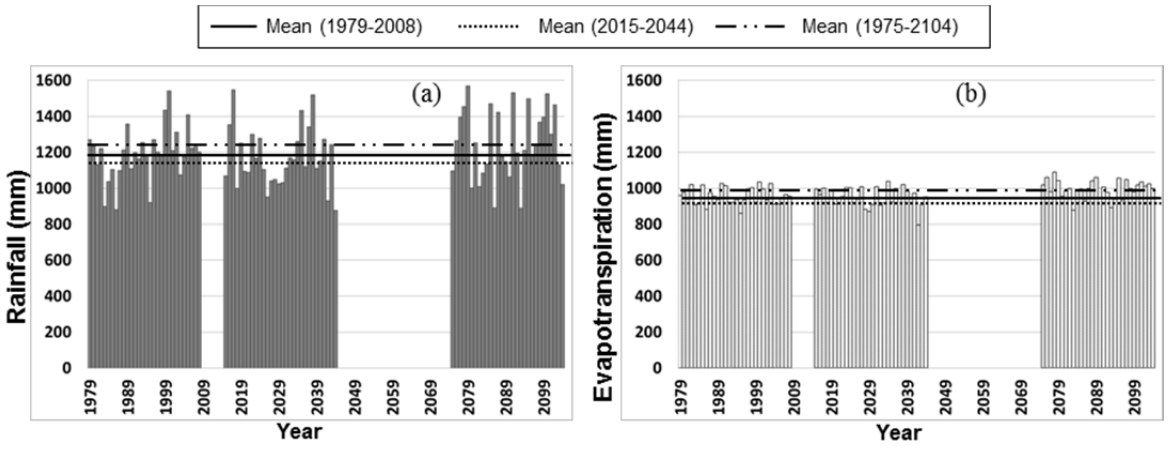

Figure 4.4-1 (a) Annual rainfall and (b) evapotranspiration data in the C.2 station grid.

Most of the northern part of the CPRB is covered by forest and mountainous areas, so the total amount of mean annual rainfall and evapotranspiration of this area is higher than the central and lower part of the basin. In terms of spatial distribution of trend the mean annual rainfall change throughout the basin has a similar rate and pattern to the C.2 grid for the near future climate experiment. The trend of mean annual rainfall has a different rate and pattern for the future climate experiment by decreasing values around the edge of the basin. The mean annual evapotranspiration trend keeps a similar rate and pattern of change throughout the basin for both near future and future climate experiments (see also Appendix B). These changes of rainfall and evapotranspiration show that the water availability trends (approximated runoff) reduced by about 7% in the near future climate and increased by about 7% in the future climate.

4.4.2 Change in river discharge

Details of change in river discharge by analysing simulated discharge from the distributed hydrological model is discussed in this section. As shown in **Figure 4.4-2**, observed daily discharge data were collected and compared with simulated discharge for the present climate experiment (1979-2008) at the C.2 station. The figure shows trends of both observed and simulated discharge are compatible to increase at the 0.18 and 0.25 % level. On the other hand, in previous study illustrated that the trend of discharge observed during 1950-1998 was significantly decrease (at the 1% level), even if the highest discharge stems from the 1990s (Kundzewicz et at., 2009). Due to no bias correction, simulated discharge generally tended to overestimate during wet seasons. But during the low flow period simulated discharge was close to the observed discharge. Therefore, it is reasonable and realistic to evaluate drought risk in this study. However, a tendency for change in overall water availability in the CPRB was also

foreseen as well.

Figure 4.4-3 shows comparison of mean monthly discharge at the monitoring station for three climate experiments. Mean monthly discharge of most of the months, excepting May, shows considerable increases for the future climate. For the near future, the mean monthly discharge in May and August is lower than the present climate experiment. According to the flow routing model including dam operation, discharge during dry season (January–April) was under regulated by the dam model. It means that most of the river discharge was released from storage water in the dams in the dry season. However, it was difficult to get a clear change on river discharge by this comparison of mean monthly discharge.

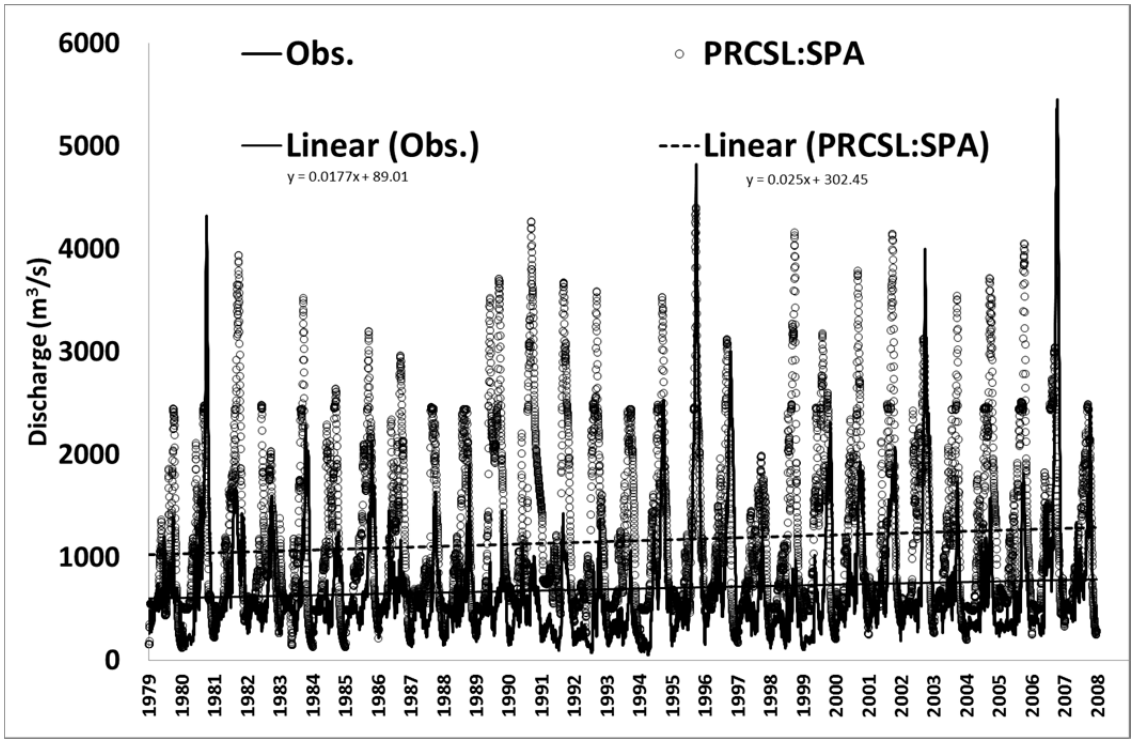

Figure 4.4-2 Comparison of observed and simulated discharge with GCM outputs for present climate (1979-2008) at the C.2 station.

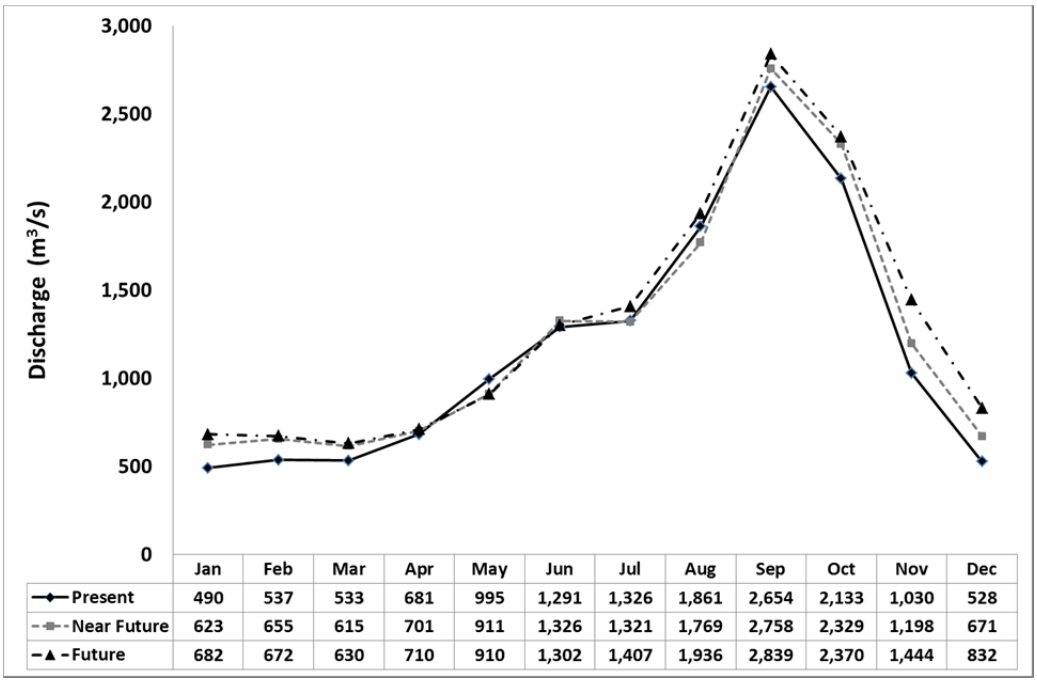

	Jan	Feb	Mar	Apr	May	Jun	Jul	Aug	Sep	Oct	Nov	Dec
Present	490	537	533	681	995	1,291	1,326	1,861	2,654	2,133	1,030	528
Near Future	623	655	615	701	911	1,326	1,321	1,769	2,758	2,329	1,198	671
Future	682	672	630	710	910	1,302	1,407	1,936	2,839	2,370	1,444	832

Figure 4.4-3 Mean monthly discharge at the C.2 station for the present, near future and future climate experiments.

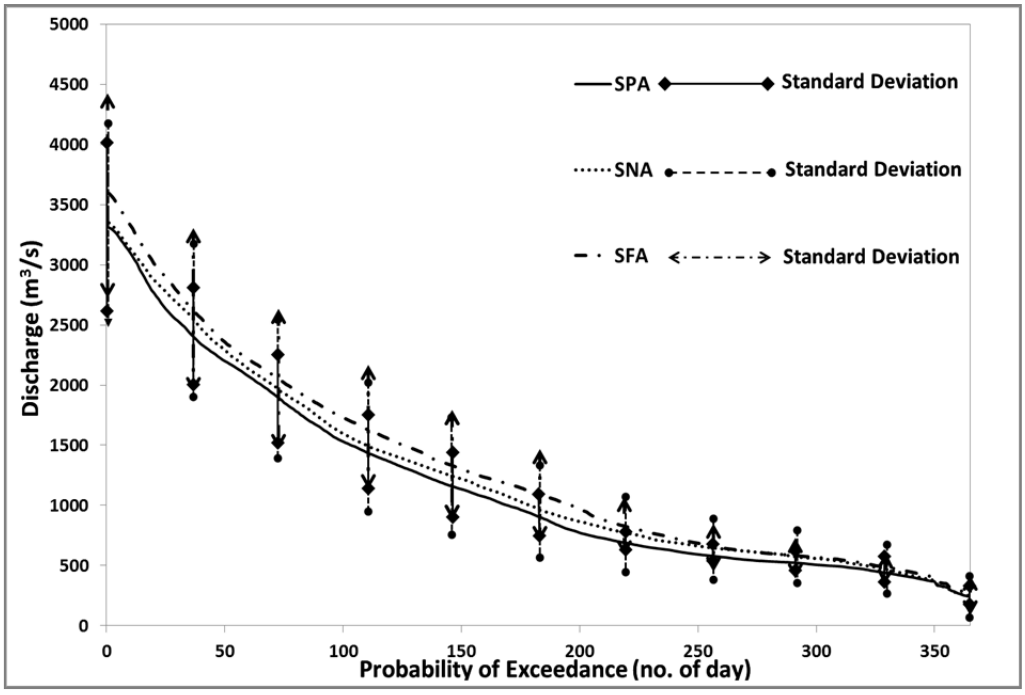

Figure 4.4-4 Mean annual flow duration curves with standard deviation of the present climate (SPA), near future climate (SNA), and future climate (SFA) experiments.

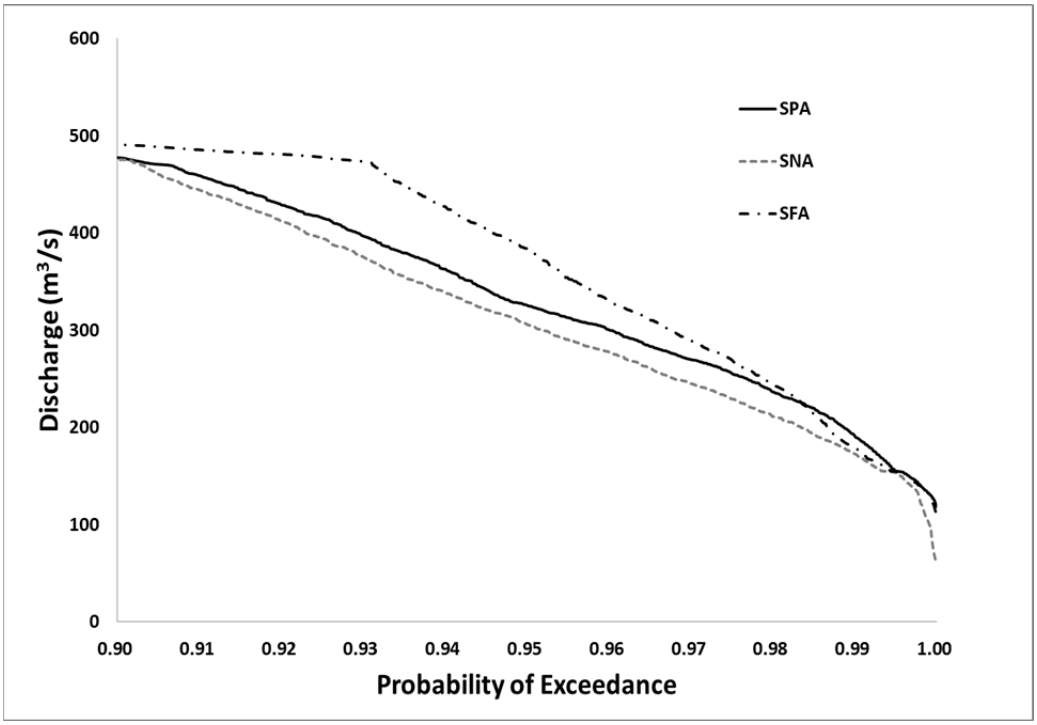

Figure 4.4-5 Low flow section of the flow duration curves constructed based on daily discharge of a period-of-record of each climate experiment.

Flow duration curves showing the probability of exceedance of flow magnitude and help to characterize the response of the river to a changing climate. **Figure 4.4-4** shows mean annual flow duration curves with standard deviations for the three climate experiments. For the future climate, a considerable increase in all discharge rates (both high and low flow section) is consistent with the rate of rainfall increases rather than evapotranspiration. For the near future climate, a slight increase in mean discharge rates at the middle flow section and a decrease at the low flow section was detected. To enlarge the low flow section, **Figure 4.4-5**, therefore, compares the flow duration curves constructed based on daily discharge of a period-of-record of each climate experiment at the low flow section. Hence, it is clear that the low flow values tend to decrease significantly in the near future experiment which result in increased drought risk in the CPRB.

4.5 Conclusion

In this chapter, a regional distributed hydrological model, including the effect of dam operation and inundation and outputs of the MRI-AGCM3.2S, PRCSL, TRNSL and EVPSL, were applied to the CPRB for projected river discharge in the present climate (1979–2008), the near climate future (2015–2044) and the future climate (2075–2104) experiments. Changes of rainfall and evapotranspiration, which were derived for the GCM outputs, showed that the water availability trends reduced in the near future climate experiment and increased in the future climate experiment. This result was comparable with the result from our simulation from the model. Broad trends of projected discharge showed that water availabilities in the CPRB increase all year round, both in the wet and dry seasons in the future climate experiment. For the near future climate annual water budget slightly increases, but during dry season trends of projected discharge considerably reduced.

According to our study results, reduction of water availability led to an increase in drought risk in the near future climate. By using the application of the dam operation model, an adaptive measure for managing dam operation rules to deal with the risk of drought is recommended for further study. It was difficult to achieve reliable estimates of peak discharges under climate change conditions at this stage. Therefore, a statistical method based on the relationship between observed and simulated peak discharges was suggested to be conducted for further study on the projection of water resources of the CPRB. From the information of change of drought risk and flood risk, proposed dam operation rule might be helpful for sustainable planning of water resources management of the basin.

Chapter 5

Bias correction of GCM precipitation and evapotranspiration

5.1 Introduction

Global Circulation Models (GCMs) are accepted as the important to for predicting and assessing the impacts of a changing climate and assisting to design adaptation measures for the future situation. Prediction of the Chao Phraya River discharge has been conducted in the previous chapter for water resources assessment of the basin by utilizing outputs of the MRI-AGCM3.2S (20 km resolution) without bias correction. However, for a reliable prediction result, the bias correction should be applied to the GCM output.

Previous studies on bias correction in the Chao Phraya River Basin (CPRB) have been carried out by Koontanakulvong and Chaowiwat (2010) using Standard Deviation ratio downscaled rainfall and Modified Rescale downscaled rainfall to remove the bias form the MRI-AGCM3.1 precipitation and temperature datasets. In the Ping River basin, sub-basin of the CPRB, Sharma et al. (2007) improved the quality of EHCHAM4/OPYC SERS A2 and B2 precipitation by applying gamma-gamma transformation bias-correction.

Several studies around the world conducting the precipitation bias correction based on a relationship of cumulative distribution functions (CDFs) of the GCM and observation data have been shown to perform well for hydrologic simulations and climate change studies. (Lafon et al., 2013; Piani et al., 2010; Themeßl et al., 2010; Wood et al., 2004). Therefore, I attempted to remove biases form the GCM dataset, not only the precipitation data but also the evapotranspiration, using a relationship of the CDFs of the precipitation data and introduced a straightforward method to the evapotranspiration.

5.2 Data

5.2.1 GCM precipitation and evapotranspiration

I proposed to remove the bias from the MRI-AGCM3.2 variables in three (3) different climate experiments: the present climate experiment (1979–2008), the near future climate experiment (2015–2044), and the future climate experiment (2075–2104). The GCM precipitation is rainfall reaching to soil layer (PRCSL) and the GCM evapotranspiration is a summation of evaporation from bare soil (EVPSL) and transpiration from root zone soil (TRNSL). The GCM variables covering the CPRB were extracted total 1,120 grids resolution 0.1875 (Cols=28 and Rows=40), which is defined as being between Latitude = 12.094 - 19.406 N and Longitude = 98.060 – 103.123 E.

5.2.2 APHRODITE data

The Asian Precipitation–Highly-Resolved Observational Data Integration Towards Evaluation of Water Resources (APHRODITE) project has been begun since 2006 to develop daily precipitation datasets on high-resolution grids covering the whole of Asia. The goal was to provide the product for the validation of high-resolution model and for studies on hydrological process. A daily gridded precipitation dataset covering a period of more than 57 years (1951-2007) recorded data was created by collecting precipitation data from a local organization in each country and analyzing rain gauge observation data across Asia. The latest version which has been released open-access is APHRO_V1101 datasets for monsoon Asia, the Middle East, and northern Eurasia (at 0.5° × 0.5° and 0.25° × 0.25° resolution). The product was compared with the product

of the Global Precipitation Climatology Center (GPCC). It shown that in most of areas, APHRO_V1101 estimated less precipitation than the GPCC product. However, APHRODITE's daily gridded precipitation is presently the only long-term, continental-scale, high-resolution daily product (Yatagai et al., 2012).

In our study, I selected the APHRO_V1101 datasets for monsoon Asia 0.25° × 0.25° resolution to be the reference truth data during 1979-2007 for conducting the bias correction of GCM precipitation. There are total 770 grids (Cols=22 and Rows=35) covering the CPRB were clipped from the domain of the APHRODITE data.

5.2.3 Reference evapotranspiration

Evapotranspiration is a combining of two processes, evaporation and transpiration. Evaporation is defined as the rate of liquid water transformation to vapor from open water, bare soil, or vegetation with soil beneath. Transpiration is defined as rate of water which enters the atmosphere from the soil through the plants (Shuttleworth, 1993).

To remove bias from the GCM Evapotranspiration data, the long term observed data are needed for the reference truth data. Unfortunately, there is no direct observation of the evapotranspiration. Many methods to estimate the evapotranspiration have been conducted, for example by the atmospheric water balance method, by weather forecast model, by hydrologic model and by formulas (Attarod et al., 2006; Ohba and Ponsana, 1987; Oki et al., 1994; Kosa and Pongput, 2007; Watanbe et al., 2004; Xu and Li, 2003). Basic information requires for the estimation are the recorded climatology data, wind speed, temperature, sunshine duration, humidity and etc.

In our study, I obtained a reference crop evapotranspiration (ET_o) calculated by the Royal Irrigation Department of Thailand (RID) using the FAO Penman-Monteith

method (Allen et al., 1998) with recorded climatology data for the 30 years from 1981 to 2010 to be the truth reference data. The data were collected from 26 observing stations and reformatted by using nearest method to be a grid based data covering the CPRB with the same resolution to the evapotranspiration from the GCM (0.1875 degree). The detail of FAO Penman-Monteith equation is explained follows.

FAO Penman-Monteith Equation

The FAO Penman-Monteith is currently recommended as the only standard method for the definition and estimation of the reference evapotranspiration (ET_o) that I use as the truth reference data for removing the bias form GCM evapotranspiration. The original Penman-Monteith equation allows the calculation of evaporation (E) from meteorological variables and resistances which are related to the stomatal and aerodynamic characteristics of the crop, and has the form

$$E = \frac{1}{\lambda}\left[\frac{\Delta(R_n - G) + \rho_a c_p \,{}^{(e_s - e_a)}/_{r_a}}{\Delta + \gamma(1 + {}^{r_s}/_{r_a})}\right] \qquad \text{mm day}^{-1} \qquad (5\text{-}1)$$

where λ is the latent heat of evaporation (MJ kg^{-1}), R_n is the net radiation (MJ m^{-2} day^{-1}), G is the soil heat flux, $(e_s - e_a)$ represents the vapor pressure deficit of the air (kPa), ρ_a is the mean air density at constant pressure (kg m^{-3}), c_p is the specific heat of the air (= 1.013 kJ kg^{-1}°C^{-1}), Δ is the slope of the saturation vapor pressure temperature relationship (kPa °C^{-1}), γ is the psychrometric constant (kPa °C^{-1}), and r_s and r_a are the (bulk) surface and aerodynamic resistances (s m^{-1}).

Aerodynamic resistance r_a controls the rate of water vapor transfer away from the ground by turbulent diffusion. It is a relationship of wind speed and the height of the vegetation covering the ground that can be determined by the following equation.

$$r_a = \frac{ln[(z_m - d)/Z_{om}]\, ln[(z_h - d)/z_{oh}]}{(0.41)^2 U_z} \quad (5\text{-}2)$$

Where z_m and z_h are the respective heights of the wind speed and humidity measurements (m), d is zero plane displacement height (m), z_{om} is roughness length governing momentum transfer (m), z_{oh} roughness length governing transfer of heat and vapor (m), U_z wind speed (ms^{-1}). (Bulk) surface resistance (r_s) terms the resistance of vapor flow through the transpiring crop and evaporating soil surface. The relationship between the surface resistance and leaf cover, soil water status, and environmental variables can be described by

$$r_s = \frac{r_l}{LAI_{active}} \quad (5\text{-}3)$$

where r_l bulk stomatal resistance of the well-illuminated leaf ($s\ m^{-1}$), and LAI_{active} active (sunlit) leaf area index in unit of m^2 (leaf area) m^{-2} (soil surface). From the original Penman-Monteith equation (Eq. 5-1), the equations of the aerodynamic (Eq. 5-2) and surface resistance (Eq. 5-3), the FAO Penman-Monteith method to estimate ET_o can be derived as

$$ET_o = \frac{0.408\Delta(R_n - G) + \gamma \frac{900}{T+273} U_2 (e_s - e_a)}{\Delta + \gamma(1 + 0.34U_2)} \quad (5\text{-}4)$$

where G is soil heat flux density ($MJ\ m^{-2}\ day^{-1}$), T is mean daily air temperature at 2 m height (°C), U_2 is wind speed at 2 m height ($m\ s^{-1}$), e_s is saturation vapor pressure (kPa), and e_a is actual vapor pressure (kPa).

5.3 Methodology

To make to bias correction on the GCM precipitation (P_{GCM}) and evapotranspiration (E_{GCM}), I applied two simple methods for each variable. The basic idea is to remove biases from the GCM data before applying the data to hydrological simulation. The correction was conducted regarding to a relationship of the reference truth data and GCM data based on grid by grid. Each combination of precipitation and evapotranspiration bias correction methods was evaluated it performance by simulated discharge of the hydrological models at the C.2 station. The training period was set for 29 years from 1979 to 2007 (present climate, SPA) and the projection periods were set from 2015 to 2043 for near future period (SNA) and from 2075 to 2103 for future period (SFA). I apply the bias correction separately for each calendar month. The framework of the bias correction is illustrated in **Figure 5.3-1.** Details for each correction method are explained in the following sections.

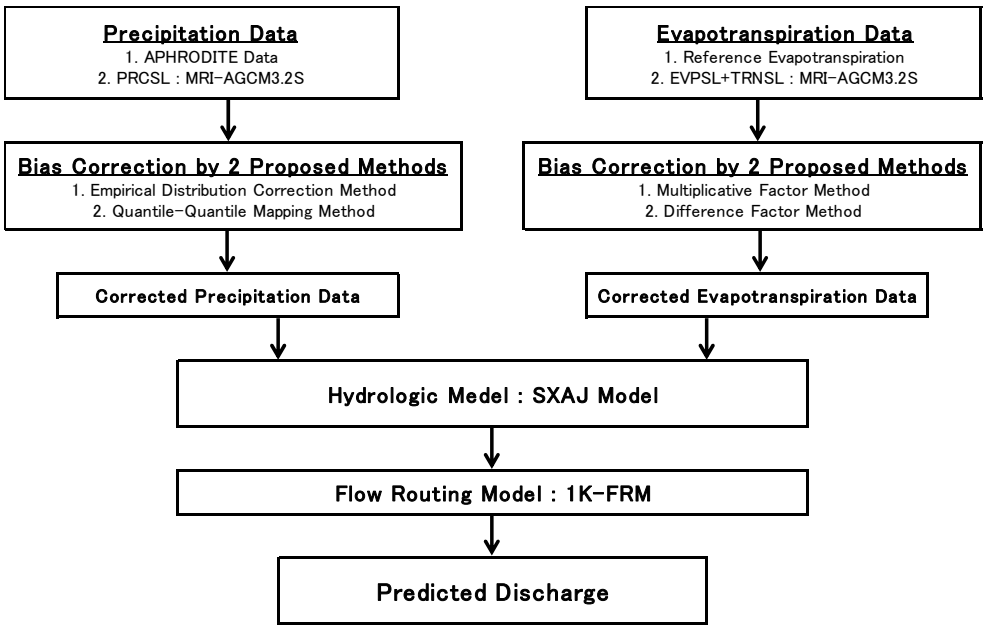

Figure 5.3-1 Bias correction framework.

5.3.1 Bias correction of daily precipitation

Figure 5.3-2 illustrates the flowchart of bias correction method. Due to difference in resolution of GCM precipitation (*P*) and APHRODITE precipitation (referred as observation data, *O*), the nearest grids were paired for identifying the bias pattern. Wet day was defined as the day that rainfall occurred more than 0.1 mm. Generally, the daily GCM precipitation contains biases in frequency and intensity distribution. Firstly, the bias in frequency distribution is represented by a number of wet days. Based on Cumulative Distribution Functions (CDFs) of daily GCM precipitation and the observation data of each month for entire training period, bias in precipitation frequency can be corrected by adjusting the wet days of GCM precipitation to match with observation data by setting the GCM precipitation to 0.0 mm for every day with the Non-exceedance probability (NEP) lower than the threshold where O = 0.1 mm. Secondly, the bias in intensity distribution of GCM precipitation can be corrected by our proposed two techniques as follows.

Empirical distribution method

This method is to correct the daily GCM precipitation by a linear transform function. The linear correction factor (*C*) can be obtained by dividing the CDFs of the truncated GCM and observation precipitation into a number of discrete quantiles, 25Q 50Q 75Qand 100Q (**Figure 5.3-3**), and then getting a mean precipitation data at each division of the quantiles (Lafon et al., 2013). The corrected daily precipitation data in each quantiles division (nQ : n = 25 50 75 and 100) were calculated as

$$P_{i\_cor:SPA} = c_{nQ} P_{i\_GCM:SPA} \quad (5\text{-}5)$$

where $P_{i\_cor:SPA}$ is corrected GCM precipitation and $P_{i\_GCM:SPA}$ is raw present GCM data. Subscript i indicates the relative position of data within the CDF. Factor C_{nQ} is calculated by dividing mean observation ($\bar{O}$) by mean GCM precipitation ($\bar{P}_{GCM}$) in each quantile as

$$c_{nQ} = \frac{\bar{O}}{\bar{P}_{GCM:SPA}} \tag{5-6}$$

For the projection periods, I assumed that the bias of the intensity distribution occurring in the near future and future GCM precipitation data come from the same sources of uncertainty variables in the GCM. Therefore, to remove the bias in those future periods, C_{nQ} can be directly multiply to the near future and future GCM according to **Eq.5-5**.

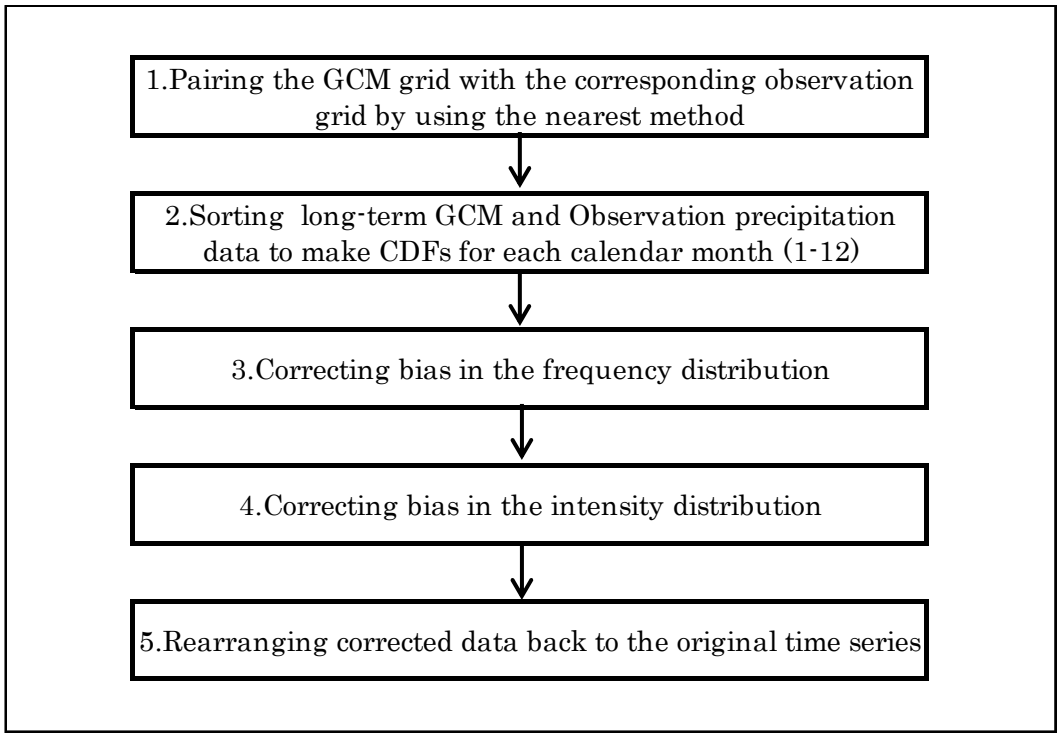

Figure 5.3-2 Flow chart of the precipitation bias-correction work.

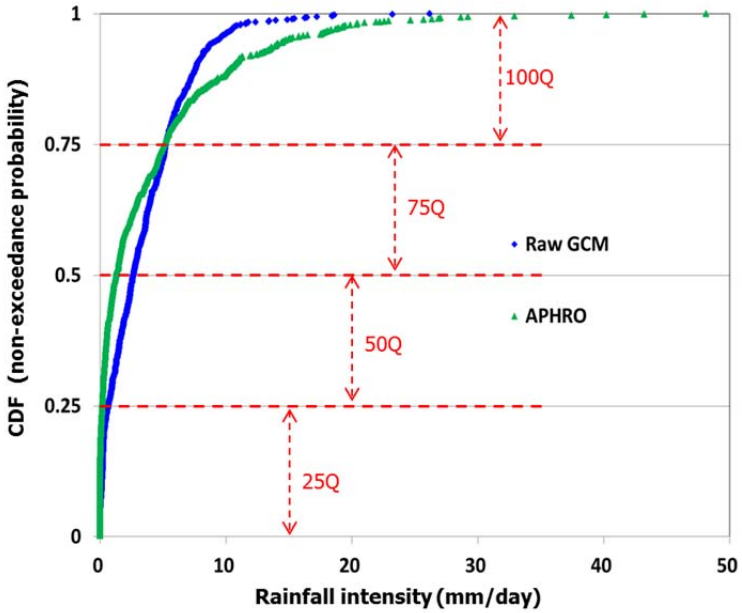

Figure 5.3-3 Cumulative distributed functions of the long-term daily GCM and observation precipitation at a particular location.

Quantile-quantile method

Quantile-quantile (Q-Q) bias correction method was proposed for removing intensity bias from the GCM precipitation based on the assumption that correction can be conferred from ranked historical simulation or observation data to equivalent ranks in future projection. The quantile-quantile correction has been used in several northern hemisphere studies to improve the utility of regional climate model (RCM) outputs. The technique has the advantage of preserving complex changes in the RCM projections – e.g. to weather systems, dry spells, rainfall intensities, mean rainfalls, rainfall extremes – in hydrological modelling (Bennett et al., 2011 and 2013). Many studies apply the quantile-quantile method by fixing the data with shape of statistical distribution (e.g. Ines and Hansen, 2006; Lafon et al., 2013; Mishra and Herath, 2011). I did not assume the shape of the theoretical. To remove the bias in the training period, CDFs of both raw GCM and observation precipitation were created accordingly. **Figure 5.3-4** illustrates

transformation of the raw GCM precipitation data. The GCM precipitation is mapped onto the observation precipitation at respective NEP of GCM data to observation data (or GCM quantile to observation quantile). This relationship can be mathematically expressed by the inverse of the observation data CDF as.

$$P_{i\_COR:SPA} = F_{obs}^{-1}(F_{RAW:SPA}(P_{i\_RAW:SPA})) \quad (5\text{-}7)$$

This method is straightforward. However, to apply for the projection periods I implicitly assumed that the variability in the climate experiment is unchanged (Boe et al., 2007). With respect to a relationship of the CDF of GCM precipitation in the training period (current climate: SPA) and the CDF of projection period (near future or future climate: SNA or SFA), the bias correction of the projection periods was proposed by using the following equations:

$$P_{i\_COR:SNA} = P_{i\_RAW:SNA}\left[\frac{F_{obs}^{-1}((F_{RAW:SNA}(P_{i\_RAW:SNA}))}{F_{RAW:SPA}^{-1}((F_{RAW:SNA}(P_{i\_RAW:SNA}))}\right] \quad (5\text{-}8)$$

or $$P_{i\_COR:SNA} = P_{i\_RAW:SNA}\left[\frac{X_{i\_SNA}}{Xi\_SPA}\right] \quad (5\text{-}9)$$

where X_{i_SNA} and X_{i_SPA} are precipitation data at the corresponding quantile in the CDFs of the projection and training periods. The correction system of the projection periods are illustrated in **Figure 5.3-5**.

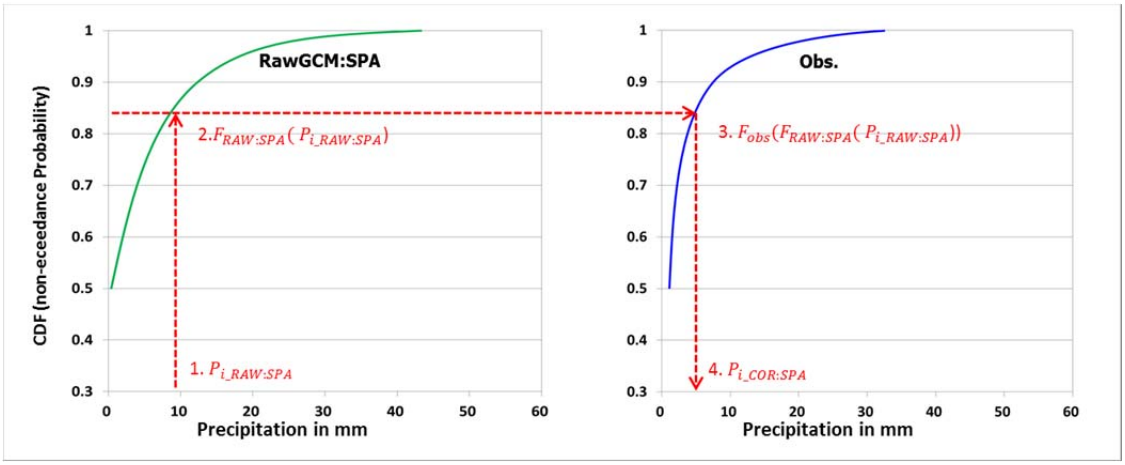

Figure 5.3-4 Transformation of the raw GCM precipitation data in baseline period.

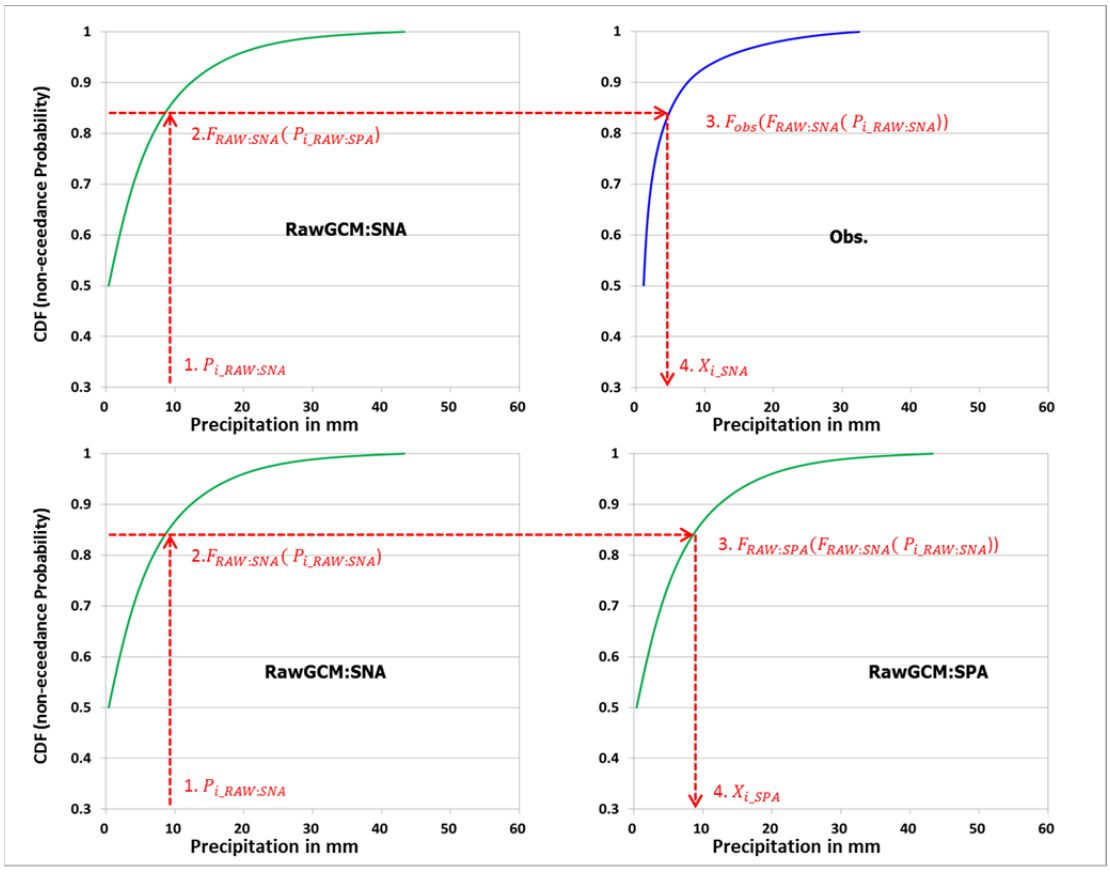

Figure 5.3-5 Transformation of the raw GCM precipitation data in projection period.

5.3.2 Bias correction on evapotranspiration

Climate input variables of the Hydrologic model were daily precipitation, temperature, daily wind speed, downward solar and long wave radiation, and dew point. The temperature, wind speed, solar radiation, and dew point are used to estimate an actual evapotranspiration. Generally, many studies removed a bias from the temperature and then input the corrected temperature to the Hydrologic model or land surface model to estimate the amount evapotranspiration, for examples the study of Bordoy and Burlando (2013); and Piani et al. (2010).

Histograms of mean daily temperature are comparable well represented by a Gaussian distribution and it's transfer function is well represented by a linear function (Piani et al., 2010). Hargreaves and Samani (1985) introduced a linear relationship of temperature and global solar radiation for predicting ET_o:

$$ETo = 0.00023 S_0 \overline{\delta_T} (T + 17.8) \quad (5\text{-}10)$$

where S_0 is the water equivalent of extraterrestrial radiation in mm per day for the location of interest, T is the temperature in $°C$, and the difference between mean monthly maximum and mean monthly minimum temperature. The Hargreaves equation **(Eq. 5-10)** shows that the evapotranspiration is a linear function of the temperature.

In case of our study I applied evapotranspiration to be hydrological model input directly. Therefore, I avoided to increase uncertainties by directly removing the bias form the evapotranspiration based on a liner function correction.

To correct bias from the GCM Evapotranspiration data, the long term observed data are

needed for the reference truth data. However, there are still limitations for the evapotranspiration measurement and estimation. The monthly mean ET_o were used to be a reference data for adjusting the GCM evapotranspiration. The evapotranspiration bias correction was proposed in two (2) methods as follows.

Multiplicative factor method

Multiplicative factors of each calendar month were calculated from the monthly mean of the GCM evapotranspiration and ET_o over the long term period (29 years) expresses as:

$$Fc_m = \frac{ETo_m}{\bar{E}_{GCM:SPA\_m}} \tag{5-11}$$

where Fc_m is a multiplicative factor of particular m month (1 – 12), ETo_m is the monthly mean reference evapotranspiration of particular m month, and $\bar{E}_{GCM:SPA\_m}$ is the monthly mean GCM evapotranspiration of particular m month in the baseline period (current climate).

And then, I applied those multiplicative factors to the daily GCM evapotranspiration values to both baseline period and projection period to correct the bias. The corrected GCM evapotranspiration are obtained as

$$E_{i\_cor:SPA} = Fc_m \times \left(E_{i\_GCM:SPA}\right)_m \quad \text{(for the baseline period)} \tag{5-12a}$$

$$E_{i\_cor:SNA} = Fc_m \times \left(E_{i\_GCM:SNA}\right)_m \quad \text{(for the projection periods)} \tag{5-12b}$$

Where $E_{i\_cor:SPA}$ and $E_{i\_cor:SNA}$ are the corrected GCM evapotranspiration for the baseline period and projection periods (near future or future climate: SNA or SFA) respectively, $E_{i_{GCM}:SPA}$ and $E_{i_{GCM}:SNA}$ are the raw GCM for the baseline period and

projection periods individually. Subscript m indicates the calendar month.

Difference factor method

To adjust monthly mean GCM evapotranspiration by adding the difference between the monthly mean of ET_o and the daily GCM evapotranspiration over the long term period. So I can be obtained daily differenced factors from the following equation.

$$Fc_m = ETo_m - \bar{E}_{GCM:SPA\_m} \quad (5\text{-}13)$$

Then, I applied those multiplicative factors to the daily GCM evapotranspiration values to both baseline period and projection period to correct the bias. The corrected GCM evapotranspiration are obtained as

$$E_{i\_cor:SPA} = \left(E_{i\_GCM:SPA}\right)_m + Fc_m \quad \text{(for the baseline period)} \quad (5\text{-}14a)$$

$$E_{i\_cor:SNA} = \left(E_{i\_GCM:SNA}\right)_m + Fc_m \quad \text{(for the projection periods)} \quad (5\text{-}14b)$$

These methods show that after adjusting the monthly mean evapotranspiration values of the base line period are same as the monthly mean ET_o, and the corrected evapotranspiration values in the projection periods are changed accordingly to the baseline period.

5.4 Result and discussion

5.4.1 Bias correction of precipitation

Both correction methods, Quantile-quantile and Empirical distribution, were constructed monthly for each grid covering the Chao Phraya River Basin and adjusted

all moments of distribution functions for each day. To evaluate performance of bias correction in frequency distribution, I investigated and analyzed the data at the particular location, C.2 station grid. Wet days were adjusted according to the wet day definition, total precipitation > 0.1 mm/day. The frequency distributions of raw GCM precipitation with low precipitation intensity is very high compared to the observed data especially in day season (December-January). After adjusting the wet days according to the threshold value of each month, diagrams comparing a number of wet days before and after correcting are shown in **Figures 5.4-1, 5.4-2 and 5.4-3** for the baseline period and projection near future and future periods, respectively at particular grid the C.2 station. **Figure 5.4-4** illustrates comparison of monthly average corrected wet days for three different periods. It shows that in among three periods thee frequency of wet days are quite similar. Trend of wet days in the projection periods slightly decreases in especially wet season by comparing with the baseline period.

In term of bias correction in intensity distribution, I applied two methods to correct the GCM precipitation. The bias correction was carried out separately across the time. Principle of both two methods of correction is to remove bias in the mean monthly of long term GCM precipitation. Therefore, it results in the same values of mean monthly precipitation from different correction method as shown in **Figure 5.4-5** for the baseline period (1979-2007). In most of the calendar months, raw GCM precipitation data are larger than the observation data, but only some months (July August October and November) the values of raw GCM precipitation are slightly lower than the observations. According to the value of law GCM in the baseline period, law GCM in the projection periods was corrected and the results in mean monthly precipitation are shown in Figures 5.4-6 and 5.4-7 for the near future climate and future climate,

respectively. However, total amount of mean annual raw GCM precipitation at the C.2 station is still higher than the observation precipitation, referring to Appendix B, **Figures B-1 and B-2**. **Figures B-1 to B-4** shows the spatial mean annual precipitation of the observation data (APHRODITE) and the raw GCM precipitation over the study area. The values of mean annual raw GCM precipitation around the central Chao Phraya River Basin are higher than those in the upper part of the basin. On the other hand, the observation data shows that the precipitation around the central part of the basin is lower than the upper part.

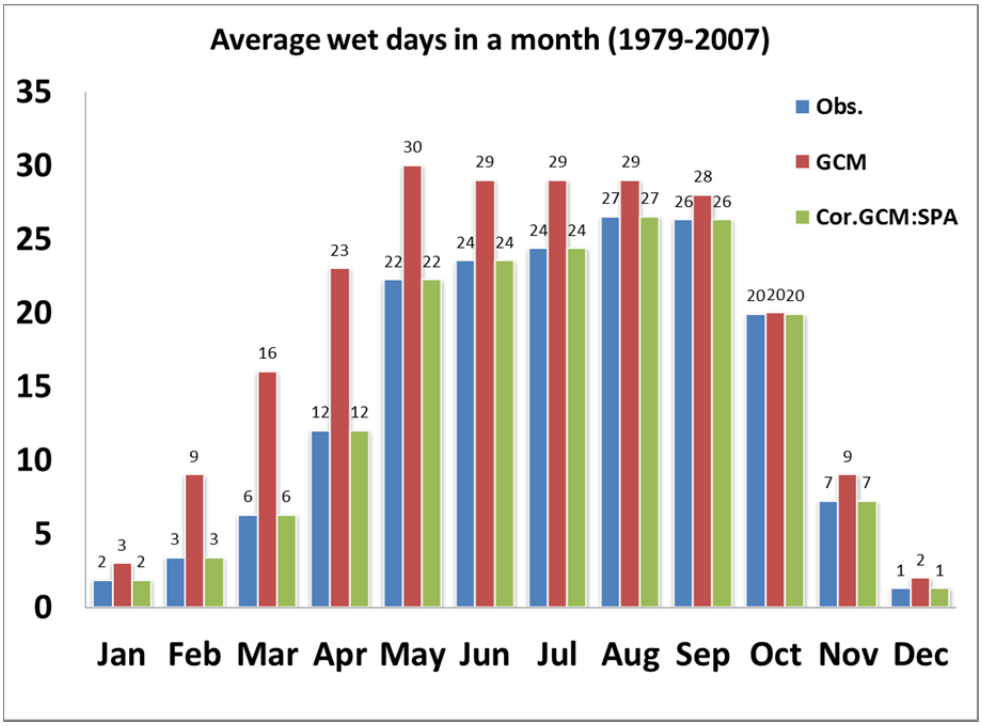

Figure 5.4-1 Number of monthly average of observation data wet days (Obs.), GCM wet days (GCM) and corrected GCM wet days for the baseline period 1979-2007 (Cor.GCM:SPA).

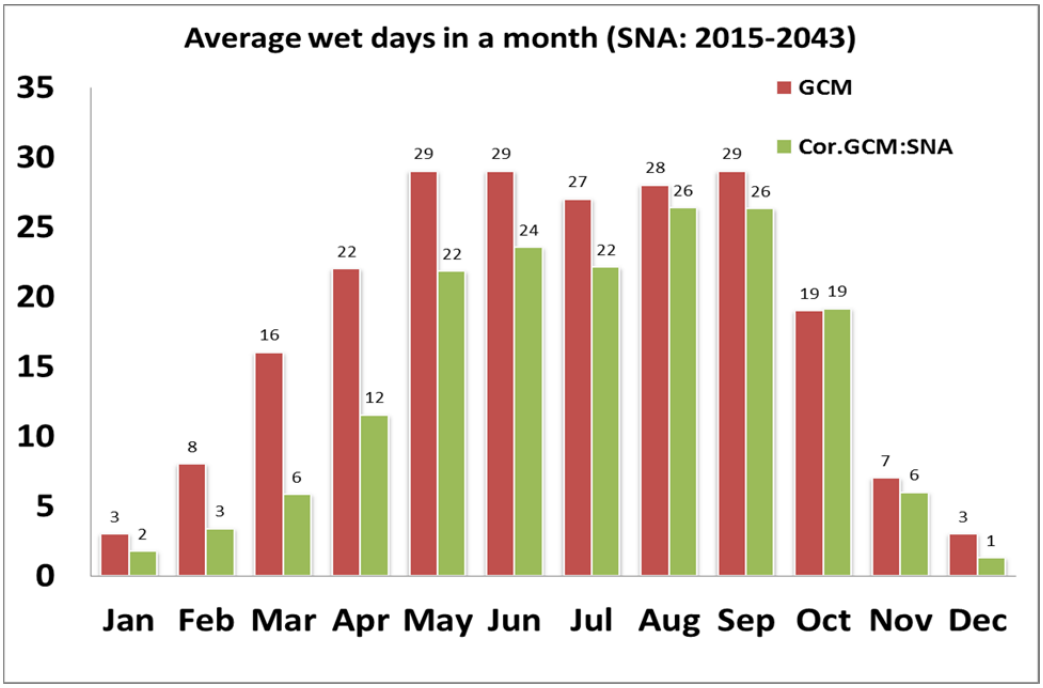

Figure 5.4-2 Number of monthly average of GCM wet days (GCM) and corrected GCM wet days for the projection period, near future climate: 2015-2043 (Cor.GCM:SNA).

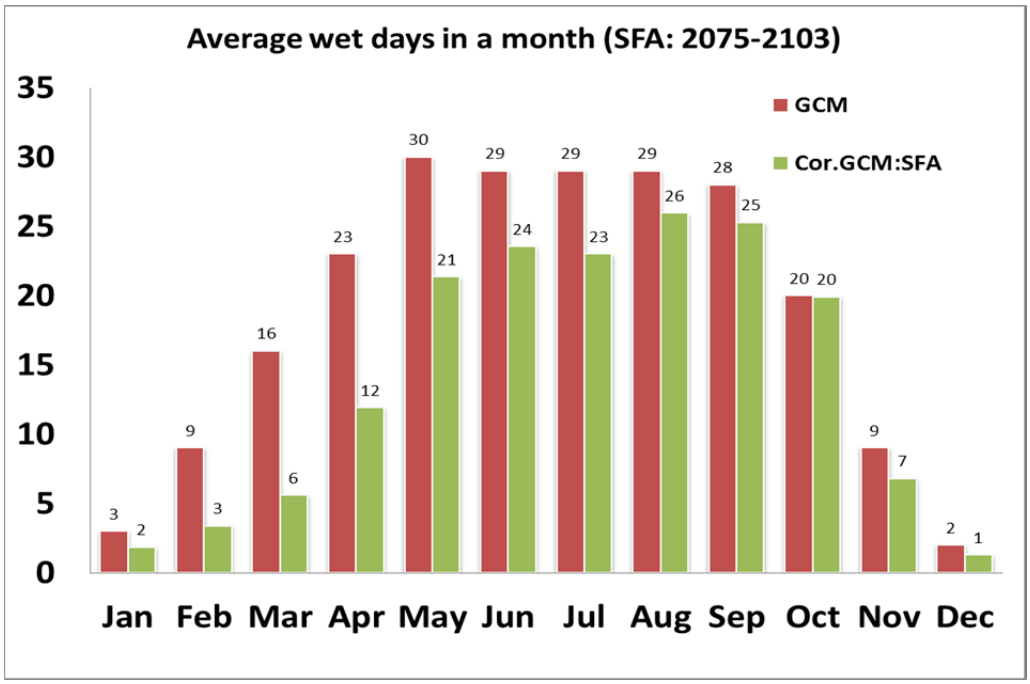

Figure 5.4-3 Number of monthly average of GCM wet days and corrected GCM wet days for the projection period, Future climate 2075-2103 (Cor.GCM:SFA).

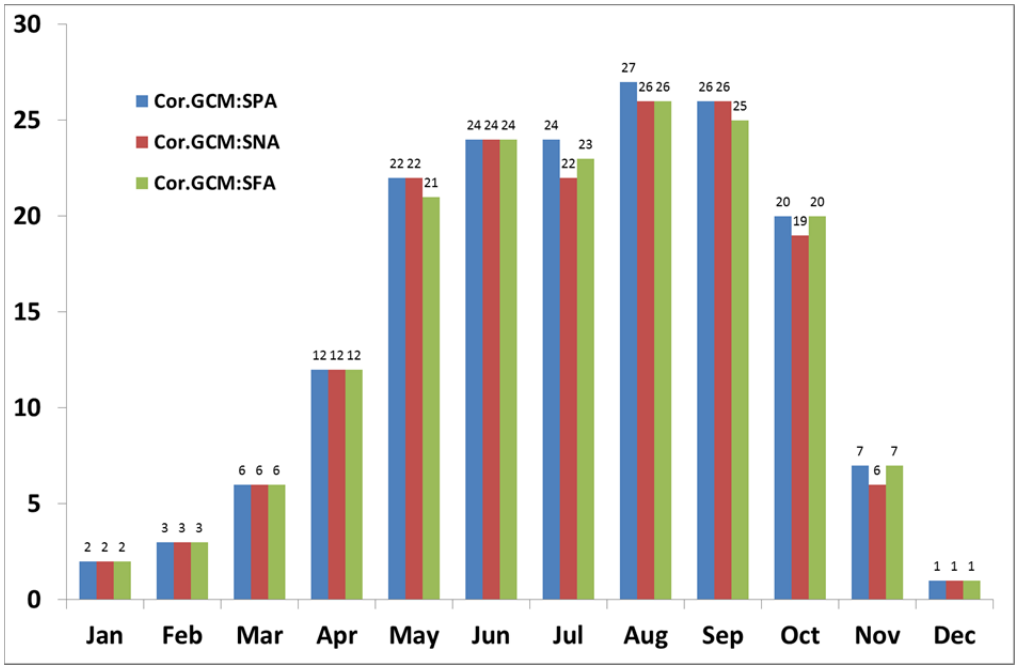

Figure 5.4-4 Comparison of monthly average corrected wet day for current climate (Cor.GCM:SPA), near future climate (Cor.GCM:SNA), and future climate (Cor.GCM:SFA).

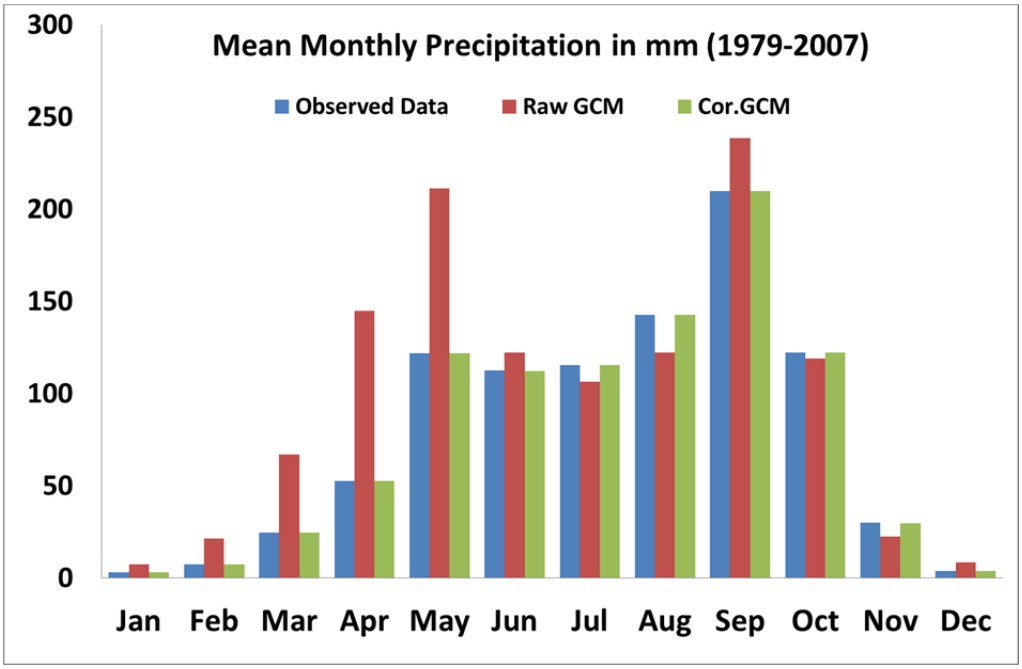

Figure 5.4-5 Mean monthly precipitation for observed precipitation data, raw GCM and corrected GCM by both empirical distribution and quantile-quantile methods.

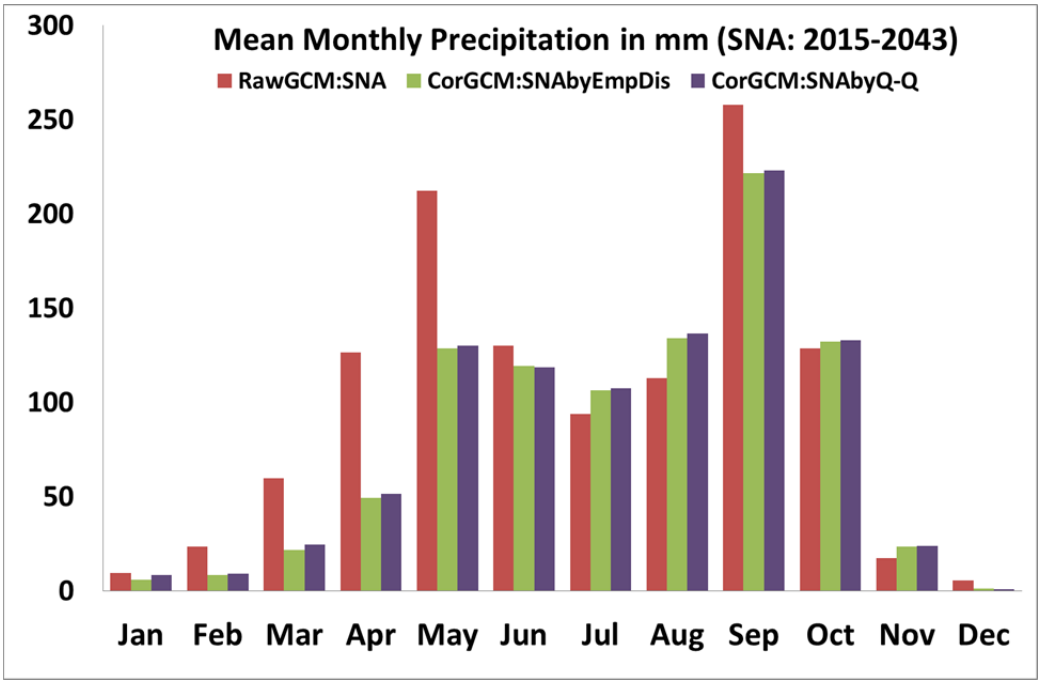

Figure 5.4-6 Mean monthly precipitation for observed precipitation data, raw GCM and corrected GCM by both empirical distribution and quantile-quantile methods in the Near Future Climate.

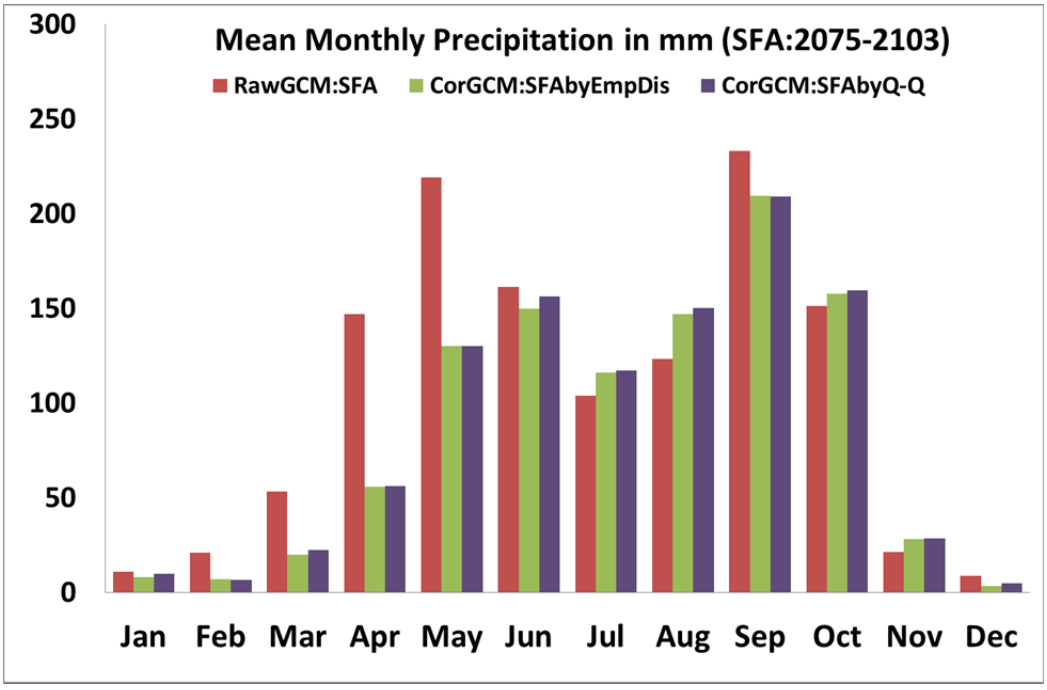

Figure 5.4-7 Mean monthly precipitation for observed precipitation data, raw GCM and corrected GCM by both empirical distribution and quantile-quantile methods in the Future Climate.

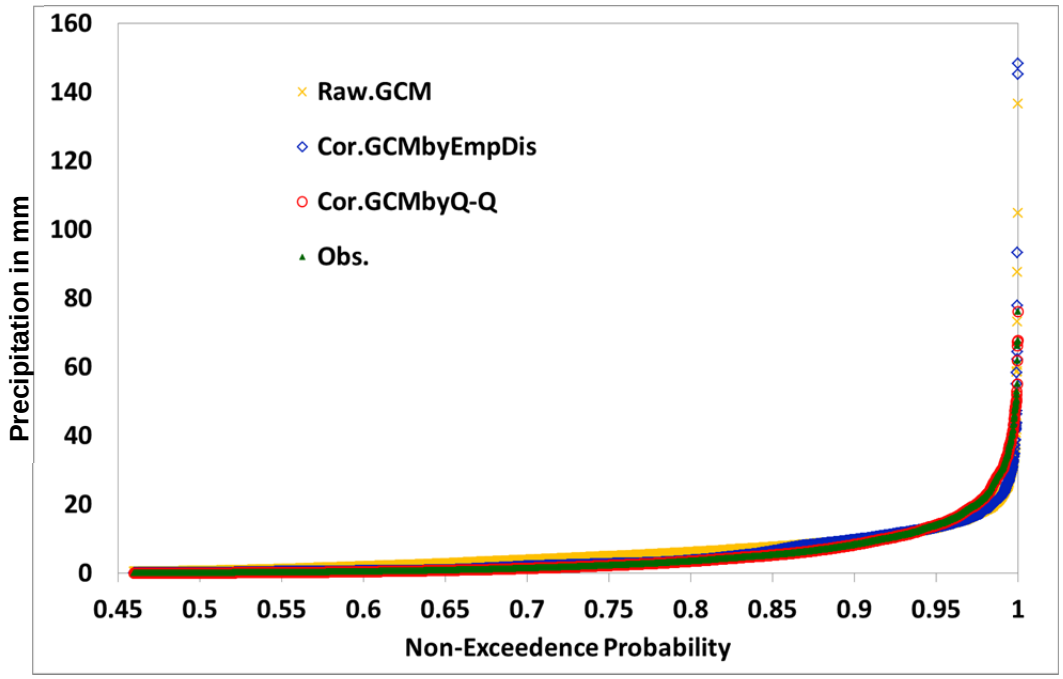

Figure 5.4-8 Duration curves of the truncated data after wet day correction of raw GCM precipitation (Raw.GCM), corrected GCM precipitation by empirical method (Cor.GCMbyEmpDis), corrected GCM precipitation by quantile-quantile method (Cor.GCMbyQ-Q), and observation precipitation (Obs).

Figure 5.4-8 illustrates duration curves of the truncated data for the raw GCM, corrected GCM (from two methods), and the observation precipitation. These bias corrections were carried out separately across the time. Consequently, the duration curve obtained for the quantile-quantile correction method is exactly same distribution with the duration curve of the observation data. The raw GCM precipitation with the low precipitation intensity (about 1-12 mm) ranged from NEP 0.55-0.95 is higher than the value of the observation data. In contrast, in range of the higher NEP (>0.95), the raw GCM precipitation intensities are lower than the observation intensities. Remark is made at the extreme points that the raw GCM precipitation seems unrealistic higher than the observation.

The empirical distribution correction also represented well adjustment of raw GCM ranged from 0.45 of NEP to 0.95 of NEP. There is some limitation of the correction of those extreme precipitation points as show in **Figure 5.4-8**. Refer to **Figure 5.4-9**; the limitation comes from that in 100 quantiles mean value of the raw GCM precipitation is much lower than mean of the observation precipitation. So the direction of remove thee bias in these quintiles is to increase values of the law GCM by multiplicative factor C_{100Q} = 1.42. That is why some unrealistic high values also were also multiplied with the factor that results in much more high value were produces.

The statistical performance of two correction methods was evaluated based on the difference of distribution functions of the GCM data and observation data. As shown in **Table 5.4-1**, the bias in the mean of GCM precipitation was removed well for both correction methods. Only the maximum difference between the observed and corrected GCM precipitation by the empirical method was increased about 19.5% as I explained before. The original GCM showed also the acceptable efficiency index (NEP = 0.90) but it was improved to 0.93 and 1.0 after I applied the empirical distribution and quantile-quantile correction methods, respectively. Root Mean square and Mean Absolute error also decreased, but the correlation coefficient of the corrected GCM by the empirical method was not change.

Direction of the bias correction was to reduce the values of the GCM precipitation in the Chao Phraya River Basin which resulting in producing over estimated discharge in the hydrological model. In Appendix B, **Figures B-5, B-6 and B-7**, ratios of change in mean annual precipitation after correcting the bias correction in three periods are shown. However, the when corrected data were arranged back into the time series basis as

shown in **Figure 5.4-10**, I need to evaluated how the corrected data improve a simulated discharge. That will be discussed in the next chapter.

Table 5.4-1 Statistical performance of cumulative distribution functions of the raw and corrected GCM precipitation data.

Performance Statistics	**Raw GCM**	**Cor.GCM by Emp.Dis**	**Cor.GCM by Q-Q**
Mean dif. (Obs-GCM)	-0.67	-0.003	0.00
Max dif. (Obs-GCM)	-60.5	-72.30	0.00
Standard Deviation : S_{obs} = 5.95			
S_{GCM}	5.39	5.59	5.95
Comparison based on the ranged data			
Efficiency Index : EI	0.90	0.93	1.0
Root Mean Square Error: RMSE (mm/day)	1.87	1.59	1.0
Mean Absolute Error: MAE (mm/day)	1.09	0.41	1.0
Correlation coefficient : R	0.96	0.96	1.0

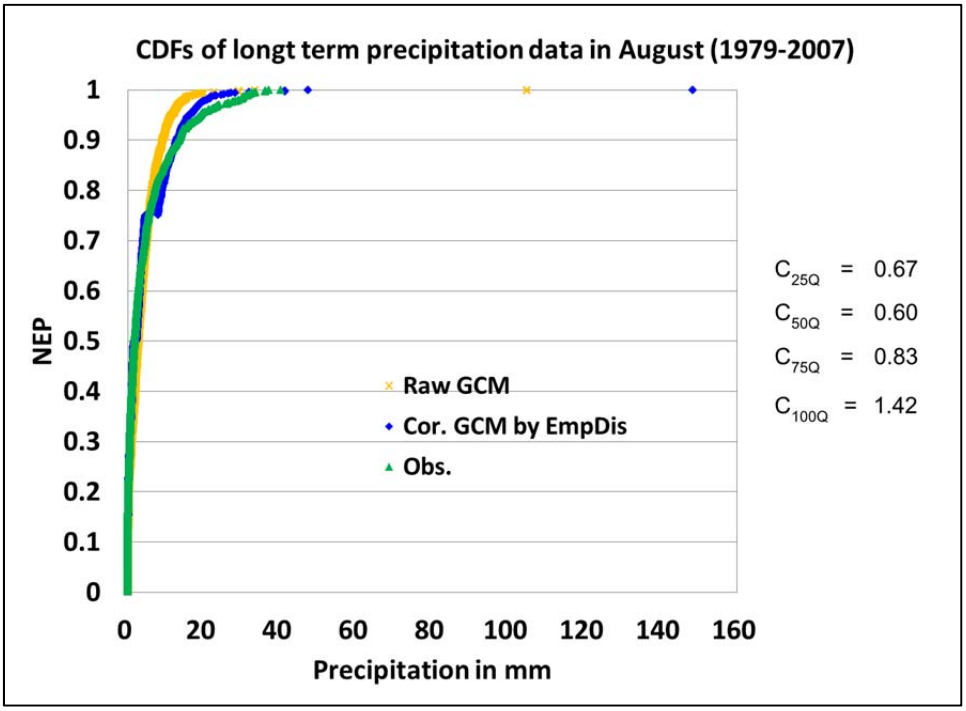

Figure 5.4-9 Cumulative distribution functions of long term precipitation data of raw GCM, corrected GCM by empirical distribution method and observation in August (1979-2007).

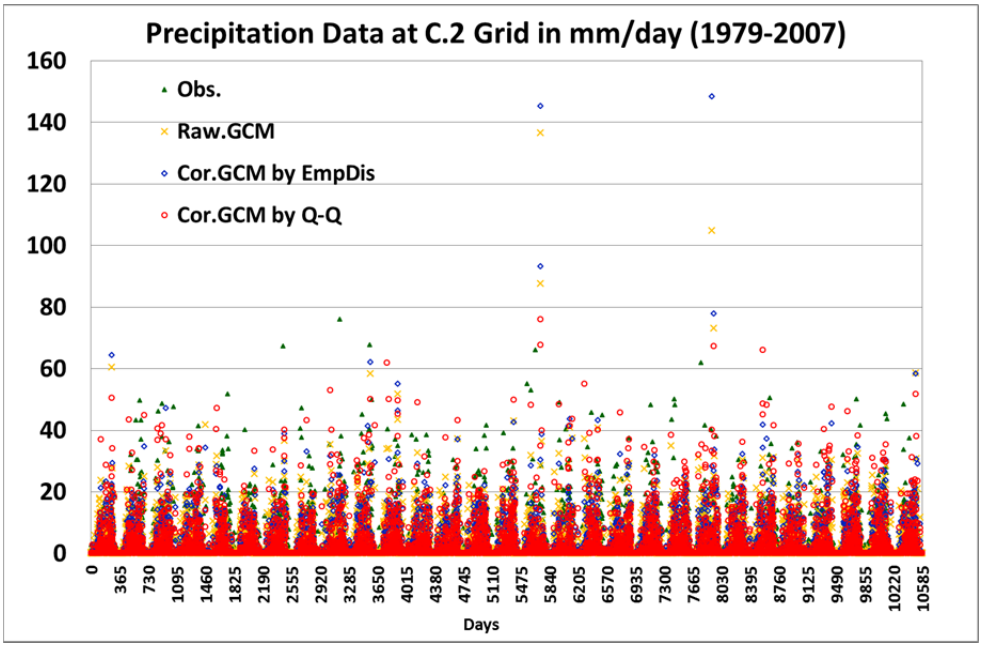

Figure 5.4-10 Comparison of time series daily precipitation data of observation, raw GCM, corrected GCM by empirical distribution method, and corrected GCM by quantile-quantile method.

5.4.2 Bias Correction of Evapotranspiration

Bias correction of evapotranspiration was directly adjusted a mean monthly GCM evapotranspiration without considering a distribution by the multiplicative factor and the difference method. The truth reference data for bias correction is mean monthly ET_o derived from the observation climatology data over 30 year. To consider the evapotranspiration at C.2 station grid, the mean annual GCM evapotranspiration is significantly low than the mean annual ET_o about 38% where total amount of annual ETo is approximately 1,544 mm. **Figure 5.4-11,** clearly shows that in dry season (December – April) the GCM evapotranspiration is considerably lower than the ET_o. This also occurred in the other grids around the center of the basin. One of the important factors leading the ET_o higher than the GCM evapotranspiration in the dry season is an effect for irrigated water. Most of the irrigation areas of the CPRB are located at the center of the basin.

Figure 5.4-12 show averages of mean monthly evapotranspiration of the baseline period total 29 year (1979-2007) for the ET_o, raw GCM evapotranspiration and corrected GCM evapotranspiration by both correction methods. **Figures 5.4-13** and **5.4-14** illustrate average of mean monthly evapotranspiration of the projection periods, near future and future. That both raw GCM evapotranspiration in the projection periods are lower than the ET_o as well.

I found a limitation of the multiplicative factor correction. At grid points and within months where the mean monthly GCM evapotranspiration is very low, while mean ET_o data are significantly higher, the multiplicative correction factor can get quite high. When I multiplied singular high daily evapotranspiration values by that high correction

factor, it leads to unphysically high values of daily corrected evapotranspiration. Therefore, the different factor correction method can avoid producing unphysically high values by the phenomena mentioned above.

Refer to **Figures B-16** and **B-19** in Appendix B, spatial differences in mean annual corrected evapotranspiration of two correction methods are illustrated and I notice that there are some particular grids in north-west of the study area show extremely high values for the near future and future climate experiments.

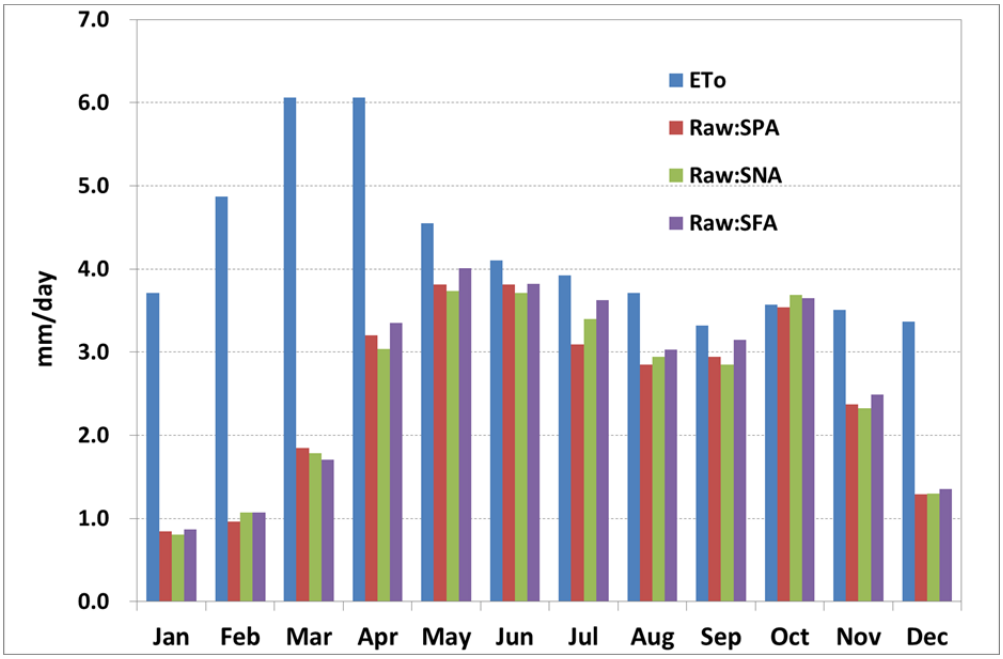

Figure 5.4-11 Histograms comparing mean monthly evapotranspiration of reference evapotranspiration (ET_o), raw current GCM evapotranspiration (Raw:SPA), raw near future GCM evapotranspiration (Raw:SNA), and raw GCM future evapotranspiration (Raw:SFA).

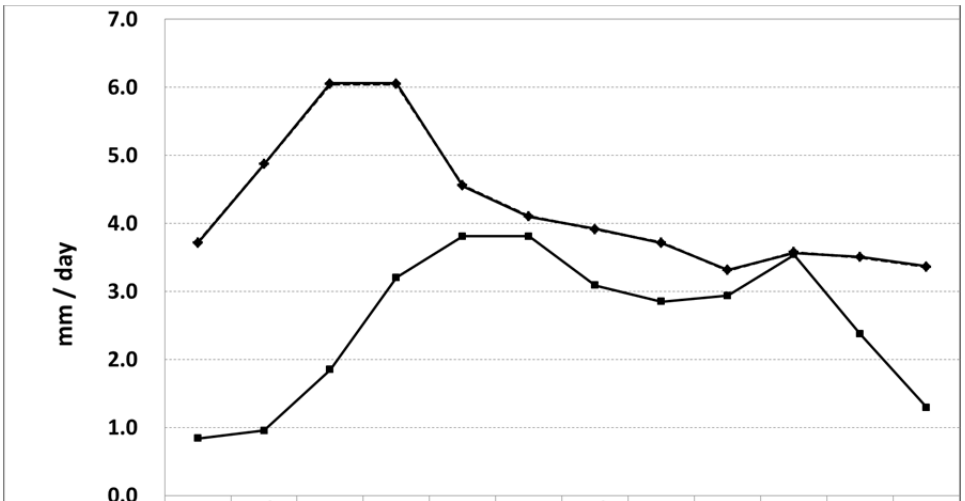

	Jan	Feb	Mar	Apr	May	Jun	Jul	Aug	Sep	Oct	Nov	Dec
ETo	3.71	4.87	6.06	6.06	4.55	4.10	3.92	3.71	3.32	3.57	3.51	3.37
Raw:SPA	0.84	0.96	1.85	3.20	3.81	3.81	3.09	2.85	2.94	3.54	2.38	1.29
Cor:SPA (MF)	3.72	4.87	6.05	6.05	4.56	4.10	3.91	3.72	3.31	3.58	3.50	3.36
Cor:SPA (DF)	3.72	4.87	6.05	6.05	4.56	4.10	3.91	3.72	3.31	3.58	3.50	3.36

Figure 5.4-12 Averages of mean monthly evapotranspiration for current climate 1979–2007 from: reference evapotranspiration (ET_o), raw GCM (Raw:SPA), corrected GCM by multiplicative factor method (Cor:SPA(MF)), and corrected GCM by different factor method (Cor:SPA(DF)).

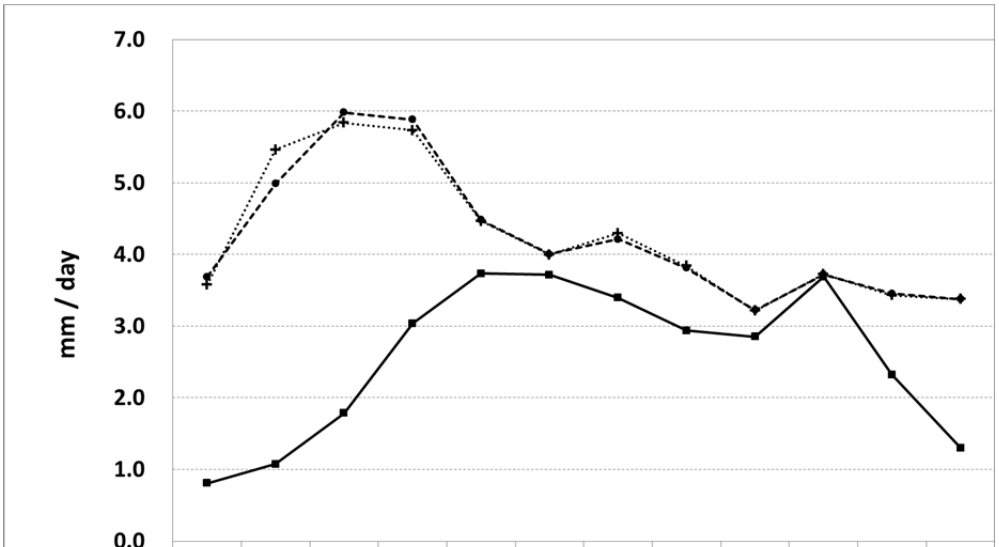

	Jan	Feb	Mar	Apr	May	Jun	Jul	Aug	Sep	Oct	Nov	Dec
Raw:SNA	0.81	1.07	1.79	3.04	3.73	3.71	3.39	2.94	2.85	3.69	2.33	1.30
Cor:SNA (MF)	3.58	5.46	5.84	5.73	4.47	4.00	4.29	3.84	3.21	3.72	3.43	3.38
Cor:SNA (DF)	3.69	4.99	5.98	5.88	4.48	4.01	4.21	3.81	3.22	3.72	3.45	3.38

Figure 5.4-13 Averages of mean monthly evapotranspiration for near future climate 2015–2043 from: reference evapotranspiration (ETo), raw GCM (Raw:SNA), corrected GCM by multiplicative factor method (Cor:SNA(MF)), and corrected GCM by different factor method (Cor:SNA(DF)).

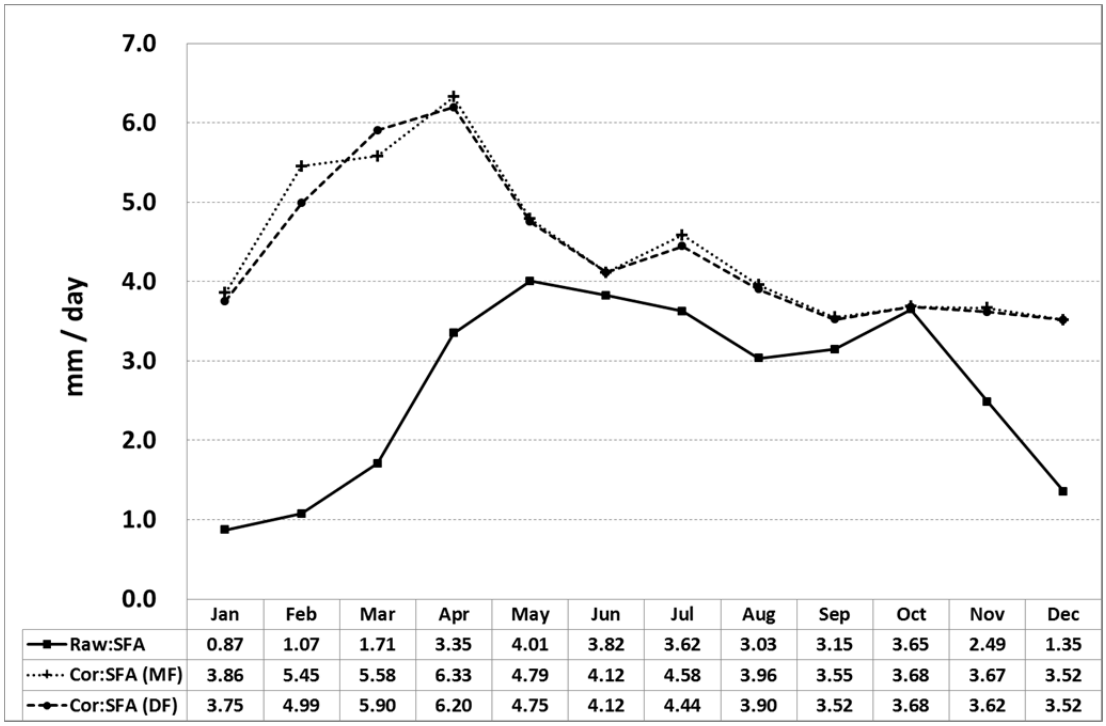

	Jan	Feb	Mar	Apr	May	Jun	Jul	Aug	Sep	Oct	Nov	Dec
Raw:SFA	0.87	1.07	1.71	3.35	4.01	3.82	3.62	3.03	3.15	3.65	2.49	1.35
Cor:SFA (MF)	3.86	5.45	5.58	6.33	4.79	4.12	4.58	3.96	3.55	3.68	3.67	3.52
Cor:SFA (DF)	3.75	4.99	5.90	6.20	4.75	4.12	4.44	3.90	3.52	3.68	3.62	3.52

Figure 5.4-14 Averages of mean monthly evapotranspiration for future climate 2075–2103 from: reference evapotranspiration (ET_o), raw GCM (Raw:SFA), corrected GCM by multiplicative factor method (Cor:SFA(MF)), and corrected GCM by different factor method (Cor:SFA(DF)).

5.5 Conclusion

In this chapter, I have applied bias correction methods to both precipitation and evapotranspiration. For the GCM precipitation and evapotranspiration data, PRCSL and EVPSL and TRNSL variables were extracted from the MRI-AGCM3.2S. APHRODITE precipitation data in resolution 0.25 degree were used as reference observation precipitation data. Reference evapotranspiration calculated by Penman-monteith equation using recorded climatological data over 30 years (1981 - 2010) has been used for the reference truth data for the precipitation. Due to an availability of the ETo, I reformat point data to 20 km resolution grid based which is same the GCM resolution. The baseline of the correction is 29 years 1979-2007 and two projection periods in the

near future and future climate experiments.

Bias in the frequency distribution of GCM precipitation has more influence by show in high number of wet days especially in the dry season. Hence, the wet days were adjusted to correct the frequency distribution bias. Also bias in the intensity distribution of GCM precipitation shows clearly with the higher intensity comparing to the truth reference data in the dry season. The empirical distribution and quantile-quantile bias correction methods effectively improved both the mean and the variance of GCM precipitation. As theses correction methods are based on the monthly CDFs of the long term precipitation data. Therefore both two bias correction methods might destroy the physical consistency of the original GCM data.

For bias in GCM evapotranspiration, two simple methods removed the bias in the data by adjusting mean monthly evapotranspiration. Both two correction methods, the Multiplicative factor and the Different factor, completely improved the mean monthly GCM evapotranspiration. However, some limitation occurred when I applied the multiplicative factor to correct daily GCM evapotranspiration in the projection period. It showed unphysically high values of the daily corrected data in some grids. By looking over spatial mean annual corrected evapotranspiration data, the different factor showed a consistency of the data in each grid over the study area.

Based on our study in this chapter, I could not make a judgment on which combination of the precipitation and evapotranspiration correction methods would provide the best result in a river discharge simulation. Therefore, all these corrected precipitation and evapotranspiration data will be input to the regional distributed hydrological model of the CPRB to simulate a river discharge and discussed in the next chapter.

Chapter 6

River discharge assessment under a changing climate in Chao Phraya River, Thailand

6.1 Introduction

Prediction of the Chao Phraya River discharge has been conducted for water resources assessment of the basin by utilizing outputs of the MRI-AGCM3.2S (20 km resolution) without bias correction. The result showed that water availabilities in the CPRB increase all year round, both in the wet and dry seasons in the future climate experiment, and during dry season of the near future climate trends of projected discharge considerably reduced (Wichakul et al., 2014). However, direct usage of hydrological variables of the GCM does not provide reliable information on scales below about 200 km (Maraun et al., 2010). Therefore, for reliable and realistic prediction result of the river discharge situation of the Chao Phraya River, I introduced several bias correction methods to the MRI-AGCM3.2S outputs, precipitation and evapotranspiration. Bias in the GCM precipitation distribution was removed by the empirical distribution and quantile-quantile correction methods. For the GCM evapotranspiration, the multiplicative factor and different factor correction methods were applied.

The chapter aims to project discharge of the Chao Phraya River and to evaluate tendency of flood and drought risks under a changing climate by using the bias-corrected GCM precipitation for a reliable result.

6.2 Methodology

6.2.1 Input data and study area

Original input data are the MRI-AGCM3.2S variables, PRCSL TRNSL and EVPSL, derived for the precipitation and evapotranspiration (Wichakul et al., 2014). Input data in this chapter have been processed to remove biases as explained in the previous

chapter. APHRODITE precipitation and the reference evapotranspiration (ET_o) were used to simulate the reference as observed discharge. There are four sets of the bias-corrected input data, which are 1) bias-corrected GCM precipitation by the quantile-quantile method with corrected GCM evapotranspiration by the multiplicative factor (PRCSL:CorQQ:CorEvapMF), 2) bias-corrected GCM precipitation by the empirical distribution method with corrected GCM evapotranspiration by the multiplicative factor (PRCSL:CorEmp:CorEvapMF), 3) bias-corrected GCM precipitation by the quantile-quantile method with corrected GCM evapotranspiration by the different factor (PRCSL:CorQQ:CorEvapDel), and 4) bias-corrected GCM precipitation by the empirical distribution method with corrected GCM evapotranspiration by the multiplicative factor (PRCSL:CorEmp:CorEvapDel).

Study area is the Chao Phraya River basin, Thailand. The discharge monitoring is at C.2 located about 5 km downstream of the Ping River and Nan River confluence, beginning of the Chao Phraya River. The location of the C.2 station can represent the overall situation of the Chao Phraya River.

6.2.2 Modeling approach

The regional distributed hydrological model composes of rainfall-runoff model and flow routing model including dam operation. The rainfall-runoff named the Simplified Xinanjiang model (SXAJ). It was established based on the concept of the variable infiltration capacity. 1K-FRM is a 1 kilometer resolution flow routing using a kinematic wave equation (Wichakul et al., 2013a). In part of flow routing, the 1K-FRM was additionally developed to include the inundation effect to improve predicted discharge for the Chao Phraya River Basin. (Wichakul et al., 2013b).

I conducted simulations by using different sets of the bias-corrected precipitation and evapotranspiration to be input data to the SXAJ model to generate runoff intensity represented 1120 (28 columns and 40 rows) grid cells covering the CPRB. Then, the 1K-FRM represents 288,000 (480 columns and 600 rows) computational grid. The predicted discharge was extracted at the C.2 grid.

6.2.3 Selecting of bias-corrected input

The simulated discharges from four sets of input data were compared to select the best fit with the reference observed discharge to be a representative of a river discharge projection in the present climate 1979-2007. The best simulated discharge that provide a reasonable result of the river discharge at monitoring point was utilized for the river discharge assessment under the impacts of climate change.

Figure 6.2-1 shows all simulated long term hydrographs generated from different input data for the present climate. To select the best set of bias corrected data, volume of the hydrographs was calculated to compare the difference with the reference observed discharge. **Table 6.2-1** shows that the simulated discharge form the bias-corrected precipitation by the quantile-quantile method with the bias-corrected evapotranspiration by the different factor (PRCSL:CorQQ:CorEvapDel) performed well with the smallest difference between the volume of its hydrograph and the reference observed hydrograph approximately 6%.

Accordingly, the future river discharge projection was conducted by using the input that bias-corrected by the quantile-quantile method and different factor method for the GCM precipitation and evapotranspiration, individually. **Figures 6.2-2, 6.2-3 and 6.2-4** illustrate comparisons of the simulated discharge by using raw GCM data versus

bias-corrected GCM data from the quantile-quantile method and different factor method for present climate, near future and future, respectively. After removing biases from the input data, simulated discharge volume of the raw GCM input was thus reduced about a 29% 24% and 22% in the present climate, near future and future climate, correspondingly. .

Table 6.2-1 Volume of simulated long term hydrographs for different input data sets.

Set of input data	Precipitation	Evapotranspiration	Total volume in MCM
APHRO_EvapETo	APHRODITE	ETo	705,652
Prcsl:CorQQ:CorEvapMF	Bias-corrected GCM by Quantile-quantile	Bias-corrected GCM by Mutiplicative factor	848,361
Prcsl:CorEmp:CorEvapMF	Bias-corrected GCM by Empirical distribution	Bias-corrected GCM by Mutiplicative factor	899,350
Prcsl:CorQQ:CorEvapDel	Bias-corrected GCM by Quantile-quantile	Bias-corrected GCM by Different factor	747,473
Prcsl:CorEmp:CorEvapDel	Bias-corrected GCM by Empirical distribution	Bias-corrected GCM by Different factor	775,143

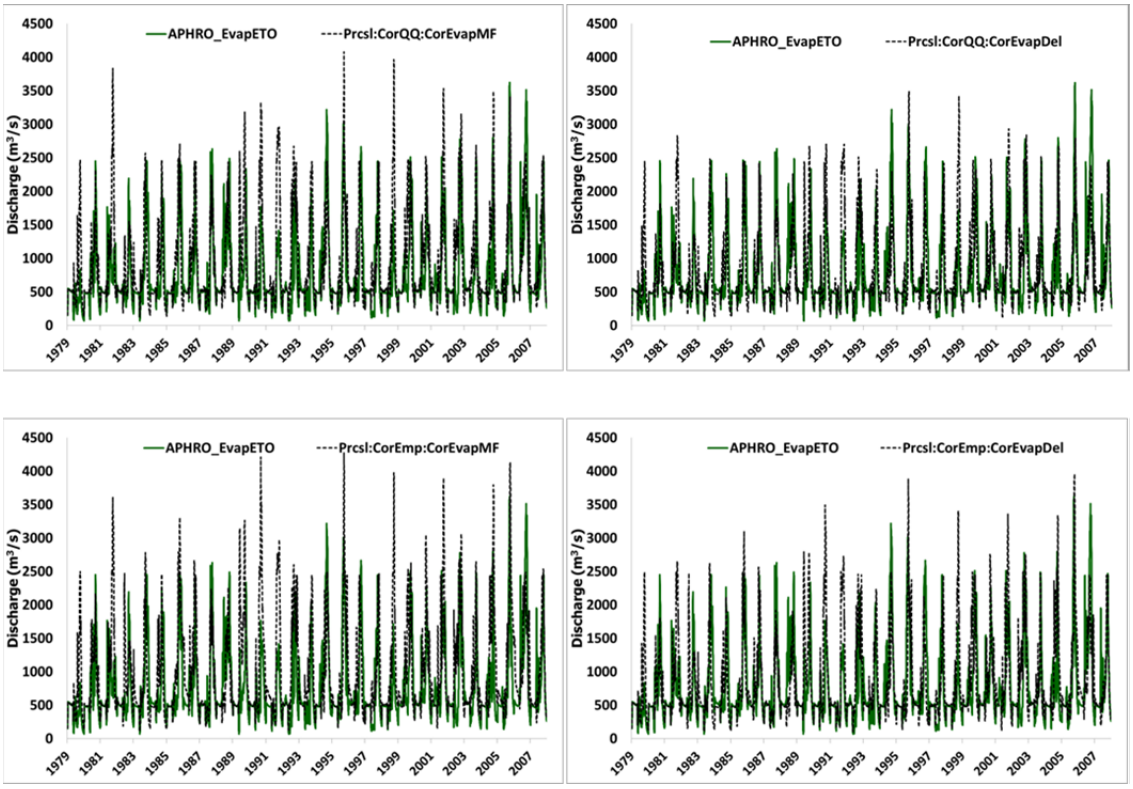

Figure 6.2-1 Comparisons of simulated discharge using different input data. Solid green line is river discharge simulated by the APHRODITE precipitation and ET_o. Dot black lines are river discharge simulated by the bias-corrected GCM precipitation and evapotranspiration.

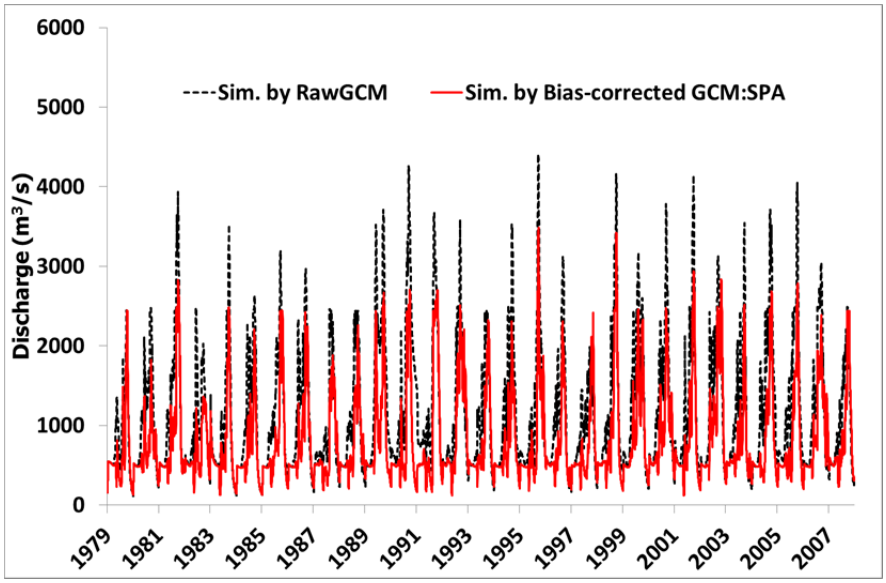

Figure 6.2-2 Daily simulated discharge by using raw GCM data versus bias-corrected GCM data at C.2 station for present climate 1979-2007.

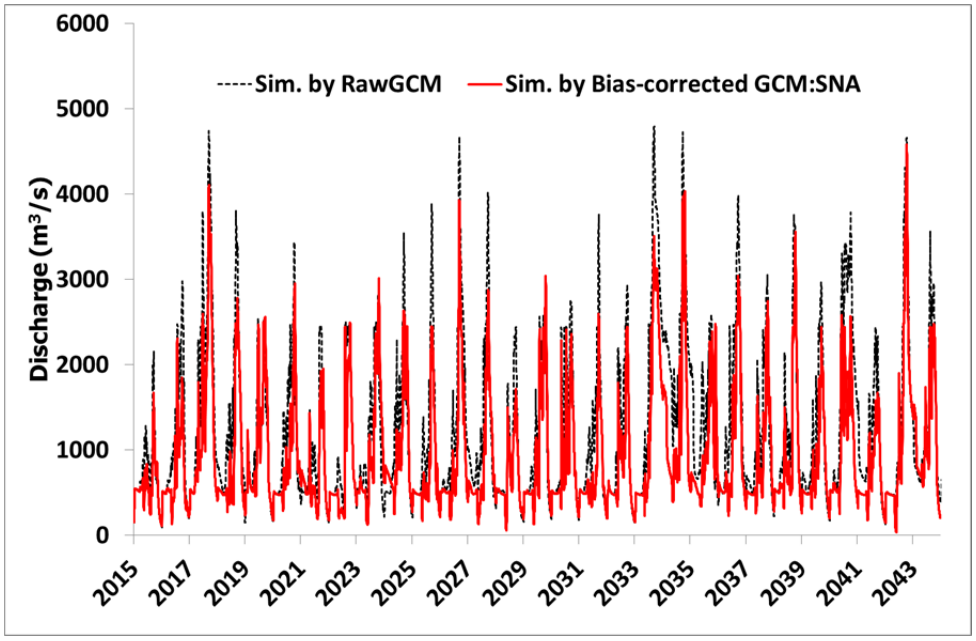

Figure 6.2-3 Daily simulated discharge by using raw GCM data versus bias-corrected GCM data at C.2 station for near future climate 2015-2043.

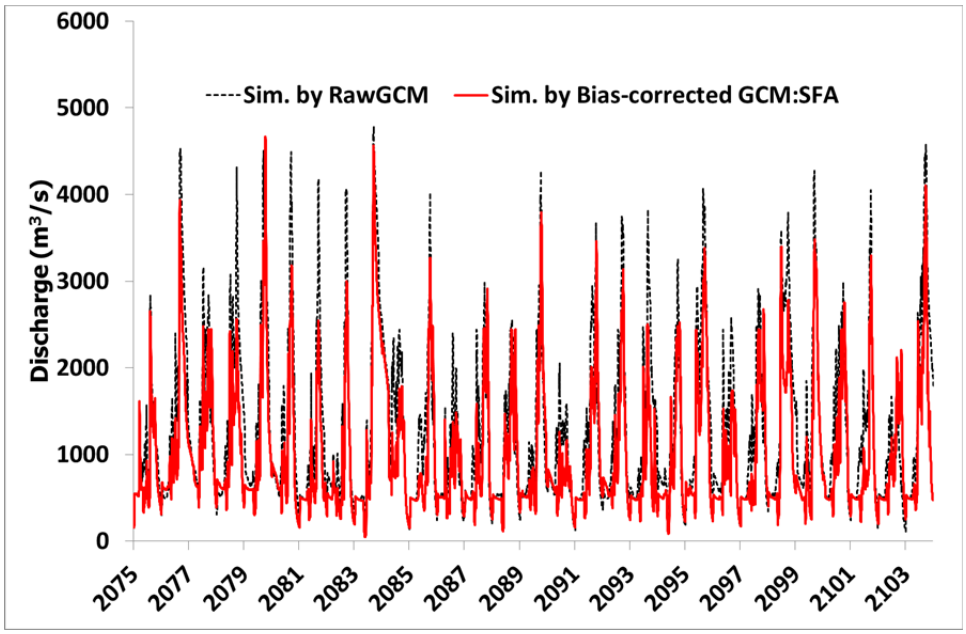

Figure 6.2-4 Daily simulated discharge by using raw GCM data versus bias-corrected GCM data at C.2 station for future climate 2075-2103.

6.3 Result and discussion

6.3.1 River discharge assessment under a changing climate

By using the bias corrected precipitation and evapotranspiration as input to the regional distributed hydrological model, I generated series of daily discharge for twenty night (29) year in each climate experiment period. Mean monthly discharge at the monitoring station, C.2 station, has been calculated to detect trend of stream flow change under a changing climate as plotted in **Figure 6.3-1**. It shows mean monthly discharge at for three climate experiments. For the future climate, comparison of the discharge of the present climate (1979-2007) and the future climate (2075-2103) shows significant increases about 10% to 41% of the mean monthly discharge in the present climate. For the near future, most of the months the mean monthly discharge shows a bit increase about 10% to 25% of the mean monthly discharge in the present climate. On the other hand, the discharge of the near future climate extremely rises up in October at the same rate of increase as the next three decades. Only in May, the mean discharge does not much change. According of the Thailand climatology, May is the end of summer season and beginning of rainy season. That is why effect of changes of temperature (or evapotranspiration) and rainfall intensity have less effect to the mean discharge in this month.

One of important tools to characterize the response of the river to a changing climate is flow duration curve. The probability of exceedance (P) of mean annual flow magnitude of each climate experiment periods are illustrated in flow duration curves. **Figure 6.3-2** presents mean annual flow duration curves with standard deviations for the three climate experiments. It clearly shows that the magnitudes of river flow considerably rise

up for $P < 0.6$ in both the near future and future climate experiments. The magnitude of river discharge in the future period has a tendency to increase for all occurrence time.

For $P > 0.6$, there is no a significant signal of changes in mean annual flow for the near future and future period. According to the dam operation model embedded in the flow routing model for generating stream flow, discharge during low flow season was influenced by the dam model (Wichakul et al., 2011). It means that future inflow into dams dose not much change, so the dam operation model still operates and releases flow from storage water to downstream as operating in the current climate. However, to enlarge the low flow section, **Figure 6.3-3** compares the flow duration curves constructed based on daily discharge of a period-of-record of each climate experiment at the low flow section. Therefore, it is clear that the low flow values tend to decrease in the near future experiment which might result in increased drought risk in the CPRB. Conversely, for the 21st century the low flow values tend to increase roughly 15 % of the flow in the present climate period. For the flood risk assessment, the frequency analysis of the extreme events is generally applied to evaluate to risk that I discuss in the next paragraph.

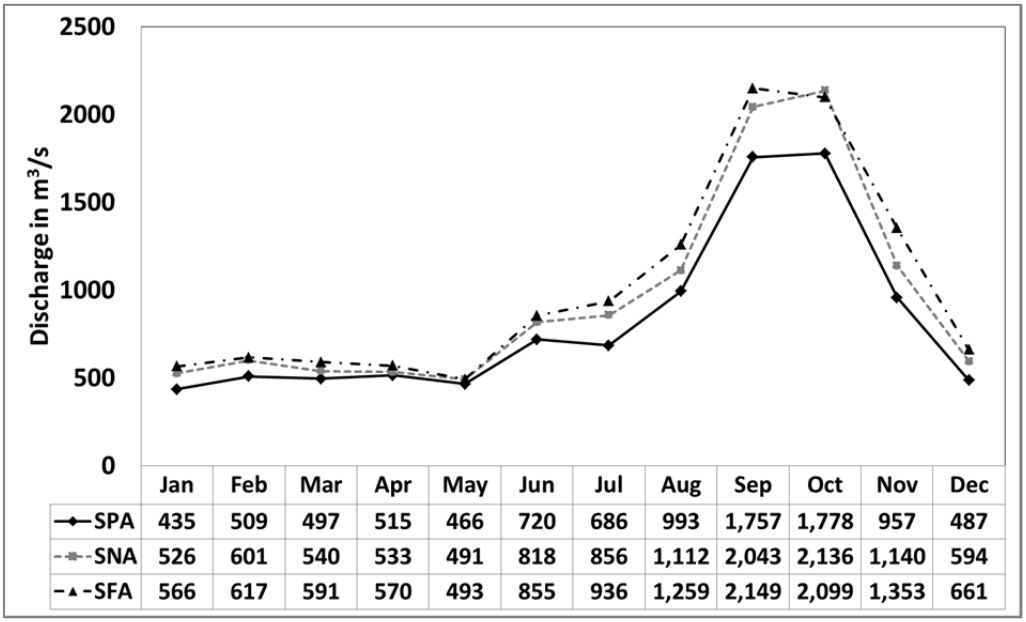

	Jan	Feb	Mar	Apr	May	Jun	Jul	Aug	Sep	Oct	Nov	Dec
SPA	435	509	497	515	466	720	686	993	1,757	1,778	957	487
SNA	526	601	540	533	491	818	856	1,112	2,043	2,136	1,140	594
SFA	566	617	591	570	493	855	936	1,259	2,149	2,099	1,353	661

Figure 6.3-1 Mean monthly discharge at the C.2 station for the present (SPA), near future (SNA) and future climate experiments (SFA).

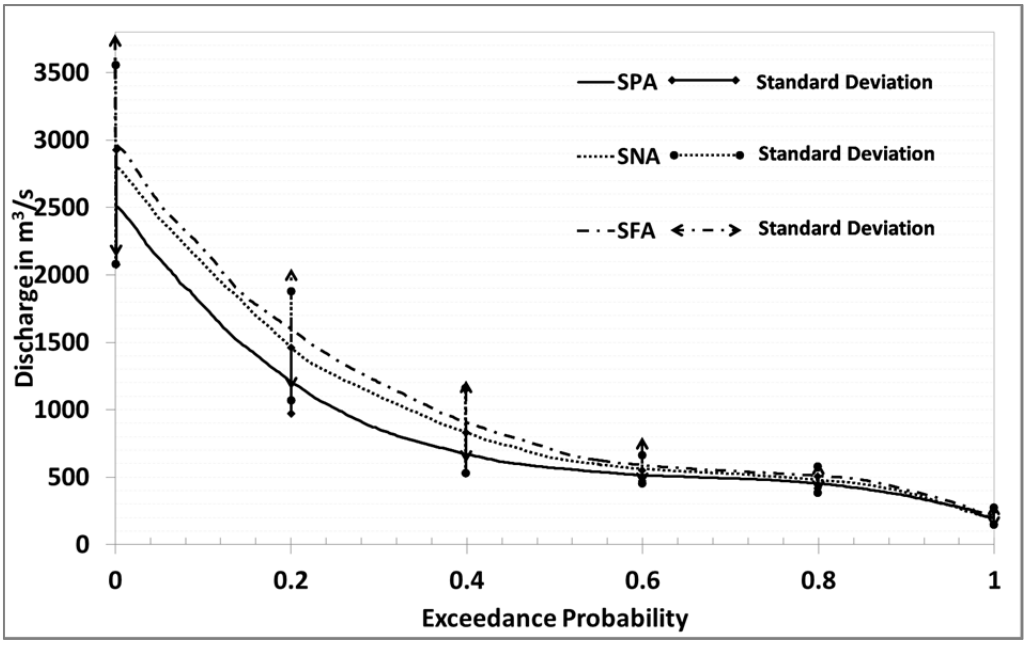

Figure 6.3-2 Mean annual flow duration curves with standard deviation of the present climate (SPA), near future climate (SNA), and future climate (SFA) experiments.

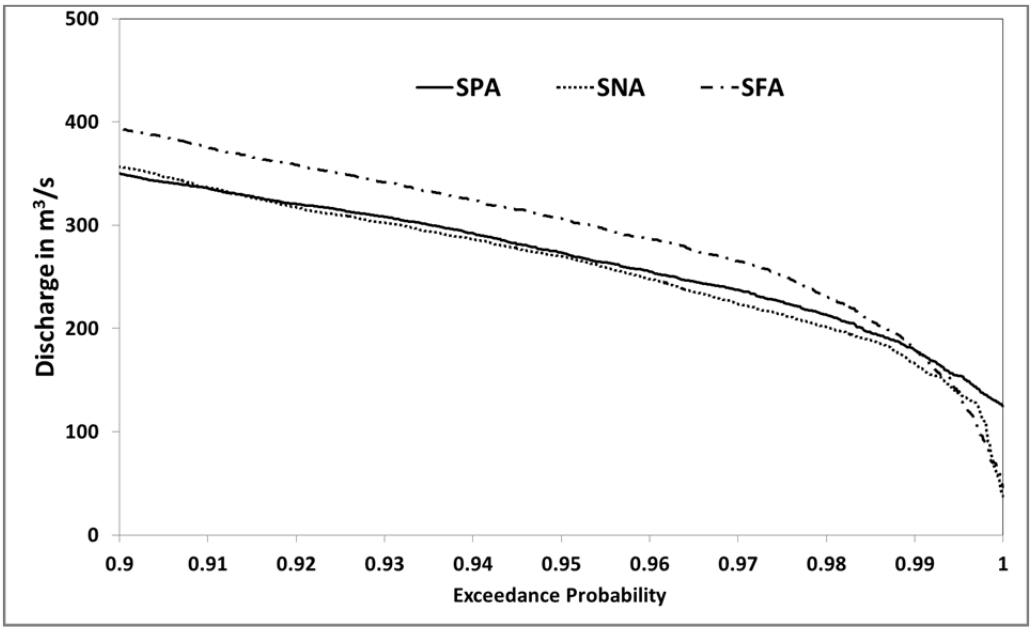

Figure 6.3-3 Low flow section of the flow duration curves constructed based on daily discharge of a period-of-record of each climate experiment.

6.3.2 Frequency analysis of extreme events

Frequency of occurrence of the extreme events is analyzed by fitting the probability distribution function (PDF) of extreme values with three families of distribution functions, Square-root exponential type maximum distribution (SqrtET), Generalized extreme value distribution (GEV), and Gumbel distribution. The following are the cumulative distribution functions (CDFs) of each distribution.

The Square-root exponential type maximum distribution's CDF is as:

$$F(x;\ \beta,\lambda) = \begin{cases} -\lambda\{\left(1+\sqrt{\beta x}\right)\ exp\left(-\sqrt{\beta x}\right)\} & x \geq 0, \\ 0 & x < 0. \end{cases} \qquad (6\text{-}1)$$

In which β is the scale parameter, and λ is the frequency parameter (Etoh et al., 1987). The generalized extreme-value (GEV) distribution has a cumulative distribution function with a parameter $k \neq 0$ as:

$$F(x;c,a) = exp\left[-\left(1-k\frac{x-c}{a}\right)^{1/k}\right] \quad (6\text{-}2)$$

where x is an annual maximum daily discharge; a is a positive scale parameter; c is a location parameter and k is a negative shape parameter. In case of $k = 0$, the GEV distribution is equivalent to the Extreme Value Type I distribution or the Gumbel distribution. The cumulative distribution function of Gumbel distribution is shown as:

$$F(x;c,a) = exp\left[-exp\left(-\frac{x-c}{a}\right)\right] \quad (6\text{-}3)$$

For the Gumbel distribution, x is unbounded ($-\infty < x < \infty$) (Takara, 2009).

The annual maximum series of river flow at the C.2 station was extracted from three periods of simulation, to fit with the distribution function as mention above. **Figures 6.3-4 6.3-5, and 6.3-6** illustrate the CDFs of twenty night (29) values of annual maximum river flow fit with different functions for SPA SNA, and SFA, respectively.

Standard least-squares criterion (SLSC) is a criterion I use to evaluate goodness of fit of each distribution to the annual maximum daily discharge. It was proposed by Takara and Takasao (1998). Afterward, Tanaka and Takara (1999) proved that SLSC < 0.04 is acceptable to river discharge frequency analysis in Japan. However, the Chao Phraya River Basin topographic condition is very different to river basins in Japan. Therefore, I evaluated the acceptable SCSC by the smallest value among each probability distribution function. **Table 6.3-1** shows comparison of the goodness-of-fit for the annual maximum daily discharge at the C.2, Y.16, N.67 and P.17 stations for present climate (1979-2008) near future climate (2015-2043) and future climate (2075-2013).

The Y.16 is located at 16°45'N and 100°07'E on the Yom river upstream of the N.67

station (15°52'N and 100°15'E). Other monitoring location is at 15°56'N and 99°58'E on the Ping River named P.17 station. From the **Table 6.3-1**, it shows that among these probability distribution functions, GEV distribution function provides the best goodness-of-fit to the annual daily maximum discharge of the projection periods for all locations. Therefore, I selected the GEV for evaluating change in extreme floods and assessing flood risk.

Table 6.3-1 Goodness-of-fit criteria for each probability distribution function.

Standard Least Squares Criterion, SLSC												
PDF	C.2			Y.16			N.67			P.17		
	SPA	SNA	SFA	SPA	SNA	SFA	SPA	SNA	SFA	SPA	SNA	SFA
Gumbel	0.071	0.036	0.043	0.035	0.056	0.058	0.047	0.031	0.054	0.036	0.087	0.120
SqrtEt	0.090	0.038	0.067	0.046	0.051	0.059	0.059	0.043	0.073	0.054	0.098	0.122
Gev	0.092	0.037	0.029	0.035	0.050	0.058	0.034	0.030	0.040	0.020	0.060	0.078

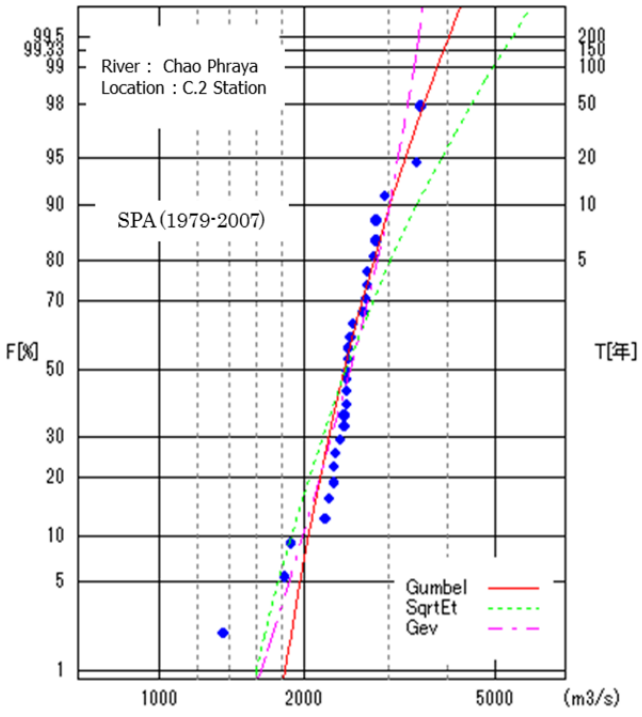

Figure 6.3-4 Cumulative distribution functions of the annual maximum daily discharge at C.2 station for present climate.

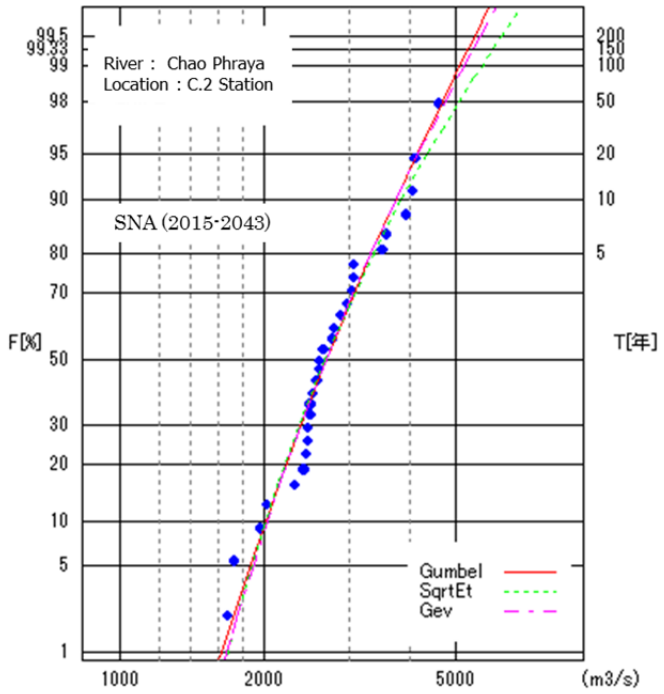

Figure 6.3-5 Cumulative distribution functions of the annual maximum daily discharge at C.2 station for near future climate.

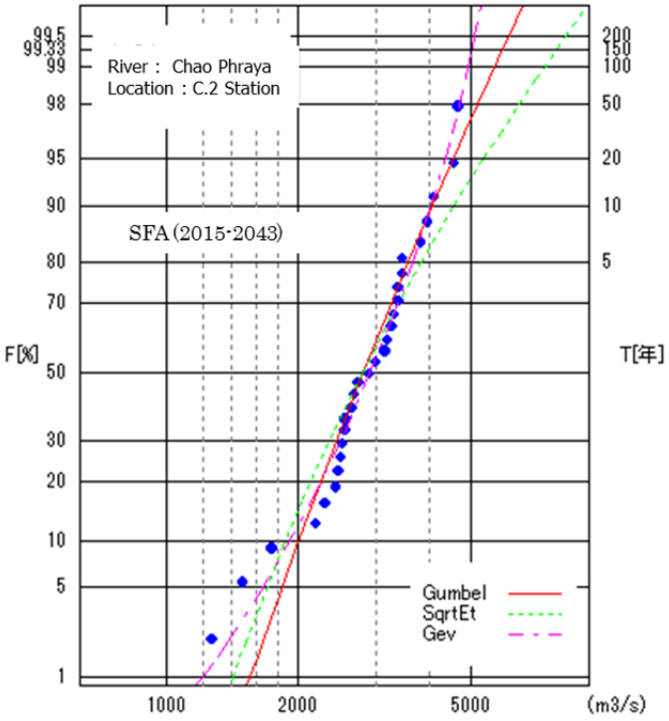

Figure 6.3-6 Cumulative distribution functions of the annual maximum daily discharge at C.2 station for future climate.

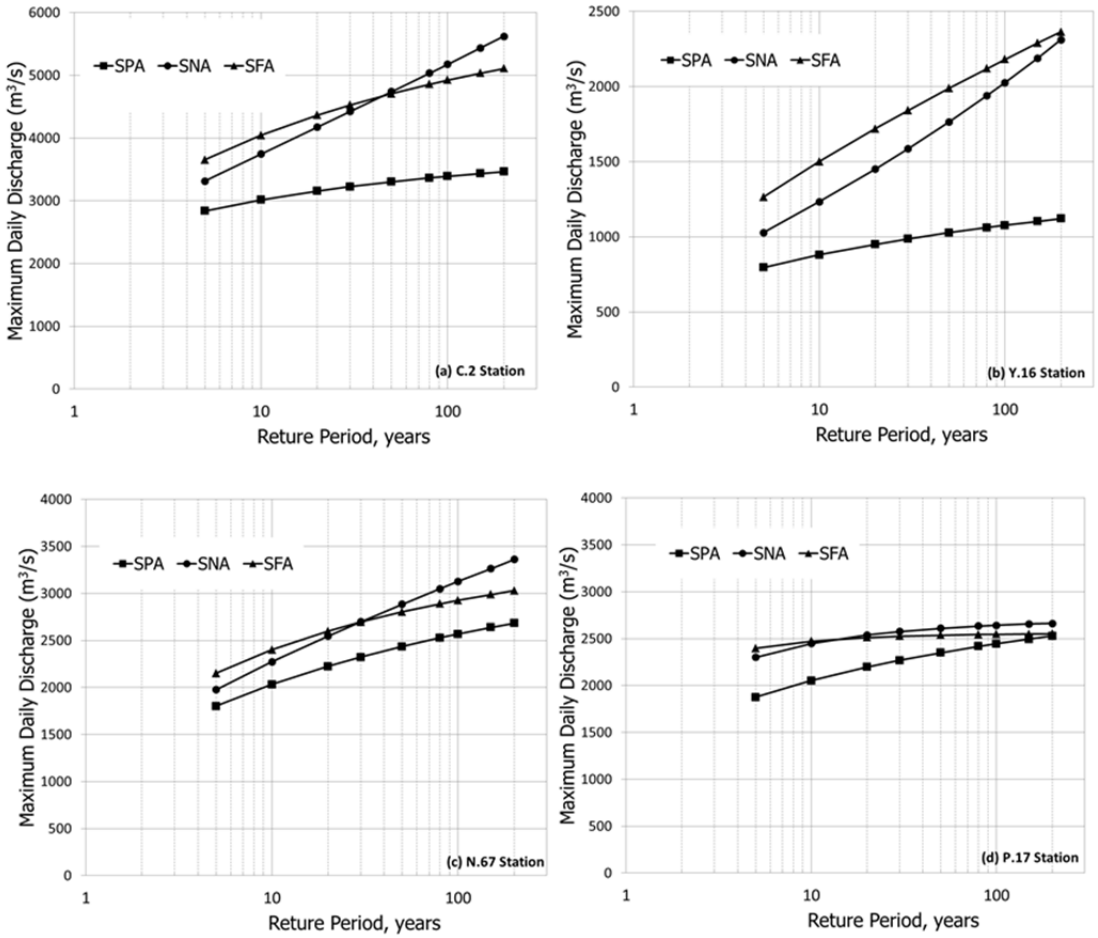

Figure 6.3-7 Maximum daily discharge corresponding to different return periods for present climate (SPA), near future climate (SNA) and future climate (SFA) for each location.

Changes in return period of flood for different periods are illustrated in **Figure 6.3-7** for four different locations; (a) for C.2 station, (b) for Y.16 station, (c) for N.67 station and (d) for P.17 station. The assessment has been conducted by comparing the return period of the 5-year, 10-year, 20-year, 30-year, 50-year, 80-year, 100-year, 150-year, and 200-year. The short return periods (shorter than 50-year return period) are relevant to flood related design structure according the impacts of climate change, such as irrigation structure, urban drainage and bridge. Refer to **Figure 6.3-7a**, in 21st century

the magnitude of extreme events at the C.2 station significantly increase for the return period shorter than 50-year and also it is larger than the magnitude of the flood events in the near future climate (2015-2143). For the long return periods (form 80-year return period), the magnitude of discharge is extremely high in the near future climate. That change in the C.2 station mostly corresponds to change in flood magnitude in the P.17 and N.67 stations for both near future and future periods, referring to **Figures 6.3-7c and 6.3-7d.** Flood frequency analysis of the Y.16 station showed different pattern from other location as illustrated in **Figure 6.3-7b** because location of the Y.16 station is far for the location of those another three stations. Flow from the Y.16 station merges with the Nan river at the confluence located upstream of the N.67 station.

The corresponding discharge of the C.2 station (5,034 m^3/s) at 80-year return period of the near future is larger than the peak discharge of Thai's flood 2011 (4,686 m^3/s). Consequently, overall trend shows the flood risk is increase in the future that will cause more damage to the CPRB.

6.4 Conclusion

Four sets of bias-corrected outputs of the MRI-AGCM3.2S, precipitation and evapotranspiration, were applied to the Chao Phraya River for projection river discharge in the present climate (1979–2007). The regional distributed hydrological model including the effect of dam operation and inundation simulated the river discharge. Simulated long term hydrographs from different sets of the input data were compared with the reference observed hydrograph. Result shows that the hydrograph simulated by using the bias-corrected precipitation by the quantile-quantile method with the bias-corrected evapotranspiration by the different factor achieved a well fit with the

reference observed discharge at the C.2 station.

Consequently, the bias-corrected GCM data have been conducted for the near climate future and the future climate experiments. Changes in the projected river discharge at the C.2 station, Nakorn Sawan province can be concluded that 1) the mean annual discharge tends to increase in both near future and future projection periods, 2) during a dry season the tendency of low flow in the near future period leads to decrease. These findings of our study are also compatible with previous studies of Hunukumbura and Tachikawa (2012), and Kure and Tebakari (2012); but it is contradictory with the study result of Champthong et al., (2013). Furthermore, the GEV was applied for flood frequency analysis which indicates that flooding frequency has increased, leading high flood risk in the future. Flood in the basin will have more severity; especially in the near future (2015-2043) the magnitude of 80-year return period flood (5,034 m^3/s) is greater than the devastating 2013 Thai flood (4,686 m^3/s). Therefore, adaptation measures to protect damages of flood in the country are critical to accomplish.

Chapter 7

Concluding Remark

The main objectives of this thesis were as follows:

- To develop a regional distributed hydrological model for the Chao Phraya River Basin, Thailand.
- To improve flood movement simulation of the extreme flood event by including a dam operation and inundation effect.
- To propose statistical bias correction methods for the daily GCM precipitation and daily GCM evapotranspiration.
- To project future discharge of the Chao Phraya River and assess a flood and drought risk of the Chao Phraya River Basin by using the bias-corrected GCM data.

All of the above objectives are involved with the development of distributed hydrological model, which is up-to-date and can reproduce historical floods in the basin, to use as a tool for better understanding of a rainfall-runoff process and river flow simulation, and to utilize the application of the model for predict a water resources situation under a changing climate of the Chao Phraya River.

In Chapter 2, the simplified Xianjiang model based on a concept of variable infiltration capacity and an aquifer condition of the study area, was applied to the study area

covering the Chao Phraya River Basin to generate runoff intensity for each computational grid. The 1-km distributed flow routing model using a kinematic wave equation, 1K-FRM, was modified to include dam operation function. To identify the parameters, the trial-and-error method was achieved by comparing the simulated hydrographs with recorded discharge at the C.2 station and inflow to the Bhumibol and the Sirikit dam in year 2011 for calibration period and Flood in 1995, 2008 and 2010 for validation periods. The agreement between observed discharge and simulated discharge, and the water balance of simulated and observed hydrographs were satisfied by the NSE ranges from 0.62 to 0.87 and the R^2 ranges from 0.63 to 0.87 for the calibration period. By utilizing the model application, the dams in the upper part of the CPRB were proved that they are useful for the flood protection in the basin, yet it also depends on size of their reservoirs.

In Chapter 3, I attempted to improve flow movement in the river channel during flooding period. An inundation model was developed and embedded into the flow routing model, 1K-FRM. Overbank flow in the inundation model was estimated by a broad crested weir equation. Not only the exchange overbank flow between the channel and floodplain pond, but also the underground flow from the floodplain pond back to the channel during recession stage were taken into account of the simulation. Additionally, the inundation model has ten parameters, which were manually identified by trial-and-error method based on experiences from the site investigation. Results demonstrated that only river flow in downstream of the Ping and Nan River basins was influenced by the inundation effect. That is clearly shown by the similar shape of simulated hydrographs at the Bhumibol and Sirikit dams. The routing model including the inundation effect improved the simulated hydrograph at the C.2 station well. The

volume of the simulated hydrograph in 2011 was slightly larger (10%) than the volume of the observed hydrograph at the C.2 station.

Chapter 4 shows simulation result of the regional distributed hydrological model forcing with outputs of the MRI-AGCM3.2S without any bias correction for the present climate (1979–2008), the near climate future (2015–2044) and the future climate (2075–2104) experiments. PRCSL is a precipitation to bare soil and summation of TRNSL and EVPSL is a total evapotranspiration. Result showed that water availabilities in the CPRB increase all year round, both in the wet and dry seasons in the future climate experiment. For the near future climate annual water budget slightly increases, but during dry season trends of projected discharge considerably reduced.

However, in Chapter 5 for a reliable result of projected discharge under a changing climate, I introduced the bias correction method for GCM precipitation and evapotranspiration, The Empirical distribution and Quantile-quantile bias correction methods effectively improved both the mean and the variance of GCM precipitation. For the GCM evapotranspiration both two correction methods, the Multiplicative factor and the Different facto, can improve the mean monthly GCM evapotranspiration.

Chapter 6, the bias-corrected precipitation by the quantile-quantile method and the bias-corrected evapotranspiration by the different factor was selected to simulate river discharge in the CPRB for the near future and future climate experiments. Result shows that the mean annual discharge at the monitoring location, the C.2 station, tends to increase in both near future and future projection periods, and during a dry season the tendency of low flow in the near future period leads to decrease. Flood frequency

analysis was conduct by the GEV distribution function – it estimated flood risk in the future will have more severity especially in the near future climate experiment.

Remark was made at the result of flood frequency analysis where the return period is longer than 80-year return period – it showed the flood magnitude was very high about 5,034 m^3/s in the near future period. It was also larger than the devastating flood in 2011 4,686 m^3/s. Therefore, to protect considerable damages to communities in along the Chao Phraya River and its tributaries caused by devastating flood, an adaptation and alleviation measures are critical to implement through the integrated and sustainable development of the nation.

APPENDIX A

List of climatological stations.

No.	Station	Latitude	Longitude
1	AYUTTHAYA	100.717	14.517
2	BANGKOKPORT	100.567	13.700
3	BANGNAAGROMET	100.617	13.667
4	BHUMIBALDAM	99.050	17.233
5	CHAINATAGROMET	100.183	15.150
6	CHIANGMAI	98.983	18.783
7	DONMUANGAIRPORT	100.600	13.917
8	KAMPHAENGPHET	99.883	16.800
9	LAMPANG	99.517	18.283
10	LAMPHUN	99.133	18.567
11	LOPBURI	100.617	14.800
12	NAKHONSAWAN	100.167	15.800
13	NAN	100.783	18.783
14	NANAGROMET	100.750	18.867
15	PATHUMTHANI	100.617	14.100
16	PHISANULOK	100.267	16.783
17	PHRAE	100.167	18.167
18	PICHITAGROMET	100.283	16.433
19	SISAMRONGAGROMET	99.867	17.167
20	SUKHOTHAI	99.800	17.100
21	SUPHANBURI	100.133	14.467
22	TAK	99.117	15.883
23	THAWANGPHA	100.800	19.117
24	THOEN	99.233	17.633
25	THUNGCHANG	100.883	19.400
26	UTTARADIT	100.100	17.617

APPENDIX B

1136	1129	1092	1113	1154	1178	1191	1126	1176	1170	1231	1251	1306	1324	1346	1401	1399	1399	1387	1440	1458	1441
1143	1130	1100	1116	1140	1178	1186	1218	1274	1312	1317	1330	1396	1409	1417	1384	1377	1349	1325	1344	1325	1317
1137	1096	1099	1109	1142	1171	1228	1259	1315	1379	1444	1463	1453	1441	1349	1300	1292	1273	1279	1249	1236	1252
1128	1090	1086	1104	1129	1172	1244	1289	1399	1468	1498	1472	1455	1383	1308	1269	1258	1239	1189	1164	1206	1293
1088	1107	1098	1088	1129	1170	1241	1386	1549	1569	1543	1466	1433	1319	1268	1199	1232	1207	1174	1250	1273	1271
1099	1084	1102	1104	1131	1165	1301	1431	1578	1519	1455	1404	1318	1256	1222	1196	1186	1181	1206	1292	1296	1286
1125	1132	1127	1115	1113	1155	1224	1426	1502	1321	1188	1256	1231	1202	1207	1156	1188	1196	1274	1387	1375	1335
1081	1117	1128	1126	1116	1078	1054	1160	1255	1231	1175	1186	1204	1202	1213	1189	1210	1293	1428	1497	1456	1461
1144	1086	1098	1112	1152	1076	972	992	1065	1077	1121	1180	1256	1234	1204	1151	1254	1397	1532	1543	1520	1399
1032	992	1019	1061	1102	1036	979	987	987	1023	1065	1149	1191	1176	1171	1153	1305	1546	1746	1715	1649	1421
858	937	944	978	1044	927	923	978	943	1011	1082	1128	1161	1124	1133	1148	1346	1662	2233	2120	1949	1481
846	834	834	865	869	821	915	965	994	1042	1050	1076	1102	1081	1088	1138	1319	1597	1798	2043	2064	2135
901	838	843	854	844	928	1006	944	943	945	1011	990	1005	1020	1083	1147	1253	1464	1665	1810	1892	2198
1026	898	908	878	856	944	934	901	940	948	969	968	977	1016	1067	1130	1237	1376	1521	1566	1656	1835
1183	976	910	872	859	891	924	1031	1039	1022	1073	1024	1000	1026	1101	1115	1172	1253	1335	1337	1437	1542
1392	1118	942	879	870	895	916	1017	1008	1115	1098	1073	1003	1015	1041	1065	1091	1165	1217	1262	1337	1386
1586	1323	1037	895	853	886	915	956	933	1022	1130	1127	1059	1034	1016	1052	1061	1083	1121	1183	1236	1229
2072	1656	1351	965	859	891	907	961	1021	1061	1170	1189	1129	1017	1008	1026	1025	1013	1020	1047	1081	1090
2898	2204	1582	1181	1039	969	933	972	1070	1066	1181	1166	1071	987	987	999	1035	984	955	965	1002	1023
3724	3256	1848	1279	1103	1060	993	999	993	1004	1115	1128	991	1024	958	916	945	936	937	977	1014	1060
3878	3274	1938	1317	1138	1095	1060	969	907	925	1016	1034	984	1037	921	881	861	857	879	977	1085	1071
3933	3111	2146	1301	1208	1060	1095	977	926	918	942	938	958	972	904	931	879	860	876	935	1023	1062
3975	3247	2396	1557	1253	1084	1112	1027	964	958	930	924	934	973	928	915	947	949	931	930	977	1014
3941	3031	2112	1664	1296	1152	1176	1078	967	908	943	930	945	1011	929	888	916	949	928	923	961	1016
3986	2533	2017	1508	1290	1244	1208	1116	945	834	860	895	923	992	951	840	844	908	942	943	977	1039
2372	2201	1990	1555	1245	1243	1171	1014	827	788	786	862	876	971	914	843	833	912	957	974	1027	1062
2261	2175	1933	1655	1264	1150	998	877	756	761	778	836	974	1004	873	850	912	1030	1041	1074	1074	1101
2826	2642	2013	1763	1350	1119	912	799	786	811	801	838	1086	1058	946	956	1016	1112	1012	1070	1073	1132
3051	3256	2466	1830	1451	1113	944	819	797	774	800	859	1003	1118	982	981	1081	1026	1033	1058	1014	1079
3084	4044	3066	1978	1451	1142	939	820	787	841	886	938	1020	1222	1414	1423	1391	1182	1090	1008	980	967
3082	3831	3149	1959	1404	1121	906	834	837	908	976	1093	1111	1163	1326	1431	1379	1337	1251	1054	925	895
–	3328	2900	2058	1411	1089	877	847	899	995	1129	1226	1080	1103	1196	1291	1354	1317	1277	1123	928	876
–	–	2358	2212	1420	1098	903	846	897	969	1029	–	1077	1082	1149	1266	1361	1314	1194	1078	975	941
–	–	2586	2416	1459	1153	950	842	857	899	–	–	1039	1059	1131	1264	1427	1332	1235	1056	1002	1038
–	–	2384	2581	1668	1203	980	867	839	878	–	–	1026	1085	1168	1371	1564	1596	1370	1033	1036	1028

Figure B-1 Mean Annual APHRODITE Precipitation Data (1979-2007)
Southwest Latitude = 12.875, Southwest Longitude = 97.875 and Grid Resolution 0.25.

368	1376	1079	680	790	620	1024	1445	775	1375	2116	1182	1407	1280	1043	950	1160	1383	997	875	1385	1786	1394	798	908	1481	1263	879
573	1295	814	443	540	981	1305	574	642	1781	1854	1189	1438	1806	1499	1142	1206	1329	1094	856	975	1404	1009	702	1412	1786	1223	765
1355	1045	855	1034	740	1101	962	344	916	1600	972	1150	1162	1444	1434	1311	1073	730	712	1143	1425	1284	833	841	1145	1041	999	1044
1636	732	655	906	925	1245	610	722	1663	1105	899	1414	911	1145	1660	1228	808	900	1075	1767	1670	1020	1188	1293	1029	733	919	1181
647	495	430	401	922	1431	382	609	1332	975	1018	1471	964	1221	2039	891	694	1855	2234	1567	911	904	1770	1417	1141	1148	1093	1051
366	719	805	463	1027	1317	306	738	1428	746	726	1329	947	950	2037	1021	733	2302	2202	984	621	1608	2341	1028	1089	1672	1175	946
559	1046	918	560	941	1094	304	1155	2290	777	760	1585	970	890	2059	1272	583	1584	1528	820	869	1944	1971	1081	1265	1401	816	1095
702	815	529	505	1109	1297	372	848	1618	567	931	1172	713	1206	2331	1164	498	1117	1343	1142	1281	1699	1581	1476	1489	1319	984	1549
613	618	508	780	1275	684	390	933	1117	623	1131	938	567	1465	2081	656	574	1363	1420	1152	1263	1569	1724	1960	1412	1096	1094	1089
654	726	646	994	989	394	621	1500	951	588	1443	1402	538	980	1617	503	658	1662	1377	831	1072	1526	1636	2077	1450	1177	1619	1193
703	791	630	731	436	821	1810	1304	530	716	1345	974	440	912	1681	852	753	1039	940	756	1147	1572	1334	1744	1714	1459	2013	2065
651	780	763	686	284	869	1799	785	534	1285	1209	623	720	1581	1339	777	684	798	1124	908	1124	1431	1358	1777	2254	1415	1272	1679
851	1004	1041	831	408	637	1202	896	989	954	824	1129	1465	1244	664	527	527	914	1249	869	877	1274	1418	1383	1824	1867	1626	1794
1152	1375	1439	764	555	904	970	925	1323	853	790	1419	1157	657	575	798	953	1104	790	522	757	1351	1655	1206	1346	1814	1872	1846
1162	1198	1346	716	562	726	614	663	1258	1017	876	1071	846	816	1167	1497	1265	712	581	1013	928	983	1569	1313	1345	1539	1575	1646
1491	1252	895	827	662	603	542	773	1387	969	945	1152	1161	1192	1231	1214	882	593	958	2043	1043	705	1299	1396	1410	1476	1488	1419
1874	1861	827	607	808	748	606	679	1130	969	1030	1261	1343	1172	1044	754	607	782	648	989	889	779	1187	1252	1242	1428	1521	1336
1451	2295	1402	542	767	917	693	511	954	1322	1299	1260	1275	1193	1194	715	978	1512	394	562	1044	1003	1279	1243	1107	1275	1429	1315
1317	1790	1634	581	504	937	808	535	937	1478	1316	1212	1349	1254	1111	1141	1907	1354	332	1001	1491	839	1093	1619	1404	1100	1123	1276
1637	1220	1512	1049	591	1259	1347	658	897	1401	1195	1164	1409	1310	839	1460	2623	843	350	1457	1442	606	642	1370	1504	1209	1215	1226
1921	973	1991	2098	562	981	1576	794	808	1406	1314	1220	1344	1486	806	1166	2128	711	553	1684	1452	896	825	1154	1453	1346	1258	1172
2088	1069	1937	3053	752	586	1690	1013	753	1262	1323	1123	1238	1565	1182	976	1211	725	804	1130	769	919	1285	1208	1245	1235	1180	1245
2016	1210	1056	2341	1301	678	1207	924	710	1198	1336	1016	1135	1294	1376	1511	1458	956	926	812	416	649	1277	1126	938	1114	1181	1289
1921	1310	821	1206	1188	803	1025	873	778	1140	1359	1021	1066	1120	1151	1493	1591	931	937	1218	805	706	972	956	1014	1198	1184	1225
1952	1352	1126	1159	775	643	1045	875	811	951	1248	1192	1053	1076	1006	1214	1467	928	930	1214	871	716	881	1016	1147	1204	1140	1176
2094	1650	1224	1243	911	709	845	800	1290	1118	1039	1196	1054	1104	1077	1163	1325	917	802	1024	872	885	1152	1200	1155	1151	1151	1183
1936	1766	1103	1081	1688	1228	674	481	1525	1225	929	1163	1012	1083	1061	1109	1260	965	695	830	842	888	1067	1071	1068	1130	1198	1288
2382	2186	1341	743	1724	1483	625	401	1172	1003	1019	1203	1059	1005	916	1045	1146	885	806	1002	975	985	1111	1119	1123	1224	1203	1267
2688	2404	1682	636	941	1261	685	804	1156	901	1068	1127	1086	1034	938	1149	1066	734	794	979	945	977	1135	1297	1313	1306	1183	1252
2777	2101	1977	976	806	839	714	898	945	814	1013	1062	1066	1032	1031	1160	931	743	724	647	660	848	917	1040	1240	1308	1173	1212
–	2789	2551	1472	855	551	732	993	929	856	1024	1079	1063	1056	1079	1174	875	1073	1408	1157	961	954	969	694	786	976	1069	1242
–	3242	2338	1551	856	634	798	1068	1048	976	1059	1074	1031	1016	1056	1239	1018	1053	1442	1351	986	912	1090	1038	986	979	1238	1548
–	3075	2131	1821	1085	734	682	800	948	1015	1044	1045	1021	996	1034	1179	1346	920	799	1031	919	735	889	1198	1208	958	1002	1140
–	–	2948	2497	1400	876	662	684	811	1062	1198	1114	1065	1028	1082	1141	1425	1466	1112	986	956	770	731	878	890	820	828	766
–	–	3446	2867	1885	1106	760	976	1093	1123	1309	1179	1111	1007	1041	1079	1144	1218	1356	1396	1411	1382	1104	790	722	850	895	951
–	–	–	3394	3076	1609	837	855	941	822	1165	1202	1079	922	960	1014	1045	1009	1007	1115	1063	1070	1068	1037	1201	940	1049	1131
–	–	–	–	3762	1922	792	955	1042	951	1211	1238	–	–	–	–	–	1017	961	1071	932	841	636	776	1092	1390	1138	1026
–	–	–	–	3617	2249	1143	1429	1327	1151	1312	1257	–	–	–	–	–	1215	1088	1145	1435	1115	804	844	978	836	1113	1231
–	–	–	–	3973	2856	1780	1630	1025	790	1093	1275	–	–	–	–	–	1212	1190	1192	1419	988	1004	1100	818	591	987	1217
–	–	–	–	–	3077	1985	1886	1097	684	925	1370	–	–	–	–	1125	1255	1235	1349	1427	1105	1025	1064	992	1260	1133	732

Figure B-2 Mean Annual GCM Precipitation Data: Current Climate (1979-2007)

Southwest Latitude = 12.094
Southwest Longitude = 98.060
Grid Resolution 0.187

403	1389	1110	747	856	676	1052	1483	839	1447	2163	1225	1434	1287	1053	961	1156	1363	999	892	1409	1820	1432	857	965	1517	1281	912
605	1291	861	505	605	1026	1359	640	714	1873	1933	1256	1479	1819	1513	1175	1227	1343	1102	880	1028	1447	1065	751	1466	1820	1250	795
1359	1067	893	1055	756	1144	1027	412	987	1665	1060	1238	1215	1482	1465	1359	1123	783	753	1160	1456	1326	871	890	1178	1069	1018	1069
1653	767	697	930	946	1242	676	784	1700	1155	959	1518	976	1186	1687	1252	873	947	1108	1783	1715	1060	1201	1303	1027	727	921	1207
706	536	466	437	938	1414	433	657	1345	1017	1104	1575	1034	1279	2064	920	728	1854	2223	1590	969	924	1731	1375	1114	1138	1079	1045
396	733	812	491	1036	1313	349	738	1395	771	802	1433	1028	1009	2057	1024	750	2300	2186	1004	687	1626	2292	993	1051	1635	1150	938
602	1067	940	586	943	1097	346	1148	2224	764	831	1668	1044	924	2060	1287	586	1610	1512	837	930	1959	1936	1058	1246	1395	803	1090
754	854	577	536	1087	1336	408	854	1557	561	957	1209	758	1235	2331	1189	510	1129	1321	1134	1329	1720	1560	1474	1493	1323	987	1557
673	658	548	792	1234	741	417	936	1104	616	1135	962	603	1489	2097	675	566	1346	1390	1139	1294	1589	1717	1960	1402	1100	1116	1087
720	754	678	992	1021	436	628	1476	948	591	1431	1411	561	986	1627	524	667	1654	1350	846	1114	1547	1642	2081	1454	1163	1610	1191
753	821	656	738	484	846	1764	1299	548	717	1336	1006	447	916	1693	871	753	1048	950	797	1212	1584	1339	1740	1704	1446	1991	2060
681	801	760	681	308	872	1727	778	550	1284	1216	612	716	1586	1335	775	680	804	1145	964	1161	1455	1359	1768	2231	1404	1255	1681
862	991	1012	785	395	647	1172	913	994	951	820	1101	1434	1229	642	500	515	919	1285	922	947	1305	1405	1388	1807	1846	1613	1816
1175	1382	1427	715	533	876	978	928	1294	834	784	1384	1130	628	544	744	909	1123	827	562	794	1352	1643	1209	1387	1817	1869	1877
1204	1236	1363	694	530	705	621	661	1195	996	867	1052	823	799	1116	1451	1239	711	607	1049	952	992	1556	1313	1352	1551	1588	1671
1591	1334	939	849	670	603	571	767	1324	942	932	1144	1153	1166	1188	1170	863	592	971	2057	1079	718	1293	1394	1385	1473	1510	1432
2032	1987	922	692	866	764	636	696	1100	940	1001	1248	1331	1155	1025	735	603	777	670	999	895	789	1186	1235	1221	1431	1530	1360
1628	2543	1555	662	865	986	722	550	961	1267	1264	1243	1248	1178	1165	688	927	1480	404	559	1003	1005	1280	1232	1100	1287	1445	1331
1519	2008	1852	692	595	1012	825	578	950	1430	1300	1197	1325	1262	1091	1080	1808	1313	334	971	1450	829	1099	1591	1385	1108	1142	1306
1862	1413	1735	1176	663	1306	1317	687	924	1370	1180	1157	1400	1312	822	1369	2554	822	333	1361	1396	601	664	1374	1496	1215	1249	1238
2148	1145	2233	2229	606	1031	1560	816	851	1415	1309	1223	1340	1493	806	1113	2086	714	533	1622	1419	892	835	1148	1447	1351	1262	1182
2297	1228	2149	3168	792	643	1708	1019	801	1290	1326	1125	1232	1558	1182	958	1193	725	785	1102	758	906	1272	1198	1242	1222	1162	1235
2230	1361	1191	2494	1383	715	1220	918	753	1208	1340	1014	1132	1299	1366	1490	1456	952	898	798	416	636	1256	1114	929	1082	1154	1253
2109	1455	935	1338	1290	863	1022	857	795	1139	1359	1021	1079	1134	1145	1491	1588	929	912	1182	785	682	945	936	985	1151	1130	1185
2157	1477	1213	1247	849	712	1060	855	804	959	1238	1179	1065	1082	1007	1214	1464	929	895	1181	847	687	843	975	1096	1140	1077	1101
2293	1806	1321	1340	956	748	845	786	1254	1111	1039	1182	1063	1098	1079	1154	1330	913	771	996	834	836	1113	1155	1105	1087	1083	1104
2136	1885	1177	1158	1727	1234	642	460	1472	1222	929	1139	1020	1075	1063	1100	1254	971	681	803	792	841	1016	1016	992	1057	1133	1222
2562	2291	1385	780	1725	1453	584	392	1127	987	1006	1201	1065	1020	929	1061	1165	890	791	965	936	944	1067	1045	1050	1160	1157	1236
2904	2553	1728	649	944	1234	667	770	1120	876	1065	1124	1085	1044	953	1165	1087	750	783	954	926	941	1098	1261	1283	1271	1167	1240
2998	2250	2048	976	789	812	691	862	918	787	1005	1047	1046	1026	1018	1175	954	751	715	644	642	835	935	1048	1250	1306	1174	1218
–	3001	2631	1475	847	541	706	949	901	859	1015	1056	1035	1041	1076	1177	906	1065	1366	1141	929	943	975	724	833	1012	1098	1292
–	3449	2482	1580	860	621	765	1028	1021	958	1040	1055	1008	999	1050	1252	1032	1059	1418	1315	969	907	1087	1055	1029	1034	1298	1615
–	3280	2300	1908	1076	722	648	765	901	986	1014	1020	995	965	1011	1191	1363	934	808	1026	907	732	891	1195	1219	985	1048	1215
–	–	3091	2569	1378	866	642	652	793	1023	1150	1090	1049	998	1056	1145	1445	1491	1145	1023	987	794	748	897	922	846	861	808
–	–	3544	2949	1844	1055	734	957	1076	1104	1262	1146	1087	990	1034	1103	1183	1255	1406	1427	1454	1411	1134	801	752	868	922	972
–	–	–	3518	3010	1546	793	819	938	836	1151	1182	1055	926	1012	1062	1105	1052	1049	1175	1107	1122	1099	1051	1215	939	1044	1123
–	–	–	–	3752	1842	740	882	1016	946	1180	1204	–	–	–	–	–	1081	1009	1121	981	907	662	788	1099	1343	1099	999
–	–	–	–	3663	2254	1094	1305	1247	1146	1303	1244	–	–	–	–	–	1273	1144	1181	1487	1161	825	858	961	817	1080	1196
–	–	–	–	3937	2881	1741	1508	966	781	1098	1262	–	–	–	–	–	1255	1226	1241	1458	1021	1020	1115	827	573	969	1185
–	–	–	–	–	3118	1997	1791	1075	699	960	1347	–	–	–	–	1149	1280	1269	1379	1453	1143	1060	1068	989	1257	1117	732

Figure B-3 Mean Annual GCM Precipitation Data : Near Future Climate (2015-2043)

Southwest Latitude = 12.094
Southwest Longitude = 98.060
Grid Resolution 0.1875

417	1376	1105	731	851	683	1066	1528	874	1443	2207	1358	1600	1422	1131	1040	1224	1413	1014	917	1451	1786	1416	853	991	1533	1316	966
605	1263	821	475	569	988	1351	673	726	1873	1969	1375	1632	1912	1538	1220	1270	1387	1109	865	1013	1442	1052	747	1477	1852	1287	851
1334	1063	861	1015	743	1106	1030	420	989	1668	1126	1333	1319	1538	1445	1359	1118	765	716	1129	1428	1298	866	895	1207	1092	1049	1104
1653	792	697	928	914	1236	710	788	1695	1185	1044	1628	1060	1218	1632	1248	843	880	1009	1706	1667	1011	1198	1296	1029	744	945	1215
720	549	479	442	934	1431	477	677	1362	1042	1158	1639	1096	1299	2013	910	700	1702	2048	1518	941	877	1687	1368	1093	1126	1072	1054
414	733	838	513	1057	1381	396	773	1403	789	838	1477	1087	1021	2027	1052	748	2151	2059	958	652	1579	2264	1011	1051	1628	1152	950
607	1075	944	612	976	1175	410	1202	2283	819	862	1721	1099	921	2067	1332	607	1535	1463	805	888	1949	1966	1087	1262	1406	834	1091
751	835	573	550	1135	1378	476	942	1675	614	989	1241	800	1249	2352	1242	529	1107	1299	1116	1284	1720	1576	1482	1520	1343	999	1545
672	644	531	793	1278	784	485	1049	1206	663	1163	981	635	1535	2130	712	600	1346	1383	1133	1278	1582	1732	1954	1416	1103	1089	1085
718	734	655	981	1038	467	690	1573	1049	639	1508	1484	595	1024	1656	572	701	1691	1359	869	1108	1544	1635	2067	1443	1141	1572	1190
755	809	634	741	499	874	1817	1350	615	779	1401	1056	477	925	1731	930	805	1098	974	812	1208	1577	1315	1715	1693	1409	1945	2017
690	768	743	700	326	909	1767	836	598	1357	1298	627	726	1636	1400	821	732	852	1182	1004	1153	1423	1323	1731	2201	1393	1209	1632
896	971	998	814	424	685	1196	945	1063	1016	877	1160	1506	1308	678	535	545	969	1320	947	952	1275	1376	1348	1791	1837	1582	1764
1212	1333	1374	722	560	905	1017	964	1350	911	844	1491	1226	680	544	779	923	1130	831	553	803	1359	1621	1186	1364	1810	1853	1840
1258	1204	1322	720	585	745	679	700	1260	1052	937	1150	885	848	1169	1487	1232	710	584	1001	945	976	1551	1336	1373	1560	1584	1657
1625	1330	920	854	696	648	600	809	1382	1009	1013	1251	1249	1253	1244	1180	853	578	930	2021	1082	721	1314	1411	1407	1478	1522	1446
2026	1951	916	683	846	785	658	724	1182	988	1084	1346	1422	1227	1071	740	562	766	643	977	896	792	1199	1256	1238	1444	1538	1360
1623	2417	1469	644	794	966	729	545	1006	1331	1323	1322	1335	1249	1220	694	887	1505	407	531	1015	1040	1298	1244	1107	1280	1433	1320
1520	1966	1777	678	546	926	795	569	947	1477	1336	1246	1408	1325	1163	1104	1773	1346	331	917	1472	845	1087	1609	1383	1095	1127	1275
1890	1415	1649	1163	663	1196	1281	662	894	1389	1206	1203	1480	1394	888	1418	2516	866	346	1313	1408	597	636	1366	1482	1196	1239	1234
2170	1150	2113	2184	648	917	1459	794	824	1404	1328	1272	1427	1583	874	1198	2184	749	553	1588	1431	902	829	1140	1433	1356	1275	1199
2337	1263	2088	3100	851	603	1546	1014	797	1279	1363	1173	1312	1675	1274	1045	1301	790	824	1132	781	911	1286	1212	1236	1241	1191	1276
2240	1400	1220	2456	1425	704	1139	920	757	1196	1379	1066	1212	1404	1484	1607	1562	1029	953	832	420	654	1296	1140	944	1121	1183	1298
2103	1457	948	1325	1311	851	989	867	812	1141	1414	1083	1157	1213	1242	1606	1704	995	969	1229	824	717	977	962	1025	1197	1192	1230
2090	1430	1183	1232	852	670	1010	861	822	954	1292	1255	1144	1163	1087	1288	1551	979	949	1208	877	724	890	1008	1136	1177	1126	1154
2188	1729	1270	1296	957	727	832	785	1234	1118	1091	1259	1132	1183	1143	1212	1382	951	824	1039	872	879	1150	1184	1128	1110	1113	1155
2014	1777	1130	1107	1624	1211	653	482	1462	1216	958	1201	1087	1156	1138	1161	1311	1008	719	843	836	885	1057	1064	1025	1084	1162	1236
2437	2166	1338	757	1593	1432	598	422	1160	1017	1051	1273	1145	1090	988	1123	1207	923	828	998	978	984	1102	1093	1076	1167	1163	1232
2824	2415	1671	643	901	1209	690	800	1160	907	1116	1203	1180	1138	1024	1246	1151	779	806	969	942	969	1124	1285	1299	1287	1164	1241
2981	2140	1889	932	783	807	707	891	967	846	1050	1122	1142	1126	1113	1257	1027	791	727	638	624	826	922	1025	1218	1295	1171	1222
–	2870	2437	1407	836	542	718	996	968	907	1071	1133	1124	1146	1178	1276	978	1120	1375	1128	905	913	929	665	768	947	1053	1243
–	3379	2326	1475	815	634	788	1077	1099	1026	1100	1120	1090	1093	1151	1349	1121	1136	1455	1316	972	913	1053	989	955	967	1247	1569
–	3287	2173	1731	1014	727	708	838	1004	1063	1087	1080	1056	1052	1122	1310	1478	1023	881	1089	943	750	871	1144	1153	919	987	1176
–	–	3027	2436	1333	871	672	725	850	1096	1216	1131	1090	1092	1163	1256	1575	1620	1225	1075	1033	811	761	887	888	826	843	802
–	–	3575	2836	1772	1060	761	965	1093	1119	1292	1182	1138	1073	1150	1208	1285	1368	1509	1521	1533	1480	1156	808	738	869	941	1008
–	–	–	3403	2857	1488	797	810	934	818	1130	1168	1104	1011	1102	1162	1194	1128	1109	1224	1155	1153	1125	1066	1223	971	1093	1189
–	–	–	–	3591	1813	741	845	972	910	1148	1186	–	–	–	–	–	1135	1038	1133	997	916	648	784	1122	1393	1180	1092
–	–	–	–	3478	2153	1040	1214	1182	1099	1269	1195	–	–	–	–	–	1312	1141	1185	1490	1169	820	845	986	847	1143	1285
–	–	–	–	3897	2756	1619	1399	916	709	1044	1207	–	–	–	–	–	1256	1224	1246	1502	1048	1051	1159	834	608	1036	1255
–	–	–	–	–	2988	1843	1610	1001	614	897	1287	–	–	–	–	1200	1315	1295	1429	1509	1193	1134	1139	1023	1327	1175	788

Figure B-4 Mean Annual GCM Precipitation Data : Future Climate (2075-2103)

Southwest Latitude = 12.094
Southwest Longitude = 98.060
Grid Resolution 0.1875

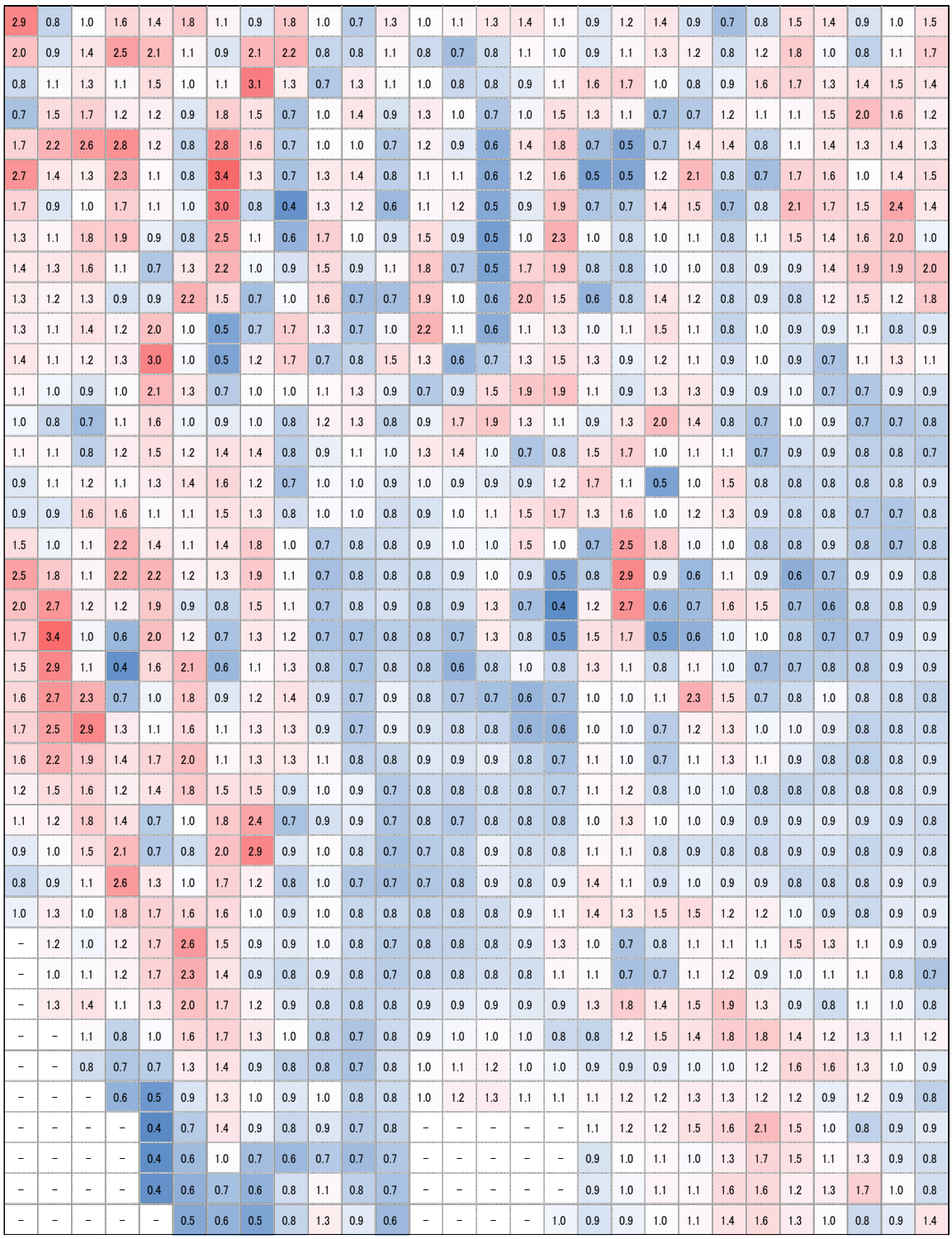

Figure B-5 Ratios of change in mean annual precipitation after correcting the bias correction in Current period (1979-2007).

3.0	0.8	1.0	1.6	1.4	1.8	1.2	0.9	1.9	1.1	0.8	1.3	1.0	1.2	1.4	1.4	1.1	0.9	1.2	1.3	0.9	0.7	0.9	1.5	1.4	0.9	1.0	1.5
1.9	0.9	1.4	2.4	2.0	1.1	0.9	2.2	2.2	0.8	0.8	1.1	0.8	0.7	0.9	1.1	1.0	0.9	1.1	1.3	1.2	0.9	1.2	1.8	1.0	0.8	1.1	1.8
0.8	1.1	1.3	1.1	1.5	1.0	1.2	3.0	1.3	0.7	1.3	1.1	1.0	0.8	0.9	0.9	1.1	1.6	1.7	1.1	0.9	1.0	1.6	1.7	1.3	1.5	1.5	1.4
0.7	1.5	1.7	1.2	1.2	0.9	1.8	1.4	0.7	1.1	1.4	0.9	1.3	1.0	0.7	1.0	1.5	1.3	1.1	0.7	0.7	1.2	1.1	1.1	1.5	2.0	1.6	1.3
1.7	2.2	2.5	2.7	1.2	0.8	2.8	1.6	0.8	1.0	1.1	0.7	1.2	0.9	0.6	1.5	1.7	0.7	0.6	0.8	1.4	1.4	0.8	1.1	1.4	1.4	1.4	1.4
2.7	1.4	1.3	2.2	1.1	0.9	3.4	1.3	0.7	1.4	1.4	0.8	1.1	1.1	0.6	1.2	1.6	0.5	0.5	1.2	2.2	0.8	0.7	1.7	1.6	1.0	1.4	1.5
1.7	0.9	1.0	1.7	1.1	1.0	3.1	0.8	0.4	1.3	1.2	0.7	1.1	1.2	0.6	0.9	1.9	0.7	0.8	1.4	1.6	0.7	0.9	2.1	1.7	1.5	2.4	1.4
1.3	1.2	1.8	1.9	1.0	0.8	2.6	1.1	0.6	1.7	1.0	0.9	1.5	0.9	0.5	1.0	2.3	1.0	0.9	1.0	1.1	0.8	1.1	1.5	1.4	1.6	2.0	1.0
1.4	1.4	1.6	1.1	0.7	1.4	2.3	1.0	0.9	1.6	0.9	1.2	1.8	0.7	0.5	1.7	1.9	0.8	0.8	1.0	1.1	0.9	0.9	0.9	1.5	1.8	1.9	1.9
1.3	1.2	1.3	0.9	0.9	2.3	1.6	0.7	1.0	1.6	0.7	0.7	1.9	1.0	0.6	2.0	1.6	0.6	0.8	1.4	1.2	0.8	0.9	0.8	1.3	1.5	1.2	1.8
1.3	1.1	1.4	1.2	2.0	1.0	0.5	0.8	1.8	1.3	0.7	1.0	2.2	1.1	0.6	1.2	1.4	1.0	1.2	1.5	1.1	0.8	1.0	0.9	0.9	1.1	0.8	0.9
1.4	1.2	1.2	1.3	3.1	1.0	0.5	1.3	1.8	0.7	0.8	1.6	1.4	0.6	0.7	1.3	1.5	1.3	1.0	1.3	1.1	0.9	1.0	0.9	0.7	1.1	1.3	1.1
1.2	1.0	0.9	1.1	2.2	1.4	0.8	1.1	1.1	1.1	1.3	1.0	0.7	0.9	1.6	2.0	2.0	1.1	0.9	1.3	1.4	0.9	0.9	1.0	0.8	0.7	0.9	0.9
1.0	0.8	0.7	1.2	1.6	1.0	0.9	1.0	0.8	1.2	1.3	0.8	1.0	1.7	2.0	1.3	1.1	0.9	1.3	2.1	1.5	0.8	0.7	1.0	1.0	0.7	0.7	0.8
1.2	1.1	0.8	1.3	1.5	1.2	1.5	1.4	0.8	1.0	1.1	1.0	1.4	1.4	1.0	0.7	0.8	1.5	1.7	1.1	1.2	1.1	0.7	0.9	0.9	0.8	0.8	0.8
0.9	1.1	1.1	1.1	1.3	1.4	1.6	1.2	0.7	1.0	1.0	0.9	1.0	1.0	1.0	0.9	1.2	1.8	1.1	0.5	1.0	1.6	0.9	0.8	0.9	0.8	0.9	0.9
0.9	0.9	1.6	1.5	1.0	1.1	1.5	1.3	0.9	1.0	1.1	0.9	0.9	1.0	1.2	1.6	1.7	1.3	1.6	1.1	1.2	1.4	0.9	0.8	0.9	0.8	0.7	0.8
1.5	1.0	1.1	2.1	1.3	1.1	1.4	1.8	1.0	0.8	0.9	0.9	1.0	1.0	1.0	1.6	1.1	0.7	2.6	1.8	1.0	1.1	0.8	0.8	0.9	0.8	0.7	0.8
2.5	1.8	1.1	2.2	2.1	1.1	1.3	1.9	1.1	0.7	0.8	0.9	0.9	0.9	1.1	0.9	0.6	0.8	3.1	1.0	0.6	1.1	0.9	0.6	0.7	0.9	1.0	0.9
2.0	2.7	1.2	1.3	1.9	0.9	0.8	1.5	1.1	0.7	0.9	0.9	0.8	0.9	1.4	0.7	0.4	1.3	3.1	0.7	0.7	1.7	1.6	0.7	0.7	0.8	0.9	0.9
1.8	3.3	1.0	0.6	2.0	1.1	0.7	1.3	1.2	0.7	0.7	0.8	0.8	0.7	1.3	0.9	0.5	1.5	1.8	0.5	0.6	1.0	1.1	0.8	0.7	0.8	0.9	1.0
1.5	2.9	1.1	0.4	1.7	2.0	0.6	1.1	1.3	0.8	0.7	0.8	0.8	0.6	0.8	1.0	0.8	1.4	1.2	0.8	1.2	1.0	0.7	0.8	0.8	0.8	0.9	0.9
1.6	2.7	2.2	0.7	1.0	1.8	0.9	1.2	1.4	0.9	0.8	1.0	0.8	0.7	0.7	0.6	0.7	1.1	1.0	1.2	2.4	1.5	0.8	0.9	1.0	0.9	0.9	0.8
1.7	2.5	2.9	1.2	1.0	1.5	1.0	1.3	1.3	0.9	0.7	1.0	0.9	0.9	0.8	0.6	0.6	1.1	1.0	0.8	1.2	1.4	1.0	1.0	1.0	0.8	0.9	0.9
1.5	2.2	1.8	1.4	1.6	1.9	1.1	1.3	1.3	1.2	0.8	0.8	0.9	0.9	1.0	0.8	0.7	1.1	1.0	0.8	1.1	1.3	1.1	1.0	0.8	0.8	0.9	0.9
1.2	1.5	1.6	1.2	1.4	1.8	1.5	1.5	0.9	1.0	1.0	0.8	0.8	0.8	0.9	0.8	0.8	1.1	1.3	0.9	1.0	1.0	0.8	0.8	0.9	0.9	0.9	0.9
1.1	1.2	1.8	1.4	0.7	1.0	1.9	2.4	0.7	0.9	1.0	0.7	0.8	0.7	0.8	0.8	0.8	1.0	1.4	1.1	1.1	1.0	0.9	0.9	1.0	0.9	0.9	0.9
0.9	1.0	1.5	2.0	0.7	0.8	2.1	3.0	0.9	1.1	0.9	0.7	0.8	0.8	1.0	0.9	0.9	1.1	1.2	0.9	0.9	0.9	0.9	0.9	0.9	0.8	0.9	0.9
0.8	0.9	1.1	2.7	1.3	1.0	1.8	1.3	0.8	1.0	0.7	0.7	0.7	0.8	0.9	0.9	1.0	1.4	1.2	0.9	1.0	1.0	1.0	0.8	0.8	0.9	0.9	0.9
0.9	1.2	1.0	1.8	1.7	1.6	1.6	1.1	0.9	1.0	0.8	0.8	0.8	0.8	0.9	1.0	1.2	1.5	1.4	1.6	1.7	1.3	1.3	1.0	0.9	0.8	0.9	1.0
–	1.1	0.9	1.2	1.8	2.7	1.5	1.0	0.9	1.0	0.8	0.8	0.8	0.8	0.8	0.9	1.3	1.1	0.7	0.9	1.2	1.2	1.1	1.5	1.4	1.1	1.0	0.9
–	1.0	1.0	1.1	1.7	2.3	1.4	0.9	0.8	0.9	0.8	0.8	0.8	0.8	0.9	0.9	1.1	1.1	0.7	0.8	1.2	1.2	1.0	1.0	1.1	1.1	0.8	0.7
–	1.3	1.4	1.0	1.3	2.0	1.7	1.2	0.9	0.9	0.8	0.8	0.9	0.9	1.0	0.9	0.9	1.4	1.8	1.4	1.6	1.9	1.4	1.0	0.9	1.1	1.0	0.9
–	–	1.0	0.8	1.0	1.6	1.8	1.4	1.1	0.8	0.7	0.8	1.0	1.0	1.1	1.0	0.8	0.8	1.2	1.5	1.5	1.8	1.8	1.4	1.2	1.3	1.1	1.2
–	–	0.8	0.7	0.7	1.3	1.5	0.9	0.8	0.8	0.7	0.9	1.0	1.1	1.2	1.0	1.0	0.9	0.9	0.9	1.0	1.0	1.2	1.7	1.6	1.3	1.0	0.9
–	–	–	0.6	0.4	0.9	1.4	1.1	1.0	1.1	0.8	0.8	1.1	1.3	1.3	1.1	1.1	1.1	1.2	1.2	1.3	1.3	1.3	1.3	0.9	1.2	0.9	0.8
–	–	–	–	0.4	0.7	1.5	1.0	0.9	0.9	0.8	0.8	–	–	–	–	–	1.1	1.2	1.2	1.5	1.7	2.2	1.6	1.0	0.8	0.9	0.9
–	–	–	–	0.4	0.6	1.0	0.7	0.7	0.8	0.7	0.7	–	–	–	–	–	0.9	1.1	1.1	1.0	1.3	1.7	1.6	1.1	1.3	0.9	0.8
–	–	–	–	0.4	0.6	0.7	0.6	0.9	1.2	0.8	0.7	–	–	–	–	–	0.9	1.0	1.2	1.1	1.6	1.6	1.3	1.3	1.9	1.1	0.9
–	–	–	–	–	0.5	0.6	0.5	0.9	1.4	0.9	0.7	–	–	–	–	1.0	0.9	1.0	1.0	1.1	1.4	1.5	1.3	1.1	0.8	0.9	1.5

Figure B-6 Ratios of change in mean annual precipitation after correcting Q-Q bias correction in near future period (2015-2043).

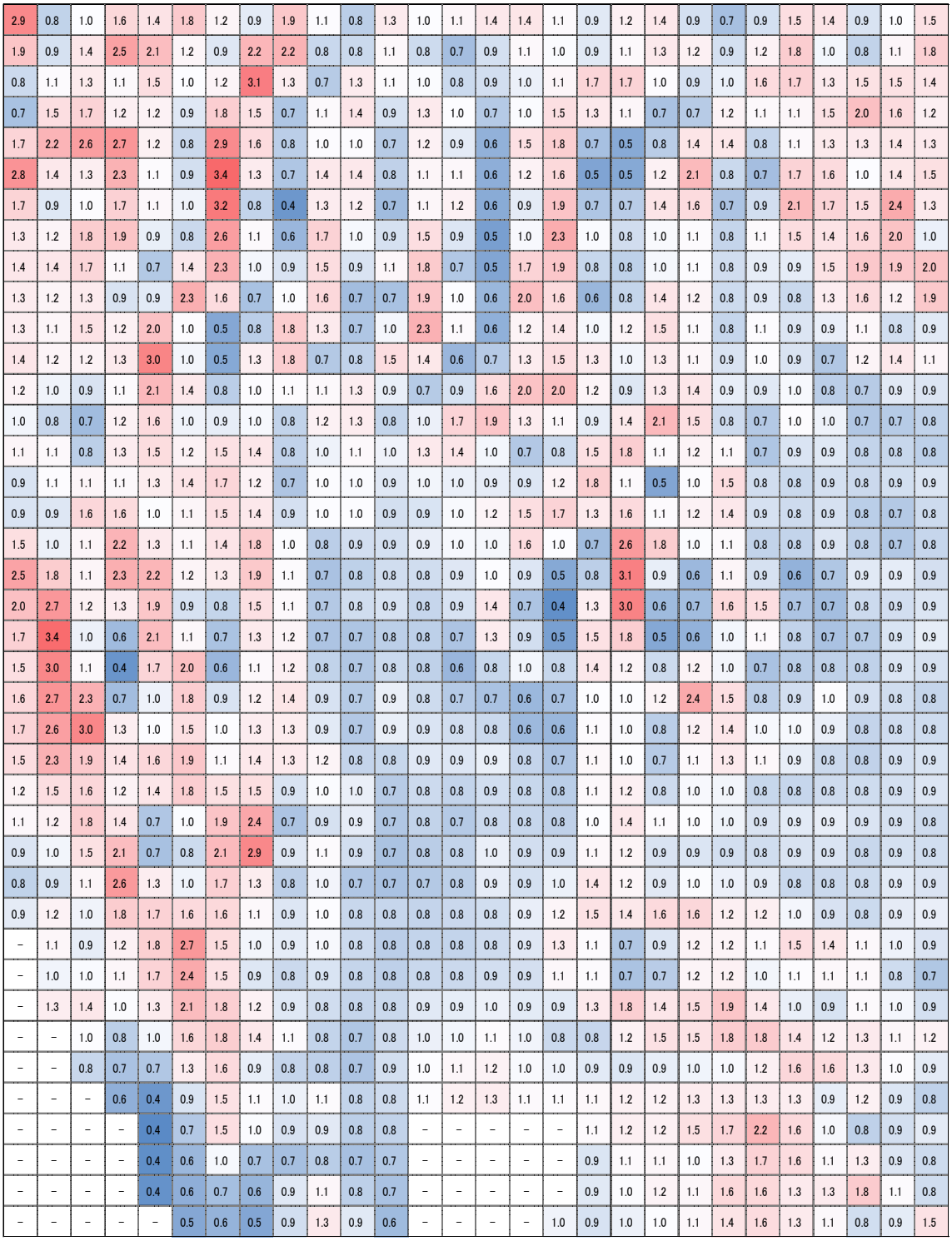

Figure B-7 Ratios of change in mean annual precipitation after correcting Emp.Dis bias correction in near future period (2015-2043).

2.9	0.8	1.0	1.6	1.4	1.8	1.1	0.9	1.8	1.0	0.8	1.3	1.0	1.1	1.3	1.3	1.0	0.9	1.2	1.3	0.9	0.7	0.9	1.6	1.4	0.9	1.0	1.4
1.9	0.9	1.4	2.4	2.0	1.1	0.9	2.1	2.1	0.8	0.8	1.1	0.8	0.7	0.8	1.0	1.0	0.9	1.1	1.3	1.2	0.9	1.2	1.8	1.0	0.8	1.1	1.7
0.8	1.1	1.3	1.1	1.5	1.0	1.1	2.9	1.3	0.7	1.3	1.1	1.0	0.8	0.8	0.9	1.1	1.6	1.6	1.0	0.9	1.0	1.6	1.7	1.3	1.4	1.4	1.4
0.7	1.5	1.7	1.2	1.2	0.9	1.8	1.4	0.7	1.1	1.4	0.9	1.3	1.0	0.7	1.0	1.5	1.3	1.1	0.7	0.7	1.2	1.1	1.1	1.4	1.9	1.5	1.2
1.7	2.2	2.5	2.6	1.2	0.8	2.8	1.5	0.8	1.0	1.0	0.7	1.2	0.9	0.6	1.5	1.8	0.7	0.5	0.7	1.4	1.4	0.8	1.1	1.3	1.3	1.4	1.3
2.6	1.3	1.2	2.1	1.1	0.9	3.2	1.3	0.7	1.3	1.4	0.8	1.1	1.1	0.6	1.2	1.7	0.5	0.5	1.2	2.1	0.8	0.7	1.6	1.6	1.0	1.4	1.5
1.6	0.9	1.0	1.7	1.1	1.0	3.1	0.8	0.5	1.3	1.3	0.7	1.1	1.2	0.6	0.9	2.0	0.7	0.8	1.4	1.6	0.7	0.9	2.1	1.7	1.5	2.4	1.3
1.3	1.1	1.7	1.8	1.0	0.9	2.5	1.1	0.6	1.7	1.0	0.9	1.5	0.9	0.5	1.0	2.4	1.0	0.9	1.0	1.1	0.8	1.1	1.5	1.4	1.6	2.0	1.0
1.4	1.3	1.6	1.1	0.8	1.3	2.2	1.0	0.9	1.6	0.9	1.2	1.8	0.7	0.5	1.7	1.9	0.8	0.8	1.0	1.1	0.9	1.0	1.0	1.5	1.9	1.9	2.0
1.3	1.2	1.3	0.9	0.9	2.2	1.5	0.7	1.0	1.6	0.7	0.7	1.9	1.0	0.6	2.0	1.6	0.6	0.8	1.4	1.2	0.8	0.9	0.8	1.3	1.6	1.2	1.9
1.3	1.1	1.4	1.2	1.9	1.0	0.5	0.8	1.8	1.3	0.7	1.0	2.2	1.1	0.6	1.2	1.4	1.0	1.2	1.5	1.1	0.8	1.1	0.9	1.0	1.1	0.9	0.9
1.4	1.1	1.2	1.3	3.0	1.0	0.6	1.2	1.7	0.7	0.8	1.6	1.4	0.6	0.7	1.3	1.5	1.3	1.0	1.3	1.1	0.9	1.0	0.9	0.7	1.2	1.4	1.1
1.2	1.0	0.9	1.1	2.1	1.3	0.8	1.0	1.1	1.1	1.3	1.0	0.7	0.9	1.6	1.9	1.8	1.1	0.9	1.3	1.3	0.9	0.9	1.0	0.8	0.8	0.9	0.9
1.0	0.8	0.7	1.2	1.6	1.0	0.9	1.0	0.8	1.2	1.3	0.8	1.0	1.8	2.0	1.3	1.1	0.9	1.3	2.0	1.4	0.8	0.7	1.1	1.0	0.7	0.7	0.8
1.2	1.1	0.8	1.3	1.5	1.2	1.5	1.4	0.8	1.0	1.1	1.0	1.4	1.5	1.0	0.7	0.8	1.4	1.7	1.1	1.2	1.1	0.7	0.9	0.9	0.8	0.8	0.8
0.9	1.1	1.1	1.0	1.2	1.4	1.6	1.2	0.7	1.0	1.0	0.9	1.0	1.0	1.0	0.9	1.2	1.8	1.1	0.5	1.0	1.5	0.9	0.8	0.9	0.8	0.9	0.9
0.9	0.9	1.6	1.5	1.0	1.1	1.5	1.4	0.9	1.0	1.1	0.9	0.9	1.0	1.2	1.6	1.7	1.4	1.6	1.1	1.2	1.4	0.9	0.8	0.9	0.8	0.7	0.8
1.5	1.0	1.1	2.1	1.3	1.1	1.4	1.9	1.0	0.8	0.9	0.9	1.0	1.0	1.0	1.6	1.1	0.7	2.6	1.8	1.0	1.1	0.8	0.8	0.9	0.8	0.7	0.8
2.5	1.8	1.1	2.2	2.1	1.2	1.4	2.0	1.1	0.7	0.8	0.9	0.9	0.9	1.1	0.9	0.6	0.8	2.9	1.0	0.6	1.1	0.9	0.6	0.7	0.9	1.0	0.9
2.0	2.7	1.2	1.2	1.8	0.9	0.8	1.6	1.1	0.7	0.9	0.9	0.8	0.9	1.4	0.7	0.4	1.3	2.8	0.7	0.7	1.6	1.5	0.7	0.7	0.8	0.9	0.9
1.8	3.4	1.0	0.6	2.0	1.1	0.7	1.4	1.2	0.7	0.7	0.8	0.8	0.7	1.3	0.9	0.5	1.5	1.7	0.5	0.6	1.0	1.1	0.8	0.7	0.8	0.9	1.0
1.5	3.0	1.1	0.4	1.7	1.9	0.6	1.1	1.3	0.8	0.7	0.8	0.8	0.6	0.8	1.0	0.8	1.4	1.1	0.8	1.2	1.0	0.7	0.8	0.8	0.8	0.9	0.9
1.6	2.7	2.2	0.7	1.0	1.8	0.9	1.2	1.4	0.9	0.8	1.0	0.9	0.7	0.7	0.6	0.7	1.1	1.0	1.2	2.3	1.5	0.8	0.9	1.0	0.9	0.9	0.8
1.7	2.5	2.9	1.3	1.0	1.5	1.0	1.2	1.3	0.9	0.7	1.0	0.9	0.9	0.8	0.6	0.6	1.1	1.0	0.8	1.2	1.4	1.0	1.0	1.0	0.8	0.9	0.9
1.6	2.2	1.8	1.4	1.7	1.9	1.1	1.3	1.3	1.2	0.8	0.8	0.9	0.9	1.0	0.8	0.7	1.1	1.0	0.8	1.1	1.3	1.1	1.0	0.9	0.8	0.9	0.9
1.2	1.5	1.6	1.2	1.4	1.8	1.4	1.5	0.9	1.0	1.0	0.8	0.8	0.8	0.9	0.8	0.8	1.1	1.3	0.9	1.0	1.0	0.8	0.9	0.9	0.9	0.9	0.9
1.2	1.2	1.7	1.4	0.7	1.0	1.9	2.4	0.7	0.9	1.0	0.7	0.8	0.8	0.8	0.8	0.8	1.1	1.4	1.1	1.1	1.0	0.9	1.0	1.0	1.0	0.9	0.9
0.9	1.0	1.5	2.1	0.7	0.9	2.0	2.9	0.9	1.1	0.9	0.7	0.8	0.8	1.0	0.9	0.9	1.1	1.2	0.9	0.9	0.9	0.9	0.9	0.9	0.9	0.9	0.9
0.8	0.9	1.2	2.6	1.4	1.0	1.7	1.3	0.8	1.0	0.7	0.7	0.7	0.8	1.0	0.9	1.0	1.4	1.2	0.9	1.0	1.0	1.0	0.8	0.9	0.9	1.0	0.9
0.9	1.3	1.0	1.8	1.7	1.6	1.6	1.1	0.9	1.1	0.8	0.8	0.8	0.8	0.9	1.0	1.2	1.5	1.4	1.6	1.7	1.3	1.3	1.0	0.9	0.8	0.9	1.0
–	1.2	1.0	1.2	1.7	2.6	1.6	1.0	1.0	1.0	0.9	0.8	0.8	0.8	0.9	0.9	1.3	1.1	0.7	0.9	1.2	1.2	1.1	1.5	1.4	1.1	1.0	0.9
–	1.0	1.1	1.2	1.7	2.2	1.4	0.9	0.9	0.9	0.8	0.8	0.8	0.8	0.9	0.9	1.1	1.1	0.7	0.8	1.2	1.2	1.0	1.0	1.1	1.1	0.8	0.7
–	1.3	1.4	1.1	1.4	1.9	1.7	1.2	0.9	0.9	0.8	0.8	0.9	1.0	1.0	0.9	0.9	1.4	1.8	1.4	1.6	2.0	1.4	0.9	0.8	1.1	1.0	0.9
–	–	1.1	0.8	1.0	1.5	1.7	1.3	1.1	0.8	0.7	0.8	1.0	1.0	1.1	1.0	0.8	0.8	1.2	1.5	1.5	1.9	1.9	1.5	1.2	1.3	1.1	1.2
–	–	0.8	0.7	0.8	1.3	1.5	0.9	0.8	0.8	0.7	0.9	1.1	1.2	1.2	1.0	1.0	0.9	0.9	1.0	1.0	1.0	1.3	1.7	1.6	1.4	1.0	0.9
–	–	–	0.6	0.5	0.9	1.3	1.0	0.9	1.1	0.8	0.9	1.1	1.3	1.3	1.1	1.1	1.1	1.2	1.2	1.3	1.3	1.3	1.3	1.0	1.2	0.9	0.8
–	–	–	–	0.4	0.8	1.4	1.0	0.9	0.9	0.8	0.9	–	–	–	–	–	1.1	1.3	1.3	1.5	1.7	2.3	1.7	1.0	0.8	0.9	0.9
–	–	–	–	0.4	0.7	1.1	0.7	0.6	0.8	0.7	0.8	–	–	–	–	–	0.9	1.1	1.2	1.0	1.4	1.8	1.6	1.1	1.3	0.9	0.9
–	–	–	–	0.4	0.6	0.7	0.6	0.9	1.2	0.8	0.7	–	–	–	–	–	0.9	1.0	1.2	1.1	1.7	1.7	1.3	1.4	2.0	1.1	0.9
–	–	–	–	–	0.6	0.6	0.5	0.8	1.3	0.9	0.7	–	–	–	–	1.0	0.9	1.0	1.1	1.1	1.5	1.6	1.4	1.1	0.9	1.0	1.5

Figure B-8 Ratios of change in mean annual precipitation after correcting Q-Q bias correction in future period (2075-2103).

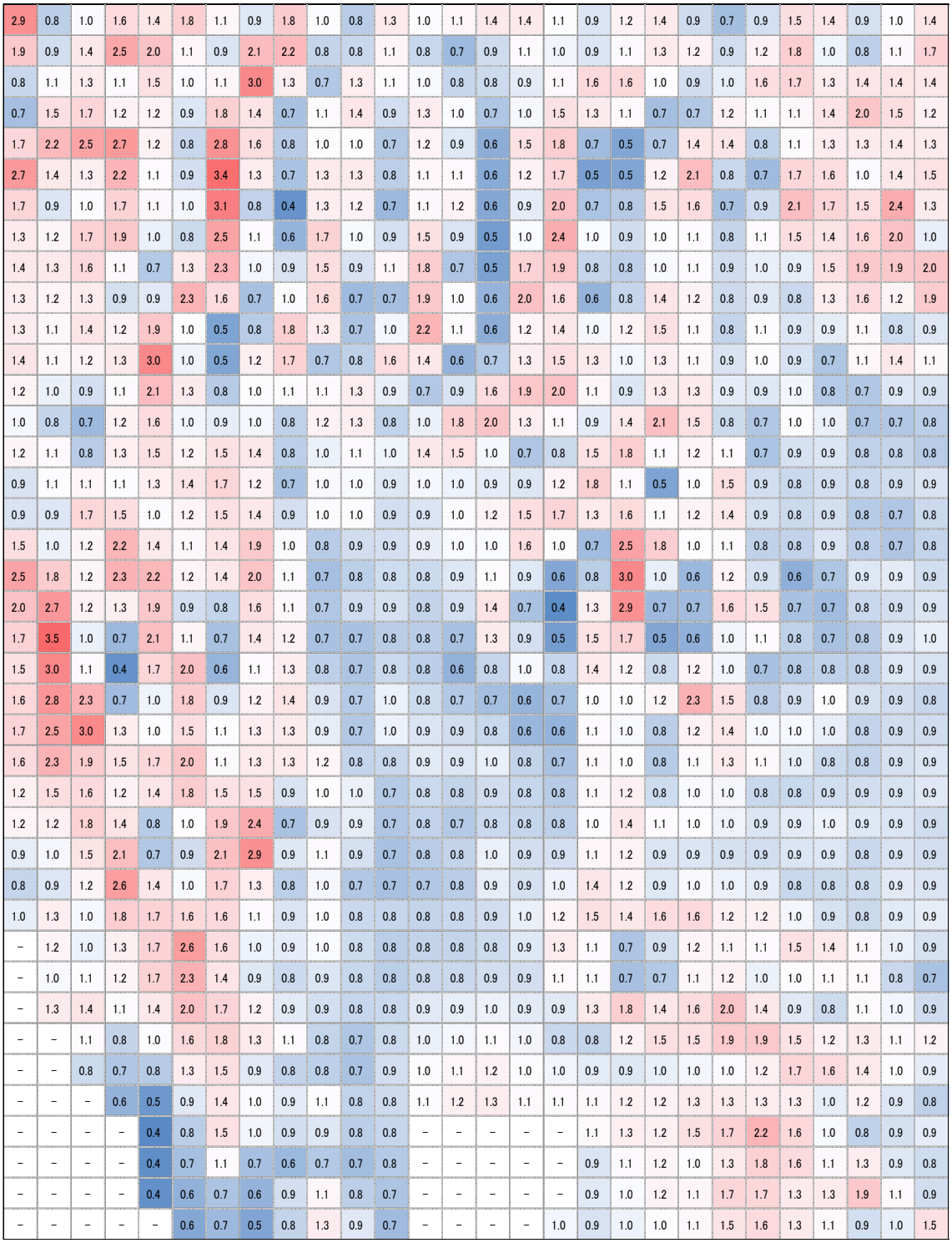

Figure B-9 Ratios of change in mean annual precipitation after correcting Emp.Dis bias correction in future period (2075-2103).

375	854	864	681	768	635	769	755	750	785	829	639	654	650	889	867	851	768	809	792	721	733	853	778	830	842	866	842
581	846	789	450	553	801	800	533	647	775	869	638	628	868	827	846	848	786	800	788	799	781	856	703	793	727	821	764
812	825	780	788	729	792	836	346	795	796	645	649	639	886	791	800	876	730	700	787	786	822	805	810	816	819	823	824
820	724	654	781	785	800	608	723	785	568	635	636	650	896	760	795	788	809	760	704	798	845	776	758	793	727	790	773
653	502	435	405	772	796	381	615	840	569	620	888	858	893	743	813	676	786	667	716	828	813	712	719	750	742	775	736
367	716	776	463	788	826	305	739	833	585	599	871	649	614	761	826	689	734	679	808	615	802	639	729	759	695	755	763
565	841	797	562	795	847	307	902	781	583	573	841	625	601	774	829	583	801	740	774	779	769	715	772	793	787	752	764
695	765	533	502	815	857	371	592	886	531	802	846	589	585	782	872	507	835	742	772	810	787	794	798	813	819	757	704
614	622	507	735	880	662	390	842	928	622	834	847	528	878	823	656	578	845	792	785	816	806	813	810	873	864	785	777
649	692	641	790	901	394	609	908	648	549	565	578	519	884	853	491	666	781	797	782	822	819	830	822	616	879	755	773
671	735	630	723	434	745	841	876	517	613	590	610	431	858	822	576	740	818	827	741	840	818	857	838	588	863	763	763
645	722	727	690	280	814	831	772	515	912	897	621	718	840	853	755	681	773	852	586	887	841	841	824	826	599	856	838
745	757	768	782	406	547	863	828	814	869	794	873	848	868	661	523	474	573	592	604	613	595	575	586	578	825	829	828
774	735	713	718	549	776	804	767	855	812	766	883	869	562	493	722	827	541	616	493	606	601	564	592	610	849	845	846
764	734	701	661	558	698	607	647	854	859	827	909	778	627	819	844	817	545	534	579	626	612	572	593	618	861	859	851
726	757	699	685	659	604	548	759	885	831	848	910	907	903	826	904	762	573	753	773	638	678	869	860	857	854	858	848
625	770	708	584	708	727	615	652	883	866	897	932	933	912	845	679	562	714	620	794	612	739	874	876	860	588	593	842
621	777	773	534	653	751	667	505	830	927	942	921	931	919	891	653	734	821	381	533	577	604	884	871	860	850	836	826
656	798	754	566	501	752	799	524	800	919	943	915	934	937	863	850	773	819	326	757	554	595	824	853	876	861	843	835
709	689	751	768	540	792	880	655	755	894	935	919	936	945	750	875	755	767	339	768	819	585	610	872	867	858	853	845
716	792	782	769	553	743	770	785	736	872	951	933	938	949	766	864	828	677	542	751	823	788	758	851	855	855	859	846
719	687	776	757	718	583	717	866	717	859	959	923	933	954	930	861	863	694	694	809	724	779	873	860	863	862	857	855
716	718	781	802	780	646	749	829	687	858	967	894	925	950	933	930	908	836	786	754	407	621	875	860	810	864	864	867
799	723	752	836	786	710	762	804	745	864	959	907	925	940	925	932	920	830	784	864	757	676	827	814	836	882	874	866
775	785	845	849	725	627	772	803	764	813	928	957	928	935	896	931	928	843	800	882	802	678	784	847	880	886	873	871
760	796	821	827	777	687	778	764	955	847	873	957	928	943	929	932	942	846	746	869	795	784	889	895	888	881	883	882
747	783	806	794	753	751	663	478	927	852	837	954	917	940	926	928	949	875	670	772	767	789	869	867	859	879	894	897
710	764	809	653	767	759	616	399	960	843	879	961	939	913	851	916	943	817	756	870	858	840	884	882	884	907	901	895
727	766	797	596	700	816	678	749	922	814	908	945	950	930	871	955	929	705	748	850	841	836	883	918	921	912	891	890
732	765	776	791	695	765	703	799	869	764	897	924	938	924	919	958	856	707	704	639	625	768	802	860	902	905	887	888
–	772	756	785	769	549	716	838	867	815	912	935	935	936	938	956	817	900	861	874	847	817	840	665	745	840	854	877
–	751	757	779	782	634	775	867	928	887	938	934	913	899	911	953	899	879	826	847	863	781	846	843	874	839	862	881
–	740	737	778	809	723	675	745	866	906	932	916	827	814	831	937	966	844	736	846	816	684	819	853	872	838	863	864
–	–	753	775	809	781	658	649	761	916	983	942	922	894	910	925	963	953	918	868	862	732	696	789	800	756	753	593
–	–	745	775	769	781	740	850	937	926	972	934	929	897	927	951	970	961	948	946	947	954	931	745	688	783	647	661
–	–	–	745	739	754	779	615	860	760	923	915	917	846	909	953	983	946	906	919	889	897	908	890	933	646	903	917
–	–	–	–	755	767	729	825	895	835	916	878	–	–	–	–	–	965	906	918	600	604	578	734	898	883	924	885
–	–	–	–	758	788	798	815	903	864	934	864	–	–	–	–	–	1038	960	912	864	838	752	793	888	769	900	942
–	–	–	–	761	803	793	777	893	735	873	880	–	–	–	–	–	1020	962	892	862	797	776	783	777	565	895	970
–	–	–	–	–	826	792	779	885	663	815	913	–	–	–	–	987	1029	960	900	818	787	780	799	833	879	977	704

Figure B-10 Mean Annual GCM Evapotranspiration: Current Climate (1979-2007)

Figure B-11 Mean Annual GCM Evapotranspiration: Near Future Climate (2015-2043)

420	900	906	724	813	678	818	812	802	838	894	674	690	684	927	896	905	842	854	824	796	803	918	812	882	907	936	895
604	889	801	473	579	844	853	575	710	831	920	668	661	927	889	899	906	857	854	797	845	849	903	734	871	809	898	822
849	863	803	829	733	837	880	404	838	852	679	681	665	934	852	863	913	723	688	843	854	882	829	845	889	887	887	896
856	763	685	814	825	845	709	761	837	604	664	663	673	934	822	856	785	798	807	787	869	876	848	844	860	722	834	849
710	552	477	448	811	843	472	666	878	601	651	929	898	932	811	823	671	842	760	801	854	818	789	806	818	810	838	806
411	729	806	507	834	869	393	756	876	610	633	911	672	639	817	854	702	800	767	857	648	873	713	800	808	768	823	810
607	878	825	603	833	888	407	950	842	609	604	883	645	620	824	867	600	845	821	780	818	847	793	830	850	849	772	822
738	781	570	541	861	904	482	635	932	546	829	880	613	605	834	897	526	859	818	836	866	857	860	850	870	882	803	783
663	632	538	750	932	713	464	892	968	642	869	869	554	914	867	711	591	905	863	848	866	869	874	867	932	910	842	837
678	704	654	825	946	455	655	954	675	580	599	607	553	904	898	528	692	856	871	817	865	885	895	881	655	926	826	835
685	744	628	735	501	776	893	915	576	656	623	639	457	869	879	611	771	862	871	784	889	886	911	890	627	917	827	827
661	718	716	687	330	841	887	794	558	958	940	628	713	892	901	778	712	799	899	619	951	905	893	878	882	632	892	890
776	773	792	771	419	583	919	864	852	913	839	912	892	907	668	527	479	613	635	632	648	633	614	614	610	870	873	877
811	763	744	704	550	790	840	806	894	854	808	919	919	603	504	718	859	587	647	507	631	639	609	624	640	891	890	895
794	748	732	669	571	682	638	656	897	895	873	950	831	671	860	895	889	575	529	613	662	642	614	628	648	901	902	898
745	782	716	706	671	631	598	773	936	869	890	958	955	956	868	949	777	551	780	842	680	677	903	908	901	895	899	891
656	801	735	603	730	742	649	678	935	895	938	978	980	962	893	715	553	720	617	813	643	739	904	917	902	632	633	891
654	808	805	568	659	771	688	530	882	981	989	968	975	965	936	673	757	884	402	515	620	646	922	911	900	899	889	876
692	827	772	609	516	767	790	561	837	977	992	960	975	982	916	890	834	890	331	768	612	635	847	912	927	898	887	890
743	716	771	788	580	824	947	664	780	947	982	967	980	993	812	916	836	801	342	813	904	572	602	920	925	902	898	893
743	820	808	797	629	745	834	789	744	917	1001	980	983	995	828	917	890	714	546	829	904	813	763	892	910	911	911	892
742	714	802	782	779	567	767	896	744	899	1003	968	978	993	981	910	913	744	735	857	734	786	920	908	909	914	907	913
749	743	800	829	806	663	794	848	721	897	1007	946	978	992	983	976	961	889	829	777	405	613	926	904	836	904	916	924
834	754	787	864	815	731	796	825	759	896	1003	956	981	989	970	977	968	884	831	919	772	682	849	844	877	938	924	921
808	814	874	881	763	640	808	823	763	833	976	996	980	987	951	973	972	887	839	934	817	690	809	881	933	939	920	921
795	830	854	858	806	697	793	771	995	876	916	995	980	993	980	976	984	886	784	909	808	804	939	957	937	929	929	934
777	821	840	823	786	796	656	487	985	889	871	987	966	987	975	973	999	914	696	790	773	806	908	911	901	929	946	957
732	798	850	678	794	806	602	424	992	862	912	996	984	962	908	961	989	853	779	891	872	863	925	930	928	962	953	949
762	798	837	614	699	855	688	744	939	826	943	988	992	977	921	998	978	749	761	876	849	853	922	973	975	967	941	944
771	803	819	816	707	783	699	815	878	783	922	970	977	968	960	997	917	761	708	629	610	767	833	897	953	958	937	940
–	807	787	821	778	540	707	867	878	834	937	968	975	975	976	993	886	943	905	917	848	828	851	656	739	867	900	934
–	786	793	805	779	627	785	883	936	899	946	964	950	943	952	986	942	921	858	904	896	807	900	888	887	866	909	930
–	769	770	809	834	714	690	761	879	912	936	936	870	856	872	971	996	890	791	875	843	707	831	909	933	871	909	904
–	–	783	815	836	800	672	664	788	924	986	959	941	928	948	962	997	989	951	906	901	773	724	819	816	765	771	633
–	–	774	816	796	808	732	850	945	927	989	965	955	930	968	993	1012	997	990	987	988	995	972	778	709	801	682	698
–	–	–	770	771	791	767	626	860	765	930	944	947	907	972	1019	1042	1001	959	960	925	936	952	934	971	678	938	967
–	–	–	–	790	803	704	806	888	827	924	910	–	–	–	–	–	1023	952	959	642	644	614	765	931	934	962	931
–	–	–	–	786	826	784	845	957	883	946	892	–	–	–	–	–	1071	987	944	911	881	791	829	921	795	930	983
–	–	–	–	787	828	819	823	875	690	878	901	–	–	–	–	–	1045	991	930	901	833	821	837	815	602	927	1002
–	–	–	–	–	850	821	821	897	603	810	930	–	–	–	–	1021	1060	995	944	868	823	822	848	866	924	1022	761

Figure B-12 Mean Annual GCM Evapotranspiration: Future Climate (2075-2103)

Figure B-13 Mean Annual Corrected GCM Evapotranspiration: Current Climate (1979-2007)
(Multiplicative Factor and Different Factor Methods)

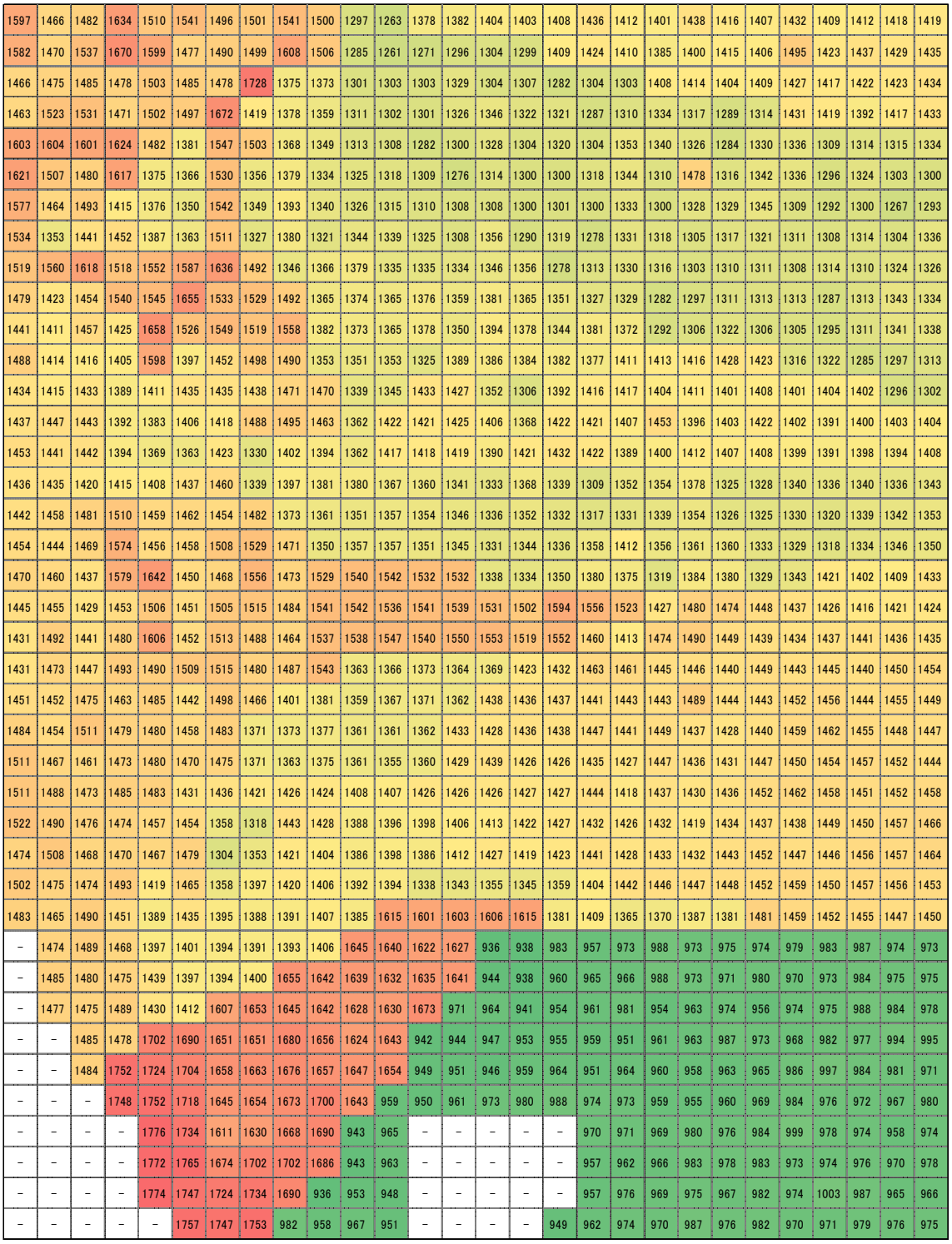

Figure B-14 Mean Annual Corrected GCM Evapotranspiration (mm): Near Future Climate (2015-2043)
(Multiplicative Factor Method)

1521	1485	1493	1546	1509	1514	1496	1496	1520	1496	1290	1279	1395	1396	1403	1402	1402	1416	1404	1400	1416	1404	1399	1414	1405	1404	1408	1412
1518	1486	1515	1541	1532	1489	1493	1499	1540	1498	1283	1279	1281	1290	1293	1291	1403	1411	1404	1391	1398	1407	1405	1431	1412	1417	1415	1418
1485	1488	1494	1488	1502	1491	1490	1538	1373	1367	1320	1323	1320	1329	1293	1295	1284	1295	1292	1402	1406	1401	1405	1413	1409	1411	1413	1419
1481	1509	1511	1485	1499	1493	1554	1393	1371	1364	1335	1321	1320	1329	1338	1313	1316	1295	1306	1316	1310	1296	1309	1414	1410	1395	1408	1416
1540	1529	1529	1526	1488	1373	1422	1406	1363	1362	1336	1325	1297	1303	1315	1304	1312	1301	1320	1319	1318	1294	1310	1317	1306	1309	1308	1319
1525	1504	1490	1521	1373	1367	1411	1363	1368	1356	1342	1333	1333	1298	1307	1301	1304	1311	1321	1306	1358	1309	1319	1319	1299	1315	1303	1298
1522	1487	1496	1385	1376	1359	1403	1359	1372	1358	1341	1329	1333	1333	1304	1301	1305	1302	1318	1302	1320	1314	1322	1304	1299	1302	1282	1296
1516	1367	1399	1396	1379	1367	1401	1356	1369	1351	1346	1340	1340	1332	1345	1296	1310	1289	1316	1311	1306	1310	1311	1306	1305	1309	1304	1321
1464	1545	1556	1524	1544	1558	1558	1517	1358	1372	1380	1340	1342	1335	1340	1351	1291	1308	1311	1310	1305	1307	1307	1305	1310	1308	1314	1315
1448	1433	1438	1534	1544	1566	1527	1531	1524	1376	1382	1379	1379	1372	1379	1379	1363	1314	1317	1296	1303	1307	1309	1308	1302	1310	1323	1319
1437	1424	1435	1425	1475	1532	1537	1525	1535	1384	1382	1379	1376	1368	1386	1381	1363	1378	1377	1303	1307	1314	1305	1304	1305	1309	1320	1319
1445	1424	1422	1416	1453	1420	1436	1521	1471	1353	1351	1367	1362	1383	1383	1406	1403	1401	1415	1417	1419	1422	1420	1310	1313	1299	1305	1312
1434	1425	1429	1406	1416	1433	1435	1436	1472	1474	1347	1346	1425	1422	1397	1390	1408	1419	1421	1411	1415	1414	1415	1411	1413	1411	1302	1306
1435	1438	1432	1404	1405	1421	1428	1483	1484	1472	1375	1421	1419	1420	1414	1395	1420	1420	1414	1419	1407	1415	1421	1413	1409	1412	1414	1412
1443	1433	1436	1405	1403	1400	1428	1357	1393	1391	1379	1425	1413	1419	1403	1417	1421	1420	1407	1414	1415	1415	1418	1413	1411	1411	1411	1416
1436	1437	1420	1419	1416	1425	1438	1369	1392	1381	1379	1363	1357	1349	1340	1364	1344	1336	1350	1354	1364	1339	1346	1352	1349	1349	1346	1349
1457	1465	1471	1474	1457	1460	1470	1465	1380	1368	1352	1358	1353	1348	1342	1351	1345	1337	1343	1345	1357	1339	1342	1346	1339	1354	1354	1357
1459	1458	1467	1495	1462	1460	1478	1476	1468	1354	1358	1357	1351	1348	1340	1349	1345	1357	1370	1351	1362	1359	1346	1344	1339	1347	1353	1353
1463	1466	1452	1502	1504	1460	1473	1494	1464	1538	1546	1541	1537	1534	1343	1344	1352	1369	1358	1335	1366	1365	1339	1353	1436	1424	1428	1438
1455	1458	1451	1463	1474	1457	1482	1487	1468	1542	1541	1537	1541	1539	1535	1525	1555	1544	1533	1435	1462	1446	1449	1443	1438	1431	1436	1435
1447	1482	1452	1461	1509	1461	1473	1475	1455	1539	1543	1544	1540	1543	1541	1533	1547	1450	1434	1454	1464	1444	1440	1438	1441	1442	1439	1439
1445	1464	1455	1460	1477	1473	1467	1472	1467	1540	1366	1365	1369	1362	1365	1428	1435	1449	1447	1442	1440	1439	1445	1441	1442	1440	1445	1447
1454	1456	1471	1458	1469	1454	1467	1465	1382	1376	1363	1368	1369	1364	1439	1438	1441	1437	1442	1441	1450	1435	1441	1446	1448	1441	1447	1445
1468	1455	1488	1468	1467	1457	1466	1374	1368	1374	1366	1366	1365	1436	1432	1437	1440	1442	1439	1447	1436	1434	1439	1451	1450	1448	1443	1444
1478	1462	1467	1466	1470	1463	1463	1375	1366	1372	1364	1362	1366	1436	1439	1432	1433	1436	1435	1448	1439	1437	1442	1446	1448	1449	1446	1443
1477	1467	1468	1468	1473	1432	1437	1435	1438	1429	1419	1420	1439	1439	1435	1434	1434	1445	1431	1439	1436	1437	1447	1454	1451	1447	1447	1450
1474	1465	1470	1466	1431	1432	1409	1408	1445	1431	1412	1412	1419	1428	1430	1433	1436	1440	1438	1440	1428	1438	1439	1442	1447	1446	1450	1456
1460	1468	1443	1441	1432	1436	1393	1424	1434	1417	1411	1415	1412	1435	1444	1436	1436	1448	1439	1437	1433	1442	1448	1444	1442	1449	1447	1453
1468	1439	1441	1449	1419	1436	1414	1414	1426	1414	1414	1415	1361	1367	1374	1363	1372	1395	1444	1444	1442	1445	1447	1453	1446	1451	1448	1448
1445	1439	1441	1437	1409	1428	1417	1410	1405	1415	1408	1640	1633	1635	1636	1638	1385	1396	1373	1371	1378	1376	1461	1449	1448	1450	1444	1448
–	1437	1434	1434	1416	1413	1413	1412	1408	1415	1666	1667	1658	1658	944	942	981	961	969	983	969	973	974	975	981	987	977	976
–	1439	1436	1435	1434	1414	1412	1414	1670	1664	1662	1660	1663	1666	950	942	961	965	962	975	976	970	984	980	973	983	977	975
–	1437	1436	1439	1425	1422	1659	1671	1666	1665	1657	1659	1686	968	963	945	953	968	980	960	969	969	962	976	982	998	999	979
–	–	1438	1429	1683	1687	1675	1669	1681	1673	1656	1668	949	950	951	955	954	956	955	968	970	979	969	968	975	972	984	988
–	–	1437	1692	1685	1687	1675	1671	1677	1672	1671	1676	958	957	949	960	964	952	961	957	957	961	967	976	980	974	979	974
–	–	–	1693	1683	1681	1669	1678	1673	1687	1670	967	958	968	975	979	986	973	974	959	956	959	968	982	975	975	967	977
–	–	–	–	1692	1683	1652	1659	1669	1684	956	973	–	–	–	–	–	971	972	969	971	971	981	982	976	977	968	971
–	–	–	–	1693	1691	1664	1681	1695	1687	955	973	–	–	–	–	–	958	963	961	969	967	976	987	974	974	968	974
–	–	–	–	1695	1680	1682	1692	1690	953	967	961	–	–	–	–	–	957	970	964	961	960	959	965	988	967	964	966
–	–	–	–	–	1682	1686	1695	981	973	979	961	–	–	–	–	951	961	970	962	973	965	960	952	961	970	976	969

Figure B-15 Mean Annual Corrected GCM Evapotranspiration (mm): Near Future Climate (2015-2043)
(Different Factor Method)

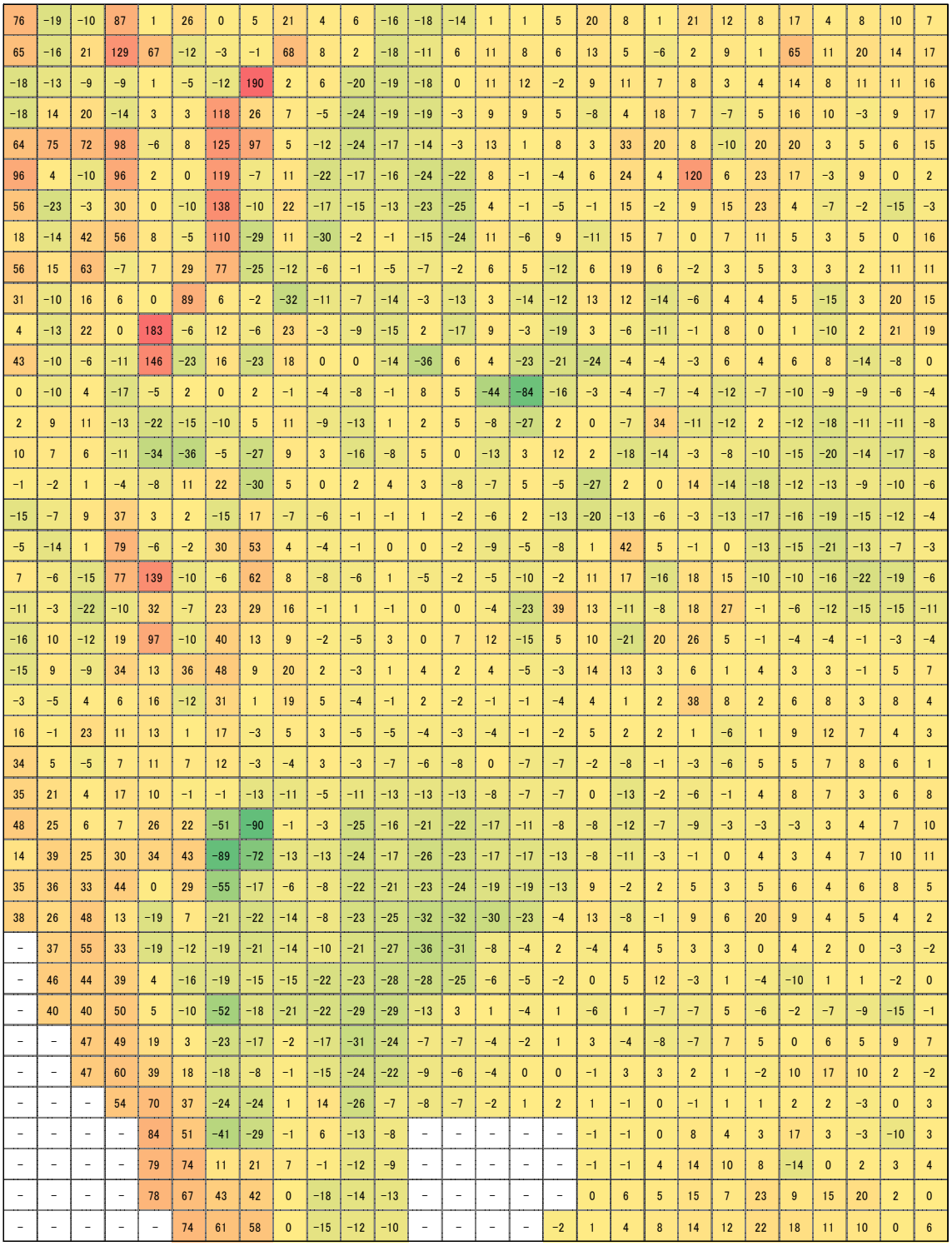

Figure B-16 Difference in Mean Annual Evapotranspiration (mm) Corrected by two correction methods: (Multiplicative Factor Method - Different Factor Method): Near Future Climate (2015-2043)

Figure B-17 Mean Annual Corrected GCM Evapotranspiration (mm): Future Climate (2075-2103)
(Multiplicative Factor Method)

1539	1540	1536	1538	1539	1537	1543	1551	1546	1547	1351	1321	1438	1436	1441	1431	1456	1477	1447	1435	1478	1472	1467	1436	1454	1467	1472	1455
1517	1537	1506	1517	1521	1538	1546	1536	1556	1550	1337	1317	1319	1345	1349	1339	1460	1473	1456	1412	1448	1470	1449	1433	1480	1484	1480	1461
1530	1533	1517	1535	1498	1539	1538	1552	1412	1419	1362	1361	1355	1376	1348	1350	1323	1280	1274	1458	1471	1462	1426	1437	1476	1470	1466	1475
1530	1533	1525	1527	1534	1539	1595	1408	1421	1400	1371	1355	1351	1367	1391	1367	1303	1296	1353	1390	1377	1337	1378	1488	1469	1397	1446	1479
1551	1544	1537	1537	1533	1416	1461	1420	1401	1395	1373	1383	1346	1345	1375	1316	1302	1362	1399	1392	1332	1311	1384	1393	1374	1374	1370	1376
1538	1507	1524	1538	1415	1413	1458	1381	1406	1389	1376	1383	1366	1331	1362	1335	1319	1373	1393	1356	1339	1378	1381	1378	1355	1380	1374	1353
1536	1531	1522	1410	1407	1411	1464	1412	1425	1390	1374	1384	1362	1362	1357	1344	1323	1350	1387	1312	1345	1384	1384	1364	1363	1368	1326	1364
1537	1385	1407	1408	1415	1417	1475	1407	1410	1378	1370	1377	1367	1363	1395	1331	1326	1331	1382	1370	1363	1376	1372	1358	1363	1369	1352	1386
1476	1540	1559	1544	1581	1580	1603	1579	1403	1399	1415	1365	1369	1379	1387	1398	1320	1365	1377	1369	1356	1370	1367	1363	1366	1352	1364	1366
1456	1439	1440	1564	1574	1591	1575	1575	1557	1411	1413	1409	1413	1400	1425	1417	1406	1381	1380	1342	1349	1373	1371	1366	1345	1353	1378	1369
1440	1436	1426	1438	1494	1560	1582	1569	1588	1423	1413	1408	1406	1391	1437	1414	1411	1424	1424	1349	1356	1374	1360	1359	1346	1360	1370	1371
1443	1424	1416	1424	1477	1453	1483	1551	1511	1389	1386	1387	1375	1431	1427	1441	1449	1444	1465	1451	1482	1482	1470	1361	1363	1340	1342	1358
1458	1443	1451	1416	1439	1463	1483	1463	1507	1513	1389	1383	1462	1457	1425	1421	1423	1458	1461	1446	1453	1456	1457	1446	1450	1463	1350	1355
1464	1455	1458	1414	1427	1441	1463	1508	1509	1512	1418	1453	1468	1459	1429	1414	1449	1463	1449	1432	1444	1456	1463	1450	1448	1460	1463	1467
1457	1441	1459	1435	1439	1411	1457	1385	1420	1413	1423	1459	1471	1462	1459	1468	1490	1449	1413	1452	1454	1448	1460	1453	1448	1458	1461	1465
1446	1452	1444	1448	1440	1454	1476	1390	1427	1415	1418	1403	1403	1407	1396	1400	1370	1332	1382	1423	1397	1353	1389	1402	1399	1396	1395	1398
1487	1487	1483	1475	1478	1470	1489	1481	1429	1405	1396	1400	1402	1404	1403	1390	1345	1360	1351	1374	1386	1355	1384	1395	1396	1398	1395	1404
1488	1486	1487	1490	1461	1476	1477	1481	1507	1409	1401	1401	1399	1400	1399	1375	1377	1418	1375	1337	1397	1397	1392	1395	1394	1404	1408	1404
1492	1485	1474	1498	1470	1471	1447	1493	1492	1599	1590	1586	1583	1586	1407	1395	1415	1426	1359	1365	1412	1394	1378	1414	1494	1479	1487	1497
1489	1482	1476	1476	1496	1488	1523	1464	1481	1594	1588	1589	1585	1589	1603	1582	1622	1576	1544	1488	1528	1430	1434	1491	1500	1487	1487	1491
1482	1483	1482	1484	1532	1458	1520	1459	1464	1586	1591	1589	1587	1587	1604	1594	1604	1480	1448	1521	1523	1467	1448	1484	1498	1499	1494	1489
1479	1483	1482	1480	1517	1440	1505	1485	1483	1580	1413	1413	1414	1407	1419	1491	1493	1493	1484	1491	1453	1449	1489	1490	1489	1495	1495	1502
1488	1480	1475	1482	1482	1473	1500	1475	1403	1408	1409	1420	1421	1411	1493	1488	1496	1495	1486	1466	1440	1434	1494	1488	1471	1485	1497	1501
1491	1486	1491	1483	1485	1477	1490	1389	1382	1400	1413	1417	1424	1493	1488	1489	1491	1497	1490	1498	1458	1450	1466	1475	1486	1501	1494	1499
1488	1484	1485	1487	1494	1468	1492	1388	1367	1389	1416	1408	1420	1495	1497	1485	1488	1487	1484	1497	1460	1456	1470	1479	1497	1498	1492	1495
1491	1490	1488	1486	1485	1438	1442	1435	1468	1457	1471	1466	1495	1493	1494	1489	1487	1485	1482	1484	1458	1464	1495	1506	1494	1493	1490	1496
1486	1494	1490	1485	1460	1473	1420	1437	1486	1465	1461	1460	1477	1492	1493	1491	1494	1484	1470	1462	1451	1462	1484	1489	1487	1494	1497	1504
1477	1490	1469	1453	1455	1475	1414	1453	1460	1447	1460	1463	1473	1493	1502	1490	1491	1480	1467	1465	1459	1468	1485	1492	1489	1499	1496	1499
1490	1460	1467	1446	1427	1467	1438	1423	1445	1439	1463	1471	1423	1427	1430	1423	1429	1424	1458	1471	1453	1461	1484	1499	1498	1500	1494	1498
1466	1466	1471	1453	1439	1446	1423	1444	1436	1447	1452	1701	1694	1699	1696	1694	1440	1434	1384	1370	1364	1380	1475	1482	1495	1497	1495	1497
–	1462	1459	1463	1437	1419	1419	1457	1439	1446	1708	1717	1723	1722	1006	1006	1037	1011	1012	1011	969	978	979	959	962	995	1014	1024
–	1462	1464	1454	1425	1420	1438	1443	1692	1695	1692	1714	1721	1728	1009	1001	1011	1010	1000	1025	1002	995	1022	1012	981	995	1015	1016
–	1457	1461	1459	1452	1419	1698	1699	1697	1690	1688	1704	1727	1010	1009	1002	998	1015	1022	997	995	991	980	1023	1028	1001	1014	1008
–	–	1457	1467	1710	1703	1697	1698	1711	1692	1687	1701	987	1002	1006	1005	1002	1004	1001	1006	1007	1009	995	998	984	976	986	1008
–	–	1457	1724	1710	1711	1676	1684	1691	1685	1701	1715	994	1001	1009	1010	1010	1004	1010	1009	1008	1008	1009	1001	989	986	1003	1005
–	–	–	1708	1715	1721	1672	1695	1684	1689	1691	997	997	1029	1031	1034	1027	1023	1021	1008	1004	1006	1012	1011	1006	999	1003	1018
–	–	–	–	1719	1719	1658	1664	1677	1676	977	1000	–	–	–	–	–	1026	1014	1008	1010	1008	1004	999	1001	1019	1006	1014
–	–	–	–	1712	1722	1670	1713	1738	1703	980	996	–	–	–	–	–	1001	995	1000	1015	1010	1007	1004	1001	994	998	1009
–	–	–	–	1709	1710	1709	1729	1666	923	973	988	–	–	–	–	–	993	997	1007	1006	1003	1013	1023	1005	1005	1000	999
–	–	–	–	–	1708	1713	1725	979	907	963	985	–	–	–	–	1002	998	1003	1012	1017	1004	1010	1017	1001	1013	1013	1026

Figure B-18 Mean Annual Corrected GCM Evapotranspiration (mm): Future Climate (2075-2103)
(Different Factor Method)

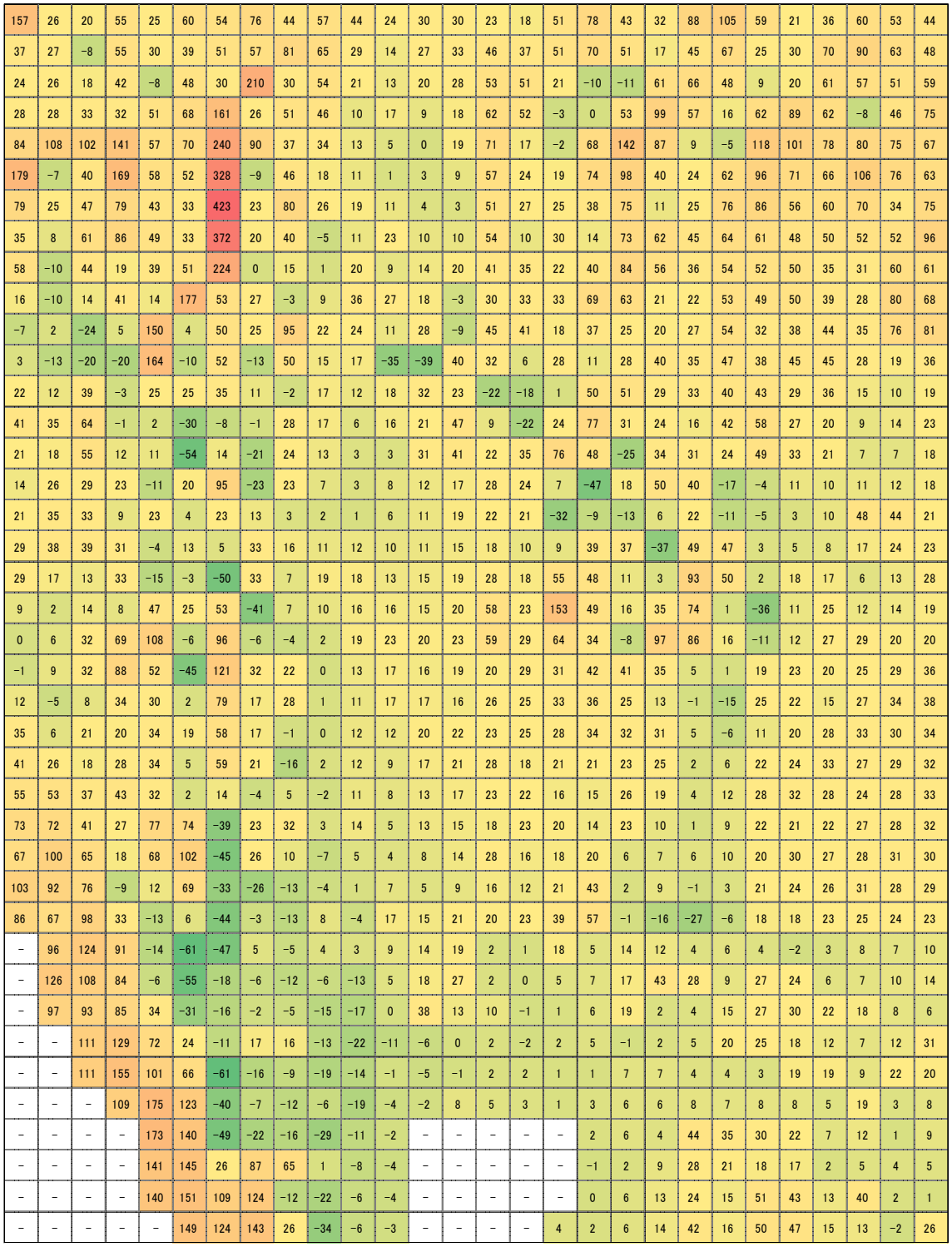

Figure B-19 Difference in Mean Annual Evapotranspiration (mm) Corrected by two correction methods: (Multiplicative Factor Method - Different Factor Method): Future Climate (2075-2103)

Bibliography

Aldous, A., James Fitzsimons, J., Richter, B., Bach, L., 2011. Droughts, floods and freshwater ecosystems: evaluating climate change impacts and developing adaptation strategies. Marine and Freshwater Research. 62(3), 223-231.

Allen, R.G., Pereira, L.S., Raes, D., Smith, M., 1998. Crop evapotranspiration - Guidelines for computing crop water requirements. FAO Irrigation and drainage paper, 56, FAO, Rome. ISBN 92-5-104219-5.

Arora, V. K. , Boer, G. J., 2001. Effect of simulated climate change on the hydology of major river basins. J. Geophys. Res. 106(D4), 3335–3348.

Bemporad, G.A., Alteracha, J., Amighettia, F. F., Peviania, M., Saccardo, I., 1979. A distributed approach for sediment yield evaluation in Alpine regions. Journal of Hydrology. 197, 370–392, doi: http://dx.doi.org/10.1016/0022-1694(95)02978-8

Bennett, J. C., Grose, M. R., Corney, S. P., White, C. J., Holz, G. K., Katzfey, J. J., Post, D. A., Bindoff, N. L., 2013. Performance of an empirical bias-correction of a high-resolution climate dataset. Int. J. Climatol.. doi: 10.1002/joc.3830.

Bennett, J. C., Grose, M. R., Post, D. A., Ling, F.L.N., Corney, S.P., Bindoff, N. L., 2011. Performance of quantile-quantile bias-correction for use in hydroclimatological projections, 19th International Congress on Modelling and Simulation, Perth, Australia, 12–16 December 2011. http://mssanz.org.au/modsim2011.

Boe, J., Terray, L., Habets, F., Martin, E., 2007. Statistical and dynamical downscaling of the Seine basin climate for hydro-meteorological studies. Int. J. Climatol.. 27, 1643–1655, doi: 10.1002/joc.1602.

Bordoy, R., Burlando, P., 2013. Bias Correction of Regional Climate Model Simulations in a Region of Complex Orography. Journal of Applied Meteorology & Climatology, 52(1), 82-101.

Champathong, A., Komori, D., Kiguchi, M., Sukhapunnaphan, T., Oki, T., Nakaegawa ,T., 2013. Future projection of mean river discharge climatology for the Chao Phraya River basin. Hydrological Research Letters. 7(2), 36–41, doi: 10.3178/HRL.7.36.

Department of Groundwater Resources of Thailand, 2012. Pilot Study and Experiment on Managed Aquifer Recharge Using Ponding System in the Lower North Region River Basin, In: Phitsanulok, Sukhothai, and Pichit Provinces (Eds.), Executive Summary Report. Khon Kaen University Press, Thailand.

Duong, D. T., Tachikawa, Y., Shiiba, M. & Yorozu, K. (2013) River discharge projection in Indochina peninsula under a changing climate using the MRI-AGCM3.2S dataset. J. Japan Society of Civil Engng B1 (Hydraulic Engng) 69(4), 37–42.

Ehret, U., Zehe E., Wulfmeyer, V., Warrach-Sagi, K., Liebert, J., 2012. HESS Opinions "Should we apply bias correction to global and regional climate model data?". Hydrol. Earth Syst. Sci. Discuss. 9, 5355–5387, doi:10.5194/hessd-9-5355-2012.

Electricity Generating Authority of Thailand. http://ichpp.egat.co.th/graphIN/hydro/bigdam.php?year=2011 (reference: Jul.18, 2012).

Electricity Generating of Authority of Thailand (EGAT). http://www.sirikitdam.egat.com, http://www.bhumiboldam.egat.com (in Thai) (reference: Aug.29, 2012)

Etoh, T., Nurato, A., Nakanishi, M., 1987. SQRT-Exponential Type Distribution of Maximum, in: Singh, V. P. (Ed.), Hydrologic Frequency Modeling. Springer, Netherlands, pp. 253-264.

Hirabayashi, Y., Kane, S., Emori, E., Oki, T., Kimoto, M., 2008. Global projections of changing risks of floods and droughts in a changing climate. Hydrological Sciences–Journal–des Sciences Hydrologiques, 53(4), 754-772.

Hopson, T. M., Webster, P. J., 2010. A 1–10-day ensemble forecasting scheme for the major river basins of Bangladesh: forecasting severe floods of 2003–07*. Journal of Hydrometeorology. 11(3), 618-641, doi: 10.1175/2009JHM1006.1.

Hunukumbura, P. B., Tachikawa, Y., 2012. River Discherge Projection under Climate Change in the Chao Phraya River Basin, Journal of the Meteorological Society of Japan. 90(A), 137-150.

Ines, A. V. M., Hansen, J. W., 2006. Bias correction of daily GCM rainfall for crop simulation studies. Agricultural and Forest Meteorology. 138, 44–53.

Intergovernmental Panel on Climate Change (IPCC), 2007a. Synthesis Report. In: Allali, A., Roxana, B., Sandra, D., Ismail, E., Dave, G., David, H., Olav, H., Bubu, P. J., Lucka, K. B., Neil, L., Hoesung, L., David, W., Eds. Climate Change 2007: Synthesis Report. Cambridge University Press, Cambridge, United Kingdom and New York, NY, USA. http://www.ipcc.ch/pdf/assessment-report/ar4/syr/ar4_syr.pdf

IPCC, 2007b. Summary for Policymakers. In: Solomon, S., D. Qin, M. Manning, Z. Chen, M. Marquis, K.B. Averyt, M.Tignor and H.L. Miller (Eds.), Climate Change 2007: The Physical Science Basis. Contribution of Working Group I to the Fourth Assessment Report of the Intergovernmental Panel on Climate Change. Cambridge University Press, Cambridge, United Kingdom and New York, NY, USA. http://www.ipcc.ch/pdf/assessment-report/ar4/wg1/ar4-wg1-spm.pdf

IPCC, 2007c. IPCC list of GCM: Model output described in the 2007 IPCC Fourth Assessment Report (SRES scenarios). http://www.ipcc-data.org/sim/gcm_monthly/SRES_AR4/index.html. (reference: April 30, 2013)

Jayawadena, A. W., ASCE, M., Mahanama, S. P. P., 2002. Meso-Scale Hdrological Modeling: Application to Mekong and Chao Phraya Basins, Journal of Hydrologic Engineering. 7(1), 12-26.

Jha, R., Heerath, S., Musiake, K., 1997. Development of IIS Distributed hydrological Model (IISDHM) and its application in Chao Phraya River Basin, Thailand. J. of Hydraulic Engineering, JSCE. 41, 227-232.

Kite, G.W., A. Dalton, and K. Dion, 1994. Simulation of streamflow in a macro-scale watershed using GCM data. Water Resources Research, 30(5):1546-1559.

Kitoh, A., T. Ose, K. Kurihara, S. Kusunoki, M. Sugi, and KAKUSHIN Team-3 Modeling Group, 2009: Projection of changes in future weather extremes using super-high-resolution global and regional atmospheric models in the KAKUSHIN Program: Results of preliminary experiments. Hydrological Research Letters, 3, 49–53, doi:10.3178/hrl.3.49.

Komori, D., Nakamura, S., Kiguchi, M., Nishijima, A., Yamazaki, D., Suzuki, S., Kawasaki, A., Oki, K., Oki, T., 2012. Characteristics of the 2011 Chao Phraya River flood in Central Thailand. Hydrological Research Letters. 6, 41-46,.

Koontanakulvong, S., Chaowiwat,W., 2010. Technical Report: Corrected MRI GCM data for Thailand, p30. Water Resources System Research Unit Faculty of Engineering, Chulalongkorn University, Thailand

Kosa, P., Pongput, K., 2007. Evaluation of spatial and temporal reference evapotranspiration in the Chao Phraya River Basin. ScienceAsia. 33, 245-252, doi: 10.2306/scienceasia1513-1874.2007.33.245.

Kundzewicz, Z. W., Mata, L. J., Arnell, N. W., Doll, P., Jimenez, B., Miller, K., Oki, T., Şen, Z., Shiklomanov, I., 2008. The implications of projected climate change for freshwater resources and their management, Hydrological Sciences Journal. 53(1), 3-10, doi: 10.1623/hysj.53.1.3.

Kundzewicz, Z. W., Nohara, D., Tong, J., Oki, T., Buda, S., Takeuchi, K., 2009. Discharge of large Asian rivers – Observations and projections. Quaternary International. 208 , 4–10, doi: http://dx.doi.org/10.1016/j.bbr.2011.03.031.

Kure, S., Tebakari, T., 2012. Hydrological impact of regional climate change in the Chao Phraya River Basin, Thailand. Hydrological Research Letters. 6, 53-58.

Lafon, T., Dadson, S., Buys, G., Prudhomme, C., 2013. Bias correction of daily precipitation simulated by a regional climate model: a comparison of methods. Int. J. Climatol. 33, 1367–1381, doi: 10.1002/joc.3518.

Li, H., Sheffield, J., Wood, E. F., 2010. Bias correction of monthly precipitation and temperature fields from Intergovernmental Panel on Climate Change AR4 models using equidistant quantile matching. J. Geophys. Res.. 115, D10101, doi: 10.1029/2009JD012882.

Liu, J., Chen, X., Zhang, J., Flury, M., 2009. Coupling the Xinanjiang model to a kinematic flow model based on digital drainage networks for flood forecasting, Hydrological Processes. 23, 1337-1348.

Maraun, D., 2013. Bias correction, quantile mapping, and downscaling: revisiting the inflation issue. Journal of Climate. 26(6), 2137-2143, doi: 10.1175/JCLI-D-12-00821.1.

Maraun, D., Wetterhall, F., Ireson, A. M., Chandler, R. E., Kendon, E. J., Widmann, M., Brienen, S., Rust, H. W., Sauter, T., Themessl, M., Venema, V. K. C., Chun, K. P., Goodess,C. M., Jones, R. G., Onof, C., Vrac, M., and Thiele-Eich, I.: Precipitation downscaling under climate change: recent developments to

bridge the gap between dynamical models and the end user, Rev. Geophys., 48, Rg3003, doi:10.1029/2009rg000314, 2010.

Mishra, B. K., Herath, S., 2011. Climate projections downscaling and impact assessment on precipitation over upper Bagmati river basin, Nepal, Paper presented at the Third International Conference on Addressing Climate Change for Sustainable Development through Up-scaling Renewable Energy Technologies, Kathmandu, Nepal.

Mizuta, R., Yoshimura, H., Murakami, H., Matsueda, M., Endo, H., Ose, T., Kamiguchi, K., Hosaka, M., Sugi, M., Yukimoto, S., Kusunoki, S. & Kitoh, A. (2012) Climate simulation using MRI-AGCM3.2 with 20-km Grid. J. Meteorol. Soc. Japan 90(A), 233–258.

Moussa, R. & Bocquillon, C., 2009. On the use of the diffusive wave for modelling extreme flood events with overbank flow in the floodplain. J. Hydrol. 374, 116–135.

Nakaegawa, T., Kitoh, A., Hosaka, M., 2013. Discharge of major global rivers in the late 21st century climate projected with the high horizontal resolution MRI-AGCMs 2013. Hydrol. Process. 27, 3301–3318, doi: 10.1002/hyp.9831.

Nirupama, Tachikawa, Y., Shiiba, M., Takasao, T., 1996. A Simple Water Balance Model for a Mesoscale Catchment Based on Heterogeneous Soil Water Storage Capacity, Bull. Disas.Prev. Res. Inst., Kyoto Univ. 45(391), 61-83.

Ogata, T., Valeriano, O. C. S., Yoshimura, C., Liengcharernsit, W., Hirabayashi, Y., 2012. Past and Future hydrological simulations of Chao Phraya River Basin, J. Japan Soc. of Civil Eng., B1 (Hydraulic Eng.). 68(4), I_97-I102.

Ohba, k., Ponsana, P., 1987. Evapotranspiration in the Northeast District of Thailand as estimated by Morton Method. J. Agricultural Meteorology. 42(4). 329-336.

Oki, T., Musiake, K., Matsuyama, H., Masuda, K., 1995. Global atmospheric water balance and runoff from large river basins. Hydrological Process, 9, 655-678.

Piao, S., Ciais, P., Huang, Y., Shen, Z., Peng, S., Li, J., Zhou, L., Liu, H., Ma, Y., Ding, Y., Friedlingstein, P., Liu, C.,Tan, K., Yu, Y., Zhang, T., Fang, J., 2010. The impacts of climate change on water resources and agriculture in China. Nature. 467, 43–51, doi:10.1038/nature09364.

Royal Irrigation Department, Ministry of Agriculture and Cooperative of Thailand. 2000. Study of Chao Phraya River Basin Management Project. (in Thai)

Sharma, D., Babel, M.S., 2013. Application of downscaled precipitation for hydrological climate-change impact assessment in the upper Ping River Basin of Thailand, Climate Dynamics. 41(9-10), 2589-2602.

Sharma, D., Gupta, A. D., Babel, M. S., 2007. Spatial disaggregation of bias-correction GCM precipitation for improved hydrologic simulation: Ping River Basin, Thailand. Hydrol. Earth Syst. Sci. Discuss. 11, 1373-1390.

Shiiba, M., Ichikawa, Y., Sakakibara, T., Tachikawa, Y., 1999. A new numerical representation form of basin topography. J. of Hydraulic, Coastal and Environmental Engineering, JSCE, 621(II-47), 1–9. (in Japanese with English summary).

Shiklomanov, I.A., 2000. Appraisal and assessment of world water resources. Water International. 25(1), 11-32, doi:10.1080/02508060008686794.

Shuttleworth W. J., 1993. Evapotranspiration, in: Maidment, D. R. (Ed.), Handbook of Hydrology. McGRAW-HILL, Inc., New York, pp.4.1-4.53

Tachikawa, Y., Ichikawa, Y., Takara, K., Shiiba, M., 2000. Development of a macro scale distributed hydrological model using an object-oriented hydrological modeling system. Proc. of 4th International Conference Hydroinformatics, Iowa, USA. CD-ROM, pp 8.

Tachikawa, Y., S. Takino, Fujioka, Y., Yorozu, K., Kim, S., Shiiba, M., 2011. Projection of river discharge of Japanese river basins under a climate change scenario. J. Japan Soc. of Civil Eng., B1 (Hydraulic Eng.). 67(1), 1-15. (in Japanese)

Takara, K., 2009. Frequency analysis of hydrological extreme events and how to consider climate change. Water Resources and Water-Related Disasters under Climate Change, -Prediction, Impact Assessment and Adaptation-, 19th UNESCO-IHP Training Course, Kyoto University.

Takara, K., Takasao, T., 1998. Criteria for evaluating probability distribution models in hydrologic frequency analysis. J. of Hydraulic Coast. Environ. Eng. 393II-9, 151–160.

Tanaka, S., Takara, K., 1999. Goodness-of-fit and stability assessment in flood

frequency analysis. Annual J. Hydraulic Eng., JSCE. 43, 127-132. (in Japanese)

Thai Ministry of Interior.
http://disaster.go.th/dpm/flood/news/news_thai/EOCReport20JAN.pdf (in Thai) (reference: Jan.20, 2012).

Themeßl, M. J., Gobiet, A., Heinrich. G., 2010. Empirical-statistical downscaling and error correction of daily precipitation from regional climate models. International Journal of Climatology. 31, 1530–1544, doi: 10.1002/joc.2168.

Tokioka, T, A. Noda, A. Kitoh, Y. Nikaidou, S. Nakagawa, T. Motori, S. Yukimoto, and K. Takata, 1995: A transient CO2 experiment with the MRI CGCM. J. Meteor. Soc. Japan, 73, 817-826.

Tokioka, T., K. Yamazaki, I. Yagai, and A. Kitoh, 1984: A Description of the MRI Atmospheric General Cirrulation Model (The MRI GCM-I). Technical Report of the Meteorological Research Institute, 13. 249 pp.

USGS (2001) HydroSHEDS. http://hydrosheds.cr.usgs.gov/ (reference: 2011)

Watanabe, K., Yamamoto, T., Yamada, T., Sakuratani, T., Nawata, E., Noichana, C., Sributta, A., Higuchi, A., 2004. Changes in seasonal evapotranspiration, soil water content, and crop coefficients in sugarcane, cassava, and maize fields in Northeast Thailand. Agric. Water Manage. 67, 133–143.

Whetton, P. H., Fowler, A. M., Haylock, M. R., Pittock, A. B., 1993. Implications of climate change due to the enhanced greenhouse effect on floods and droughts in Australia. Climate Change. 25 (3-4), 289-317.

Wichakul, S., Tachikawa, Y., Shiiba, M., Yorozu, K., 2013a. Developing a regional distributed hydrological model for water resources assessment and it application to the Chao Phraya River Basin. J. Japan Society of Civil Eng. B1 (Hydraulic Eng.). 69(4), 43‐48.

Wichakul, S., Tachikawa, Y., Shiiba, M., Yorozu, K., 2013b. Development of a flow routing model including inundation effect for the extreme flood in the Chao Phraya River Basin, Thailand 2011. J. Disaster Research. 8(3), 415–423.

Wichakul, S., Tachikawa, Y., Shiiba, M., Yorozu, K., 2014. Prediction of water resources in the Chao Phraya River Basin, Thailand. Proceeding from Hydrology in Hydrology in a Changing World: Environmental and Human

Dimensions, 7th Global FRIEND-Water Conference (IAHS). Publ. 363. Montpellier, France. (in press)

Wood A. W., Leung. L. R., Sridhar. V., Lettenmaier D. P., 2004. Hydrologic implications of dynamical and statistical approaches to downscaling climate model outputs. Climatic Change. 62, 189–216, doi: 10.1023/B : CLIM.0000013685.99609.9e.

Wood, E. F., Lettenmaier, D. P., Zartarian, V. G., 1992. A Land-Surface hydrology parameterization with subgrid variability for General Circulation Models, Journal of Geophysical Research. 97(D3), 2717-2728.

Wood, E.F., Lettenmaier, D., Liang, X., Nijssen, B., Wetzel, S. W., 1997. Hydrological modeling of continental-scale basins. Annu. Rev. Earth Planet. Sci. 25, 279–300.

World Bank, 2012. The World Bank Supports Thailand's Post-Floods Recovery Effort. http://web.worldbank.org (reference: Mar 2012)

Xu, Z. X., Li, J.Y., 2003. Estimating basin evapotranspiration using distributed hydrologic model. J. of Hydrologic Eng. 8 (2), 74-80, doi: 10.1061/(ASCE)1084-0699(2003)8:2(74).

Yang, C., Yu, Z., Hao, Z., Zhang, J., Zhu, J., 2012. Impact of climate change on flood and drought events in Huaihe River Basin, China. Hydrology Research. 43 (1/2), 14-22.

Yatagai, A., Kamiguchi, K., Arakawa, O., Hamada A., Yasutomi N., Kitoh, A., 2012. APHRODITE: constructing a long-term daily gridded precipitation dataset for Asia based on a dense network of rain gauges. Bull. Amer. Meteor. Soc., 93, 1401–1415, doi: http://dx.doi.org/10.1175/BAMS-D-11-00122.1.

Yukimoto, S., A. Noda, A. Kitoh, M. Hosaka, H. Yoshimura, T. Uchiyama, K. Shibata, O. Arakawa, and S. Kusunoki, 2006: Present-day climate and climate sensitivity in the Meteorological Research Institute Coupled GCM version 2.3 (MRI-CGCM2.3). J. Meteor. Soc. Japan, 84, 333-363.

Yukimoto, S., A. Noda, A. Kitoh, M. Sugi, Y.Kitamura, M. Hosaka, K. Shibata, S. Maeda, and T. Uchiyama, 2001: A new Meteorological Research Institute Coupled GCM (MRI-CGCM2) – Model climate and its variability - . Pap. Meteor. Geophys., 51, 47-88, doi:10.2467/mripapers.51.47.

Yukimoto, S., Yoshimura, H., K. Yamazaki, Hosaka, M., Sakami, T., Tsujino, H., Hirabara, M., Tanaka, T. Y., Deushi, M., Obata, A., Nakano, H., Adachi, Y., Shindo, E., Yabu, S., Ose, T., and Kitoh, A., 2011: Meteorological Research Institute-Earth System Model Version 1 (MRI-ESM1). Technical Report of the Meteorological Research Institute, 64.88 pp.

Zhao, R. J., Zhuang, Y. L., Fang, L. R., Liu, X. R., Zhang, Q. S., 1980. The Xinanjiang model, Hydrological Forecasting Proc., Oxford Symposium, International Association of Hydrological Sciences (IAHS). 129, 351-356.